BIOCHEMICAL PROPERTIES AND SUBSTRATE REACTIVITIES OF *AQUIFEX AEOLICUS* RIBONUCLEASE III

A Dissertation

Submitted to

the Temple University Graduate Board

In Partial Fulfillment

of the Requirements for the Degree of

DOCTOR OF PHILOSOPHY

By

Zhongjie Shi

January, 2012

Examining Committee Members:

Dr. Allen Nicholson, Advisory Chair, Chemistry and Biology
Dr. Christian Schafmeister, Chemistry
Dr. Michael Zdilla, Chemistry
Dr. Richard Waring, External Member, Biology

ABSTRACT

BIOCHEMICAL PROPERTIES AND SUBSTRATE REACTIVITIES OF *AQUIFEX AEOLICUS* RIBONUCLEASE III

Zhongjie Shi

DOCTOR OF PHILOSOPHY

Temple University, 2012

Advisor: Dr. Allen W. Nicholson

Ribonuclease III is a highly-conserved bacterial enzyme that cleaves double-stranded (ds) RNA structures, and participates in diverse RNA maturation and decay pathways. Essential insight on the RNase III mechanism of dsRNA cleavage has been provided by crystallographic studies of the enzyme from the hyperthermophilic bacterium, *Aquifex aeolicus*. However, those crystals involved complexes containing either cleaved RNA, or a mutant RNase III that is catalytically inactive. In addition, neither the biochemical properties of *A. aeolicus* (Aa)-RNase III, nor the reactivity epitopes of its cognate substrates are known. The goal of this project is to use Aa-RNase III, for which there is atomic-level structural information, to determine how RNase III recognizes its substrates and selects the target site.

I first purified recombinant Aa-RNase III and defined the conditions that support its optimal *in vitro* catalytic activity. The catalytic activity of purified recombinant Aa-RNase III exhibits a temperature optimum of 70–85°C, a pH optimum of 8.0, and with either Mg^{2+} or Mn^{2+} supports efficient catalysis. Cognate substrates for Aa-RNase III were identified and their reactivity epitopes were characterized, including the specific bp sequence elements that determine processing reactivity and

selectivity. Small RNA hairpins, based on the double-stranded structures associated with the *Aquifex* 16S and 23S rRNA precursors, are cleaved *in vitro* at sites that are consistent with production of the immediate precursors to the mature rRNAs. Third, the role of the dsRBD in scissile bond selection was examined by a mutational analysis of the conserved interactions of RNA binding motif 1 (RBM1) with the substrate proximal box (pb). The individual contributions towards substrate recognition were determined for conserved amino acid side chains in the RBM1. It also was shown that the dsRBD plays key dual roles in both binding energy and selectivity, through RBM1 responsiveness to proximal box bp sequence. The dsRBD is specifically responsive to an antideterminant (AD) bp in pb position 2. The relative structural rigidity of both dsRNA and dsRBD rationalizes the strong effect of an inhibitory bp at pb position 2: disruption of one RBM1 side chain interaction can effectively disrupt the other RBM1 side chain interactions. Finally, a cis-acting model was developed for subunit involvement in substrate recognition by RNase III. Structurally asymmetric mutant heterodimers of *Escherichia coli* (Ec)-RNase III were constructed, and asymmetric substrates were employed to reveal how RNase III can bind and deliver hairpin substrates to the active site cleft in a pathway that requires specific binding configurations of both enzyme and substrate.

ACKNOWLEDGEMENTS

I will express my heartfelt thankfulness to my advisor, Dr. Nicholson, who opened the door and led me through the ribonuclease III world, step by step. Through five years of training, I have learned both the knowledge of science and the way of doing science. He armed me, a former obstetrician and gynecologist, with modern basic theories and techniques in the biochemistry field.

I will also thank my committee members, Dr. Richard Waring, Dr. Christian Schafmeister and Dr. Michael Zdilla, who provided critical help to my course, proposal, seminar, and dissertation.

I also appreciate help from Dr. Mark Feitelson, who helped me with my proposal of HBV project. I want to thank Dr. Rhonda Nicholson for her pioneer work and my lab members for their selfless daily help and encouragement.

Finally, I would like to thank my family, who always take care of my daily life, keep encouraging me, and forgive my unavailability due to scientific work.

TABLE OF CONTENTS

LIST OF FIGURES

LIST OF TABLES

LIST OF ABBREVIATIONS

Am	ampicillin
bp	base pair
BSA	bovine serum albumin
CaM	calmodulin
CBP	calmodulin-binding-peptide
Cm	Chloramphenicol
db	distal box
dNTP	deoxynucleoside triposphate
dsRBD	double-stranded-RNA-binding domain
dsRNA	double-stranded RNA
DTT	Dithiothreitol
EB	ethidium bromide
EDTA	Ethylenediaminetetraacetic acid
$(His)_6$	hexahistidine
IPTG	Isopropyl-β-D-thiogalactopyranoside
LB	Luria-Bertani
Mb	middle box
miRNA	micro RNA
MWCO	molecular weight cut-off
nt	nucleotide
NTP	Ribonucleoside 5'-triphosphate
NucD	nuclease domain
OD	optical density
PAGE	Polyacrylamide gel electrophoresis

pb	proximal box
PCR	polymerase chain reaction
RBM	RNA-binding motif
RNAi	RNA interference
RNase	Ribonuclease
rRNA	ribosomal RNA
SDS	Sodium dodecyl sulfate
siRNA	short interfering RNA
TBE	Tris-borate-EDTA
TEMED	Tetramethylethylenediamine
tRNA	Transfer RNA
UV	ultraviolet
WC	Watson-Crick
WT	wild-type

CHAPTER 1. INTRODUCTION

1.1 The role of RNA processing and decay in gene expression

As was first disclosed by the "Central Dogma" scheme (Crick, 1970) and later delineated by the discovery of RNA interference (RNAi) pathway (Fire, 1998; Hannon, 2002), the integral function of RNA in diverse cellular processes has been established. Not only does RNA play indispensable roles in transcription, translation, and gene regulation, it can store, express, and replicate genetic information.

Primary transcription products are usually longer than the corresponding mature RNAs. Thus, RNA molecules need to be processed into their mature forms in order to properly function. RNA processing reactions include endonucleolytic cleavage; 3' or 5' exonucleolytic cleavage; insertion, deletion, or modification of nucleotides; RNA splicing; 5' capping, and 3'-end polyadenylation (Lewin, 2000). The endonucleolytic cleavage of double-stranded (ds) RNA structures is an essential step in the maturation of many eukaryotic and bacterial RNAs, and is a central participant in post-transcriptional gene silencing. A representative RNA maturation pathway that is dependent upon dsRNA cleavage is the processing of the primary transcript of the bacterial ribosomal RNA (rRNA) operons. Cleavage of dsRNA is also involved in the production of short interfering (si) RNAs, micro (mi) RNAs, and related noncoding RNAs, all of which participate in post-transcriptional gene silencing (Nicholson 2003; Lamontagne *et al*., 2001; Carmell and Hannon, 2004; Macrae *et al*., 2006).

1.2 The Ribonuclease III family

Members of the ribonuclease III (RNase III) family (Figure 1A) are broadly conserved in the Eukarya and Bacteria, and specifically recognize and cleave dsRNA. RNase III family members participate in diverse gene regulatory pathways (Court 1993; LaMontagne *et al*., 2001; Nicholson, 2003; Carmell and Hannon, 2004;

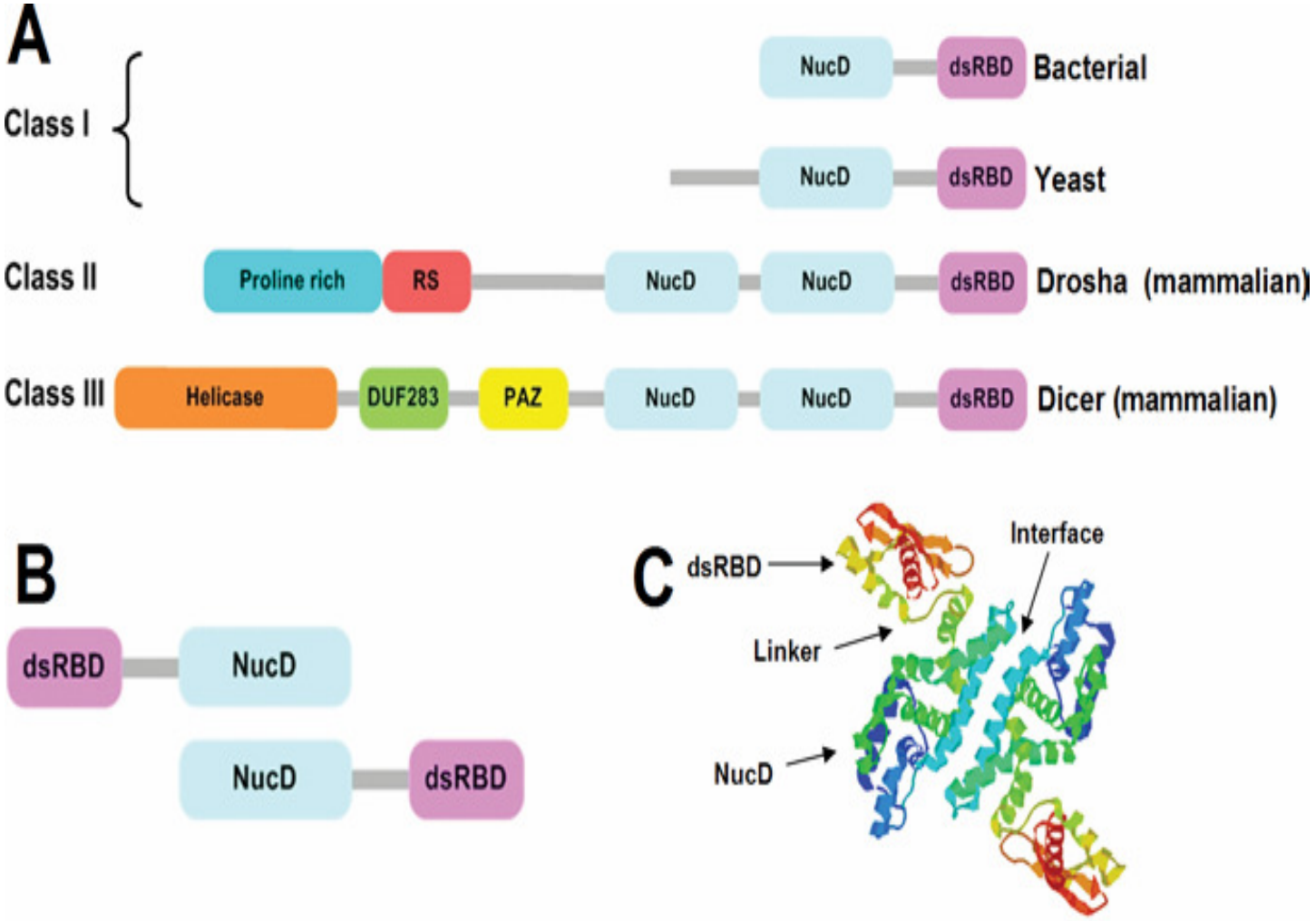
A
Class I
NucD
dsRBD
Bacterial
NucD
dsRBD
Yeast
Class II
Proline rich
RS
NucD
NucD
dsRBD
Drosha (mammalian)
Class III
Helicase
DUF283
PAZ
NucD
NucD
dsRBD
Dicer (mammalian)
B
dsRBD
NucD
NucD
dsRBD
C
dsRBD
Interface
Linker
NucD

Figure 1. The Ribonuclease III family (Meng and Nicholson, 2008).

A. The three main classes of RNase III enzymes. Class 1: Bacterial RNase III and *Saccharomyces cerevisiae* Rnt1p; Class II: Mammalian Drosha; Class III: Mammalian Dicer. Colored regions represent functional domains. Nuclease domain (NucD) is in light blue; double-stranded RNA-binding domain (dsRBD) is in light purple; Proline-rich region of Drosha is in blue; Arginine-Serine-rich (RS) region of Drosha is in red; the Helicase domain of mammalian Dicer is in orange; DUF283 (domain of unidentified function) of Dicer is in green, and the Piwi-Ago-Zwille (PAZ) domain of Dicer is in yellow.

B. Diagram of the homodimeric structure of bacterial RNase III, showing the self-association of the nuclease domain.

C. Ribbon diagram of *Thermotoga maritima* RNase III (PDB code: 1O0W). The dsRBD, NucD and linker segment are indicated: the dsRBD is shown in red–orange–yellow color, while the NucD is shown in blue–green color.

Nicholson, 2011). The eukaryotic RNase III orthologs Dicer and Drosha function in the maturation of miRNAs that control mRNA translation (Carmell and Hannon, 2004). Dicer also generates endogenous siRNAs that participate in host defense and genome maintenance (Jaskiewicz and Filipowicz, 2008). Bacterial RNases III have a conserved role in the maturation of the 16S and 23S rRNAs (Srivastava and Schlessinger, 1990; Deutscher, 2009), and also cleave diverse cellular, phage and plasmid RNAs as an integral step in their maturation or decay pathways (Price *et al*., 1999; Huntzinger *et al*., 2005; Saito and Richardson, 1981; Schmeissner *et al*., 1984).

1.3 Characteristic structural and functional features of bacterial RNase III

1.3.1 Structural features

Bacterial RNase III polypeptides are the structurally simplest members of the family, and include *Escherichia coli* (Ec), *Thermotoga maritima* (Tm), and *Aquifex aeolicus* (Aa) RNases III. A typical RNase III polypeptide possesses ~220-240 amino acids, and contains an N-terminal nuclease domain (NucD) that includes a set of highly conserved carboxylic acid residues that interact with the catalytically essential divalent metal ions. The NucD exhibits a unique, predominantly all α-helical structure (Blaszczyk *et al*., 2001). A short, flexible linker connects the NucD to the C-terminal dsRNA-binding domain (dsRBD), containing a single copy of the conserved dsRNA-binding motif (dsRBM) (Figure 1B, C; Figure 2). The linker acts as a pivot in allowing the movement of the dsRBD during dsRNA recognition and formation of the precatalytic complex. Dimerization of the NucD forms the active holoenzyme that contains two dsRBDs, both of which are needed for optimal catalytic activity (Meng and Nicholson, 2008). The dsRBD (~65 amino acids) has an α-β-β-β-α secondary structure that is the defining fold of the dsRBM (Tian *et al*., 2004). The two approximately parallel α-helices are positioned on the same face of a three-stranded,

A

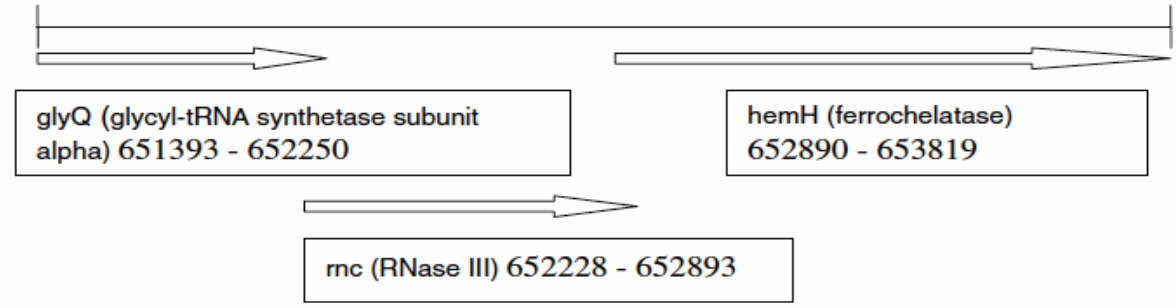

B

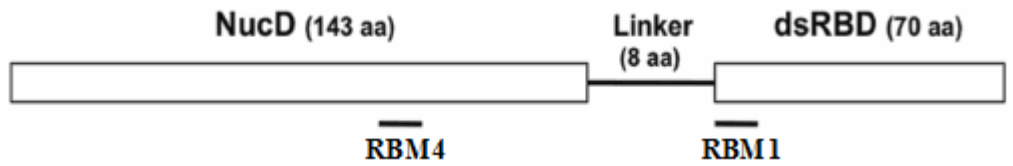

C

```
A. aeolicus          MKMLE QLEKKLGYTF KDKSLLEKAL THVSYS---- ------KKEH YETLEFLGDA   45
T. maritima       MNESERKIVE EFQKETGINF KNEELLFRAL CHSSYANEQN QAGRKD VES NEKLEFLGDA   59
M. tuberculosis      MIRSRQ PLLDALGVDL -PDELLSLAL THRSYAYENG ------GLPT NERLEFLGDA   49
E. coli              MNPIVIN RLQRKLGYTF NHQELLQQAL THRSAS---- ------SK-H NERLEFLGDS   46

                                    RBM3                                  RBM4

A. aeolicus       LVNFFIVDLL VQYSPNKREG FLSPLKAYLI SEEFFNLLAQ KL---ELHKF IRIKRG--KI  100
T. maritima       VLELFVCEIL YKKYPEAEVG DLARVKSAAA SEEVLAMVSR KM---NLGKF LFLGKGEEKT  116
M. tuberculosis   VLGLTITDAL FHRHPDRSEG DLAKLRASVV NTQALADVAR RLCAEGLGVH VLLGRGEANT  109
E. coli           ILSYVIANAL YHRFPRVDEG DMSRMRATLV RGNTLAELAR EF---ELGEC LRLGPGELKS  103

                                                                  Linker

A. aeolicus       ----NETIIG DVFEALWAAV YIDSGRDANF TRELFYKLFK EDILSAIKEG RVKKD       151
T. maritima       GGRDRDSILA DAFEALLAAI YLDQ--GYEK IKELFEQEFE FYIEKIMK-G EMLFD       168
M. tuberculosis   GGADKSSILA DGMESLLGAI YLQH--GMEK AREVILRLFG PLLDAAPTLG AGL-D       155
E. coli           GGFRRESILA DTVEALIGGV FLDS--DIQT VEKLILNWYQ TRLDEI-SPG DKQKD       155

                        RBM1                    RBM2

A. aeolicus       YKTILQEITQ KRWKERPEYR LISVEGPHHK KKFIVEAKIK -EYRTL-GEG KSKKEAEQRA  209
T. maritima       YKTALQEIVQ SEHKVPPEYI LVRTEKNDGD RIFVVEVRVN GKTIAT-GKG RTKKEAEKEA  227
M. tuberculosis   WKTSLQELTA ARGLGAPSYL VTSTGPDHDK EFTAVVVVMD SEYGS--GVG RSKKEAEQKA  213
E. coli           PKTRLQEYLQ GRHLPLPTYL VVQVRGEAHD QEFTIHCQVS GLSEPVVGTG SSRRKAEQAA  215
                        * *

A. aeolicus       AEELIKLLEE SE--------- 221
T. maritima       ARIAYEKLLK ERS-------- 240
M. tuberculosis   AAAAWKALEV LDNAMPGKTSA 234
E. coli           AEQALKKLEL E---------  226
```

NucD

dsRBD

Figure 2. Features of the *A. aeolicus* RNase III gene and polypeptide (Shi *et al*., 2011).

A. Diagram of the *A. aeolicus* chromosomal region that contains the RNase III (rnc) gene. The RNase III open reading frame (ORF) exhibits a 22-bp overlap with the ORF for the α-subunit of glycyl-tRNA synthetase, and a 3-bp overlap with the ORF for ferrochelatase, suggesting coupled expression of the tthree genes.

B. Domain structure of the Aa-RNase III polypeptide. Indicated are the N-terminal nuclease domain (NucD), linker, C-terminal dsRBD, and the positions of RNA-binding motifs 1 and 4 (RBM1 and RBM4) that interact with the substrate proximal box and distal box, respectively (Gan *et al*., 2006; Gan *et al*., 2008).

C. Sequence alignment of selected bacterial RNase III orthologs. Shown are the positions of the NucD, linker, dsRBD, RBM1 to RBM4. The asterisks indicate the highly conserved lysine and glutamine in RBM1 (K153 and Q157 in Aa-RNase III).

antiparallel β-sheet (Kharrat et al., 1995). The dsRBD recognizes ribose 2'-hydroxyl groups on both strands of the double helix, which establishes dsRNA specificity (Ryter and Schultz, 1998; Gan *et al*., 2005; Gan *et al*., 2006; Figure 3). A recently characterized *Bacillus subtilis* RNase III ortholog ('Mini-III') lacks the C-terminal dsRBD, but nonetheless retains catalytic activity and creates the mature 5'-end of 23S rRNA with the assistance of ribosomal protein L3 (Redko and Condon, 2009).

Analyses of high-resolution crystal structures of Aa-RNase III, with and without bound dsRNA, have served to rationalize a large body of genetic and biochemical data on bacterial RNases III, especially that of Ec-RNase III, and also have provided insight on the mechanisms of action of eukaryotic family members including Dicer (Blaszczyk *et al*., 2001; Blaszczyk *et al*., 2004; Gan *et al*., 2005; Gan *et al*., 2006; Gan *et al*., 2008; Ji, 2008). Salient structural features of Aa-RNase III include (i) a subunit interface created by NucD dimerization that provides a dsRNA-binding valley; (ii) the symmetric positioning of the two catalytic sites that establishes the characteristic 2-nt 3'-overhang product ends; (iii) two closely-positioned divalent metal ions in each catalytic site; and (iv) a flexible linker that confers positional mobility on the dsRBD (Figure 4).

1.3.2 Characteristic functional features of RNase III

The bacterial RNase III catalytic mechanism employs two Mg^{2+} ions (Figure 5), and involves the activation of a water nucleophile to hydrolyze target site phosphodiesters, creating 5'-phosphate, 3'-hydroxyl product termini (Nicholson, 2003; Sun *et al*., 2005). Targets sites in regular dsRNA structures are cleaved on both strands, and the relative positions of the two catalytic sites across the enzyme subunit interface provide the characteristic 2-nt, 3'-overhang product ends. RNase III has two distinct biochemical activities: dsRNA cleavage and dsRNA binding (Ji, 2006). The

A

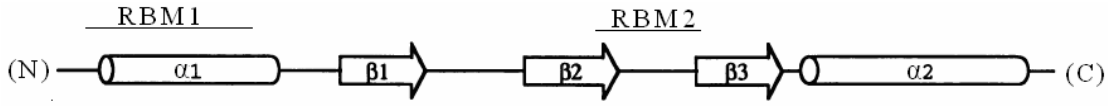
RBM1
RBM2
(N)
α1
β1
β2
β3
α2
(C)

B

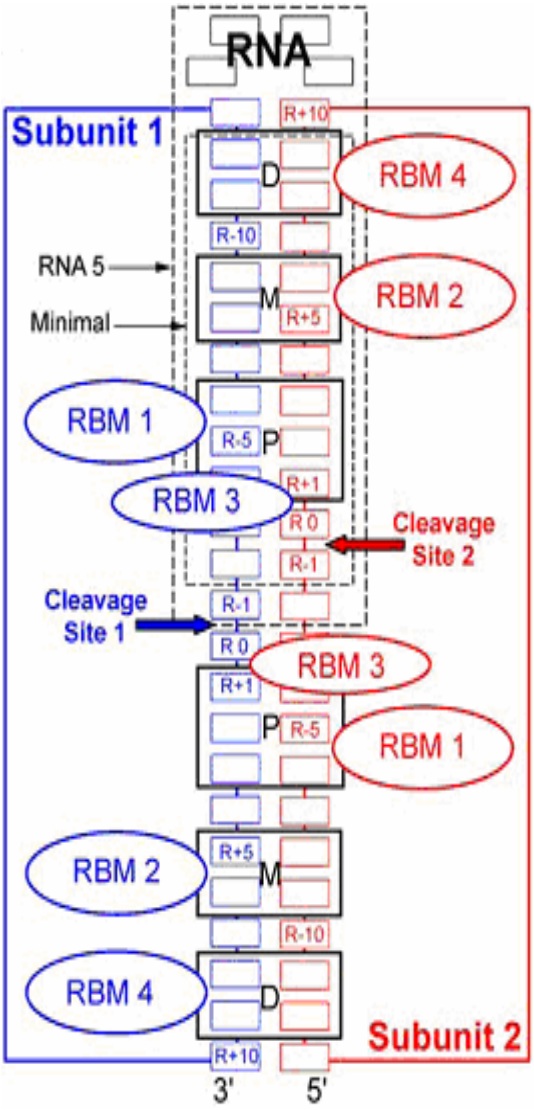
RNA
Subunit 1
Subunit 2
RNA 5
Minimal
RBM 1
RBM 2
RBM 3
RBM 4
Cleavage Site 1
Cleavage Site 2
3'
5'

C

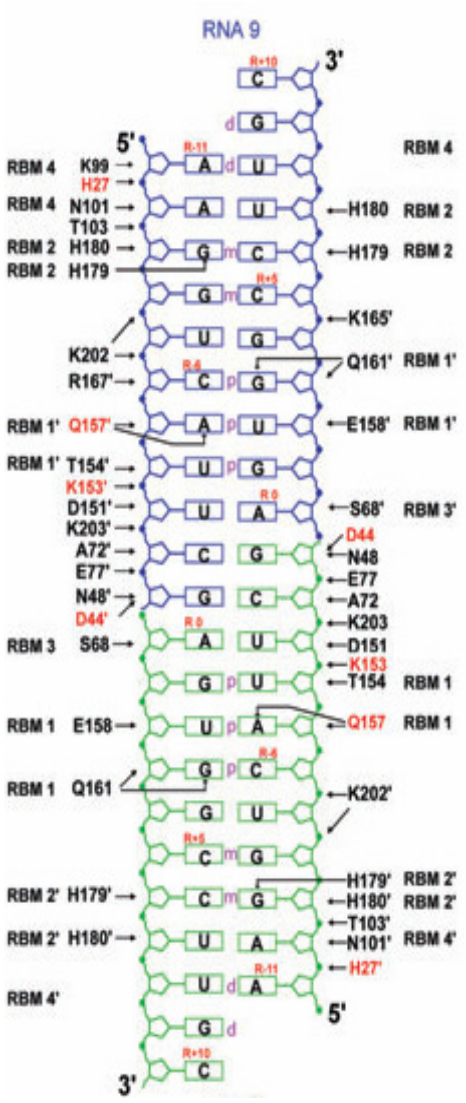
RNA 9
3'
5'
RBM 4
RBM 2
RBM 1'
RBM 3'
RBM 1
RBM 3
RBM 2'
RBM 4'
K99
H27
N101
T103
H180
H179
K165'
K202
R167'
Q161'
Q157'
E158'
T154'
K153'
D151'
K203'
S68'
A72'
E77'
N48'
D44'
D44
N48
E77
A72
K203
D151
K153
T154
Q157
E158
Q161
K202'
H179'
H180'
T103'
N101'
H27'

Figure 3. Schematic representation of RNase III-dsRNA interactions.

A. Schematic composition of the dsRBD according to its conserved secondary structural elements. The positions of RBM1 and RBM2 are shown.

B. Schematic illustrations of RNase III-dsRNA interactions as observed in the crystal structure of Aa-D44N•RNA complex (Gan *et al*., 2006). The homodimeric form of the protein is indicated as two rectangles, labeled ‘‘Subunit 1’’ and ‘‘Subunit 2’’ and the four RBMs are shown as ellipsoids. The substrate is represented by a stem-loop dsRNA with a 24 base-pair double-helical segment. The scissile bonds are indicated by arrows, and the protein-interacting regions in the dsRNA [proximal (P), middle (M), and distal (D) box] are outlined with black rectangles. The nucleotide residue immediately 3’ to the cleavage site is numbered ‘‘R0,’’ and the rest are numbered according to the polarity of the RNA strand. Subunit 1 of RNase III and the RNA strand with which it interacts are shown in blue. Subunit 2 and the associated RNA strand are shown in red. RNA 5 and a minimal dsRNA substrate are indicated by dashed lines. RBMs 1, 2, and 4 interact with the proximal (P), middle (M), and distal (D) box of the dsRNA, respectively, whereas RBM 3 interacts with nucleotide residues R0 and R+1 on one strand at the target site.

C. Schematic depiction of the hydrogen bonds between protein and dsRNA as observed in the Aa-RNase III•Mg^{2+}•dsRNA crystal structure (Gan *et al*., 2008) (PDB code: 2NUF). The two dsRNA molecules (cleavage products of a non-cognate substrate, based on an Ec-RNase III reported by Zhang and Nicholson, 1997) are distinguished with different colors; the protein-interacting boxes (proximal, middle and distal boxes) are indicated with one-letter abbreviations (p, m, and d, respectively); and the two cleaved scissile bonds (between the blue and green sequences) are located between the two RNA molecules. For the protein, the prime (′) associated with an RBM or specific residue distinguishes one protein subunit from the other. Residues strictly conserved in 100 RNase III sequences are highlighted in red. Hydrogen bonds between amino acid and nucleotide residues are indicated by black arrows.

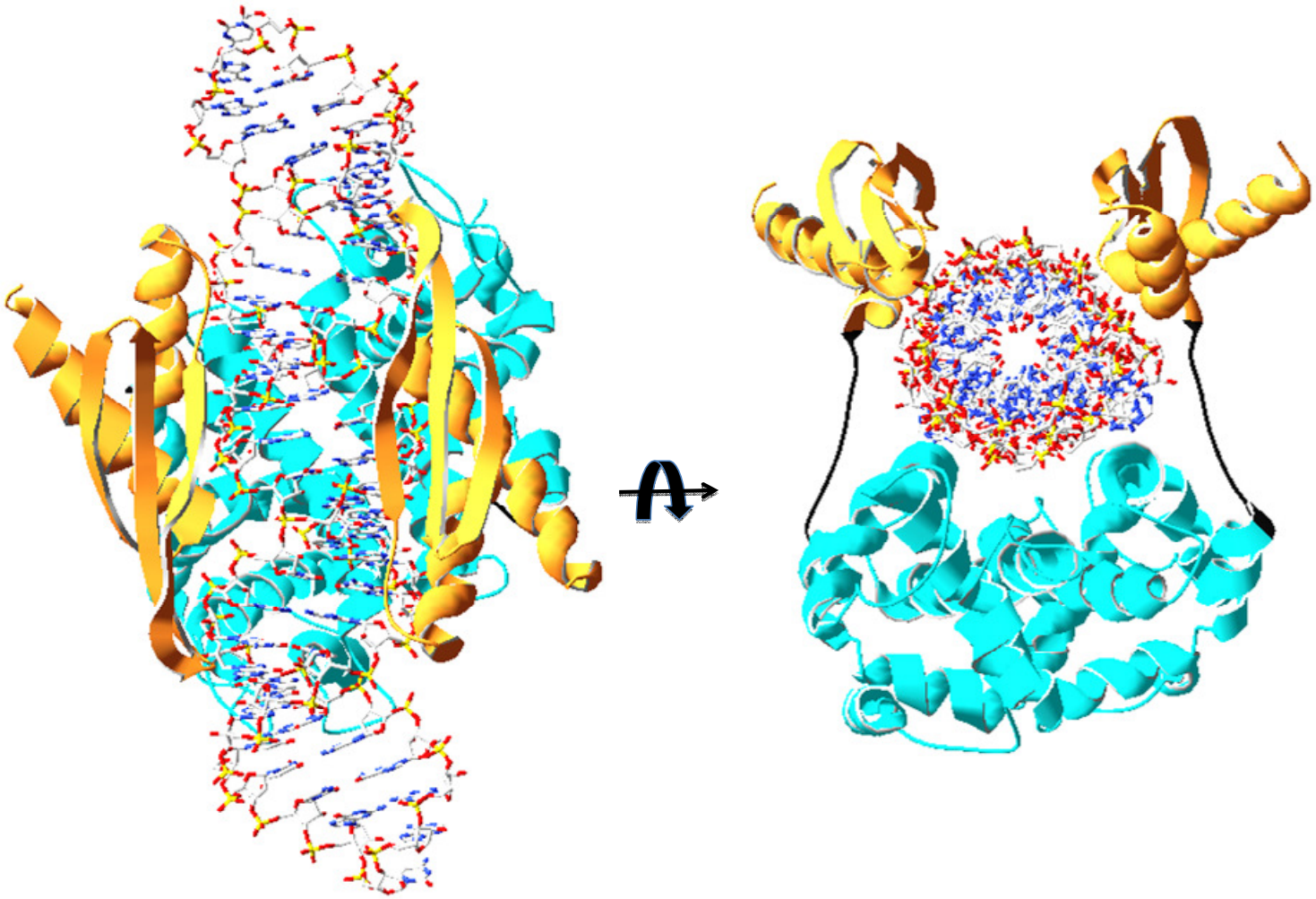

Figure 4. Two views of a crystal structure of Aa-RNase III bound to two molecules of a cleaved RNA hairpin substrate (PDB code: 2EZ6) (Gan *et al*., 2006).

Aa-RNase III used for crystallization contains the D44N mutation, which inhibits catalytic activity of Ec-RNase III (Zhang *et al*., 2004). The two dsRBDs are shown in yellow-gold while the two nuclease domains are shown in blue. The linker regions are shown in black. The dsRNA is placed in the center of cleavage valley. The RNA is illustrated as stick models in atomic color scheme (carbon in white, nitrogen in blue, oxygen in red, and phosphorus in yellow). The two views are related by a 90° rotation. The image is produced by the Swiss-PDB Viewer.

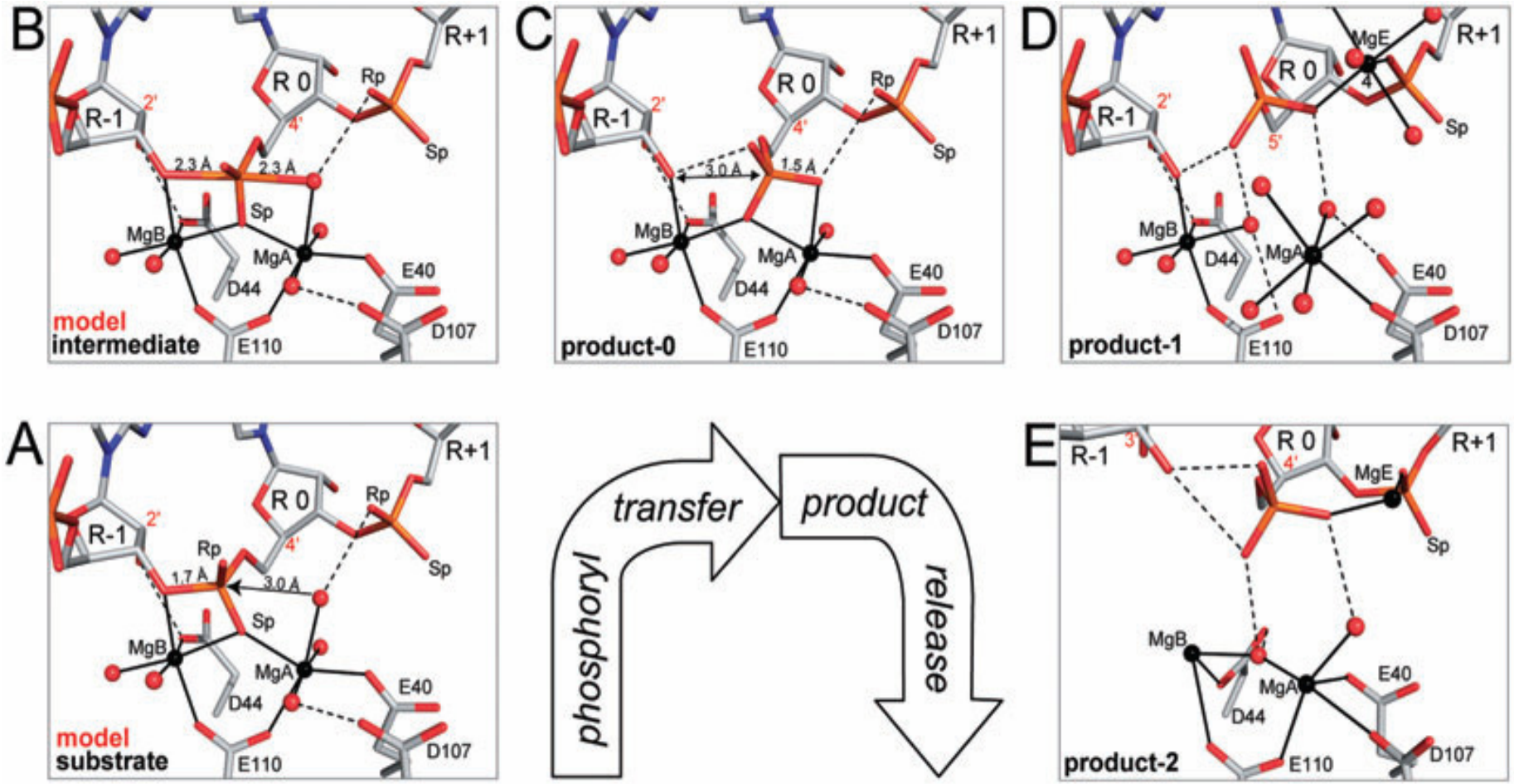
B
R-1
R 0
R+1
2'
4'
Rp
Sp
2.3 Å
2.3 Å
Sp
MgB
MgA
D44
E40
D107
E110
model
intermediate
C
3.0 Å
1.5 Å
product-0
D
MgE
5'
product-1
A
1.7 Å
3.0 Å
model
substrate
transfer
product
phosphoryl
release
E
3'
product-2

Figure 5. Proposed stepwise model for phosphoryl transfer and product release in the RNase III catalytic cycle (Gan *et al*., 2008).

A. Model of the catalytic site in the precatalytic protein–substrate complex, showing the coordination of the scissile phosphodiester by two Mg^{2+} ions (MgA and MgB).

B. Model of the intermediate complex at, or close to, the reaction transition state.

C. The catalytic site complex structure immediately after phosphodiester hydrolysis, showing a minor conformational change in the Aa-RNase III-Mg^{2+}-RNA complex.

D. The first step towards product release is represented by a major conformational change in the Aa-RNase III–Mg^{2+}-RNA structure, and a new interaction of the 5'-phosphomonoester with a Mg^{2+} ion in site E (MgE).

E. The second step towards product release, represented by the Aa-RNase III–Mg^{2+}-RNA structure. Here, the 3'-OH terminated cleavage product is disengaged from the Mg^{2+} ion in site B (MgB).

The amino acid and nucleotide residues are shown in stick form, and the Mg^{2+} ions and water oxygens as spheres (C, grey; N, blue; O, red; P, orange; Mg, black). Metal coordinate bonds are illustrated as solid lines and hydrogen bonds as dashed lines. The nucleotide residue on the 3'-side of the scissile bond is indicated as 'R0', while the rest of the nucleotides are numbered according to the polarity of the RNA strand.

first activity is exemplified by the involvement of RNase III in rRNA maturation. The 16S-23S-5S primary rRNA transcript (30S RNA; ~5500 nt) is site-specificallycleaved by bacterial RNase III in the stem structures associated with the termini of the 16S and 23S rRNAs. These reactions yield the immediate precursors to the mature 16S and 23S rRNAs (see Bram *et al*., 1980 for Ec-RNase III; Shi *et al*., 2011 for Aa-RNase III; and Nathania and Nicholson, 2010 for Tm-RNase III; Figure 6). Ec-RNase III also is responsible for the processing of the polycistronic early mRNA precursor of T7 bacteriophage. RNase III cleavage of hairpin stem-loop structures at five intercistronic sites creates the mature, fully functional mRNAs (Dunn and Studier, 1983). The second activity of RNase III as an RNA-binding protein is indicated in studies on the bacteriophage lambda cIII protein, whose synthesis is enhanced by the binding of Ec-RNase III at a site within the 5'-untranslated region of the cIII mRNA. The protein binding step is proposed to expose a ribosome binding site, thereby promoting translation of the cIII cistron (Altuvia *et al*., 1991).

1.4 Research aims and objectives

1.4.1 Challenges

In contrast to the extensive structural information, neither the biochemical behavior of Aa-RNase III, nor the structures and processing reactivities of any of its cognate substrates have been described. Such information, in conjunction with the extensive structural data, would provide mechanistic insight on the fundamental steps in the catalysis of dsRNA cleavage, and how RNase III selects its target sites. In this regard, Ec-RNase III efficiently cleaves dsRNA of broad sequence content *in vitro* into ~11-13 bp products, suggestive of the absence of a strict sequence requirement. However, cognate cellular substrates are cleaved in a highly site-specific manner *in vivo* and *in vitro*. The *in vivo* and *in vitro* processing specificities are identical, and the

A

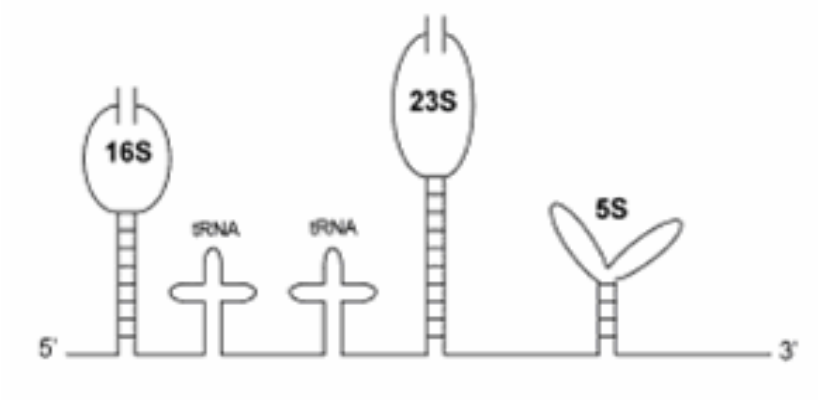
16S
23S
5S
tRNA
tRNA
5'
3'

B

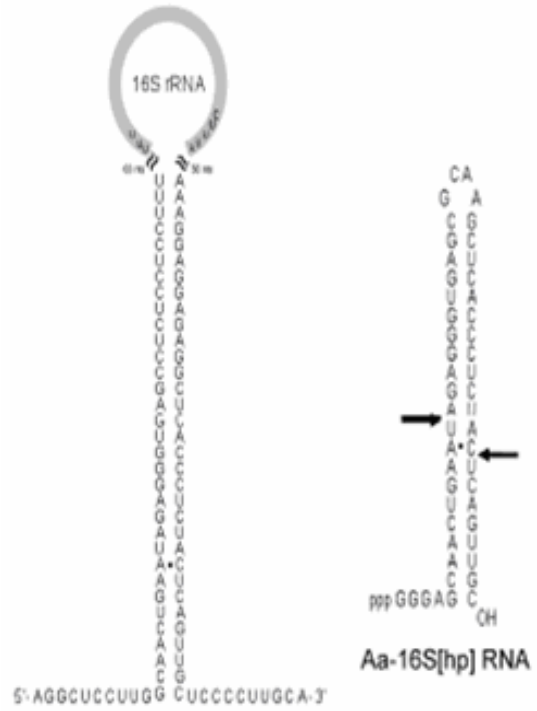
16S rRNA
Aa-16S[hp] RNA

C

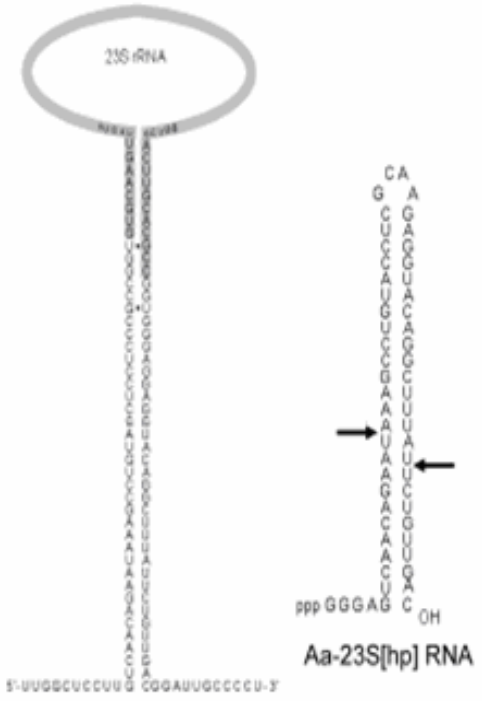
23S rRNA
Aa-23S[hp] RNA

Figure 6. Structures of the *A. aeolicus* pre-16S and pre-23S rRNA processing stems and the corresponding hairpin substrates (Shi *et al*., 2011).

A. Diagram of the primary transcript of one of the two *A. aeolicus* 16S–23S–5S rRNA gene clusters, emphasizing the base-paired stem structures associated with the 16S and 23S rRNA sequences that are cleaved by RNase III.

B. Sequence and proposed structure of the 16S pre-rRNA stem (left) and the corresponding hairpin substrate, Aa-16S[hp] RNA (right). Arrows indicate the Aa-RNase III cleavage sites.

C. Sequence and proposed structure of the 23S pre-rRNA stem (left) and corresponding hairpin substrate, Aa-23S[hp] RNA (right). In the processing stems, the nucleotide sequences within the mature rRNAs are shown in smaller size. Arrows indicate the Aa-RNase III cleavage sites.

reaction does not require additional protein cofactors. The high specificity of RNase III towards its cognate substrates is required for proper stability and/or function of the processed species. While both strands are cleaved at regular dsRNA target sites, the presence of internal loops or nucleotide bulges can limit cleavage to one strand, or inhibit cleavage without affecting RNase III binding (Calin-Jageman and Nicholson, 2003; Meng and Nicholson, 2008). However, neither helix length nor specific secondary structural elements is sufficient to identify the target site scissile bonds. As shown for Ec-RNase III (Pertzev and Nicholson, 2006), target sites are identified through specific sequence elements contained within two discrete double-helical elements, termed the proximal box (pb) and distal box (db). However, the mechanisms by which the two boxes are recognized by protein domains to establish the pathway of substrate binding and site-specific cleavage are not well understood.

The dsRBD is the primary energetic determinant of substrate binding, in addition to its selectivity for dsRNA. Thus, removal of one dsRBD from the Ec-RNase III reduces catalytic activity, mainly as a consequence of an increase in K_m (Sun *et al*., 2001), while removal of both domains essentially inactivates the enzyme under physiologically relevant conditions, due to a severely compromised ability to bind substrate (Meng and Nicholson, 2008). In addition to its importance in substrate binding energetics, it is also possible that the RNase III dsRBD participates in scissile bond selection through recognition of specific bp sequence. Structural studies of RNase III•dsRNA cocrystals identified specific regions of the dsRBD that contact substrate. One region, termed RBM1, encompasses a portion of the dsRBD α_1 helix and the N-terminal aspartic acid "cap". Conserved side chains in the RBM1 engage in a network of hydrogen bonds with sugar-phosphate and base functional groups within the proximal box of the bound substrate (Figure 7). Given the presence of multiple

A

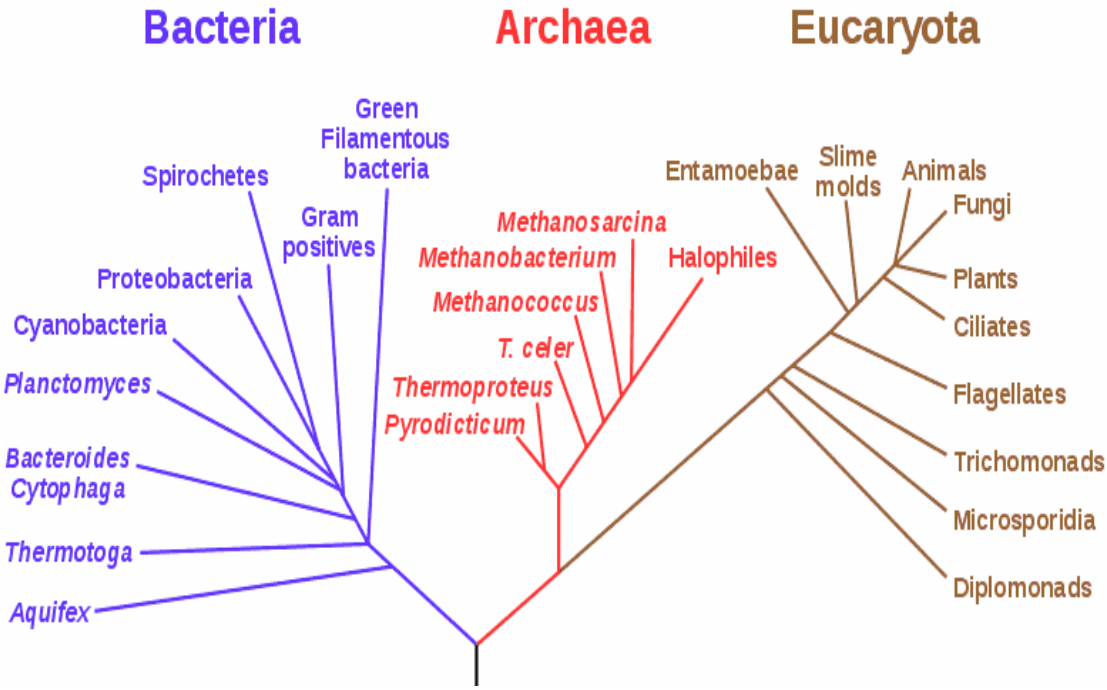
Bacteria
Archaea
Eucaryota
Green
Filamentous
bacteria
Spirochetes
Gram
positives
Proteobacteria
Cyanobacteria
Planctomyces
Bacteroides
Cytophaga
Thermotoga
Aquifex
Methanosarcina
Methanobacterium
Methanococcus
T. celer
Thermoproteus
Pyrodicticum
Halophiles
Entamoebae
Slime
molds
Animals
Fungi
Plants
Ciliates
Flagellates
Trichomonads
Microsporidia
Diplomonads

B

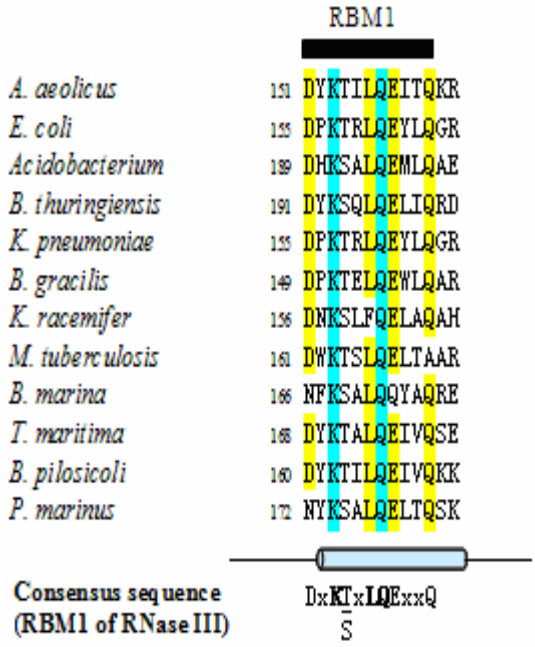
RBM1
A. aeolicus 151 DYKTILQEITQKR
E. coli 155 DPKTRLQEYLQGR
Acidobacterium 189 DHKSALQEMLQAE
B. thuringiensis 191 DYKSQLQELIQRD
K. pneumoniae 155 DPKTRLQEYLQGR
B. gracilis 149 DPKTELQEWLQAR
K. racemifer 156 DNKSLFQELAQAH
M. tuberculosis 161 DWKTSLQELTAAR
B. marina 166 NFKSALQQYAQRE
T. maritima 168 DYKTALQEIVQSE
B. pilosicoli 160 DYKTILQEIVQKK
P. marinus 172 NYKSALQELTQSK
Consensus sequence
(RBM1 of RNase III)
DxKTxLQExxQ
S

C

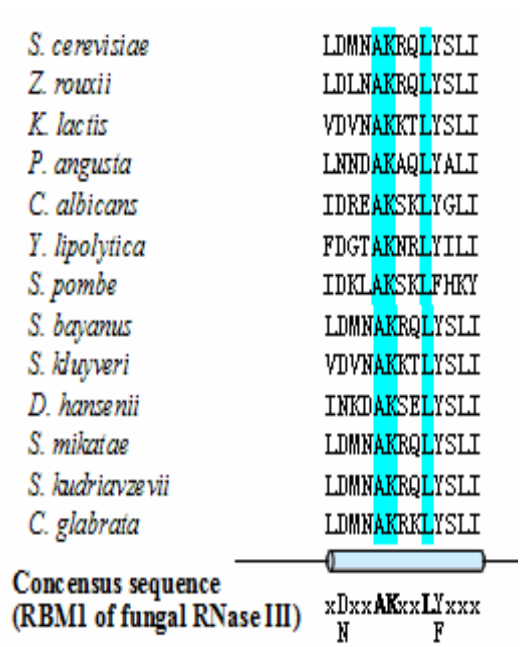
S. cerevisiae LDMNAKRQLYSLI
Z. rouxii LDLNAKRQLYSLI
K. lactis VDVNAKKTLYSLI
P. angusta LNNDAKAQLYALI
C. albicans IDREAKSKLYGLI
Y. lipolytica FDGTAKNRLYILI
S. pombe IDKLAKSKLFHKY
S. bayanus LDMNAKRQLYSLI
S. kluyveri VDVNAKKTLYSLI
D. hansenii INKDAKSELYSLI
S. mikatae LDMNAKRQLYSLI
S. kudriavzevii LDMNAKRQLYSLI
C. glabrata LDMNAKRKLYSLI
Concensus sequence
(RBM1 of fungal RNase III)
xDxxAKxxLYxxx
N F

D

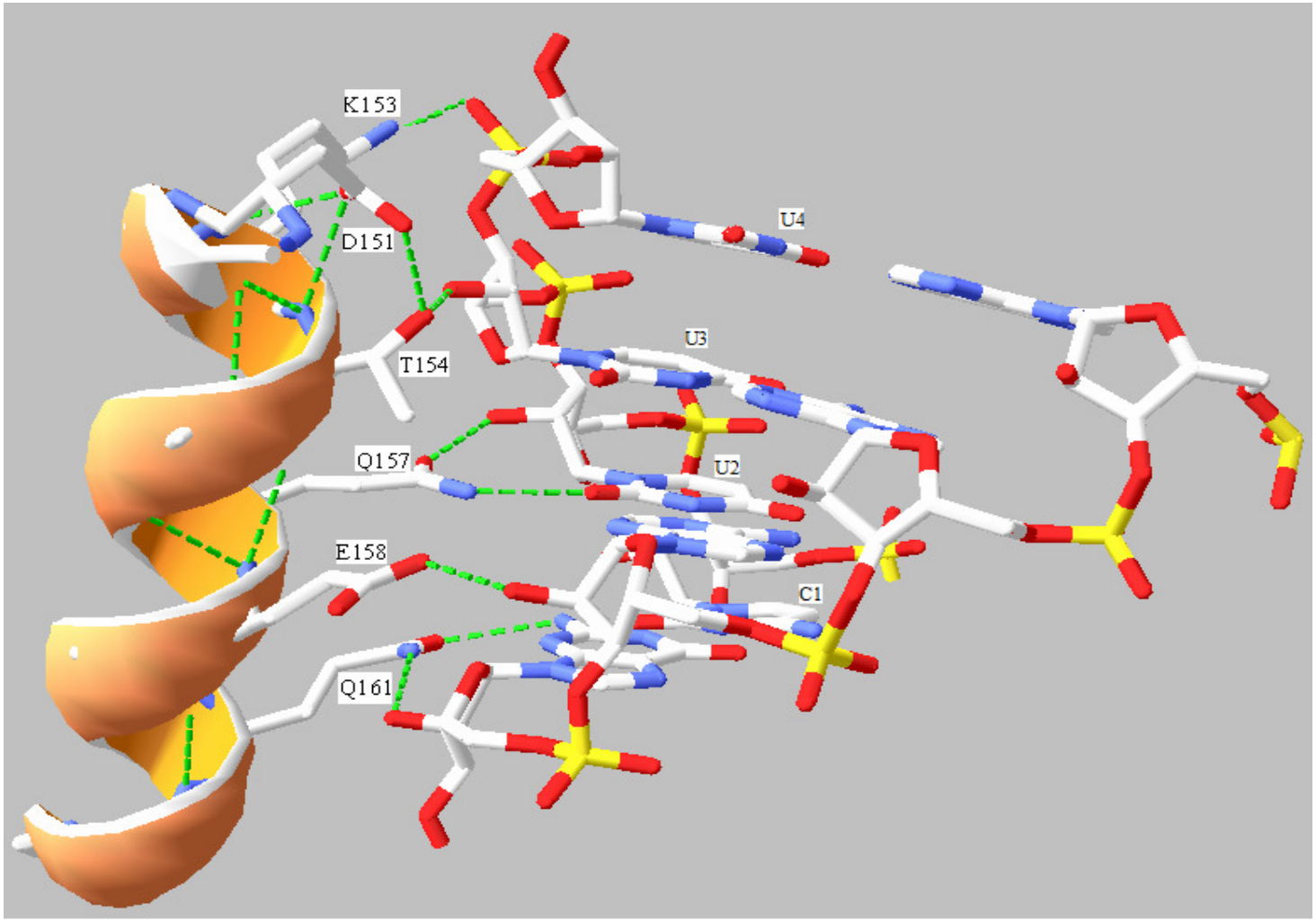

Figure 7 Alignment of dsRBD α_1 helix of selected RNase III polypeptides, and the interaction of the α_1 helix with dsRNA.

A. The phylogenetic tree of life (from Woese *et al*., 1990).

B. Alignment of the α_1 helices of bacterial RNases III. The selections are from each of the major branches of the bacterial phylogenetic tree (see panel A). The listed α_1 helices are from RNase III of Aquificales (*A. aeolicus*); Proteobacteria (*E. coli*); Gram positive (*B. thuringiensis, K. pneumoniae*); Bacteroidetes (*B. gracilis*); Green Filamentous bacteria (*K. racemifer*); Actinobacteria; (*M. tuberculosis*); Planctomycetes (*B. marina*) (the Q at position 173 is conserved among the family members); Thermotogales (*T. maritima*); Spirochetes (*B. pilosicoli*); and Cyanobacteria (*P. marinus*). Residues highlighted in cyan are the most highly conserved, and residues highlighted in yellow are less highly conserved. The α_1 helix is represented by the blue cylinder, and the RBM1 region (Gan *et al*., 2006) is indicated by the black bar. For Aa-RNase III, the α_1 helix spans Y152 to R163, and RBM1 includes D151 through Q161.

C. Alignment of the dsRBD α_1 helix of fungal Class 1 RNases III. The α_1 helix is indicated by the blue cylinder. For *S. cerevisiae*, the α_1 helix includes residues 366 to 378. Alignments were generated by ClustalW2 (http://www.ebi.ac.uk/Tools/msa/clustalw2/).

D. Interactions of the α_1 helix of Aa-RNase III dsRBD with dsRNA based on an Ec-RNase III reported by Zhang and Nicholson, 1997. The side chains of K153, T154, Q157 interact with U4, U3, and U2, respectively, on one strand, and the E158 and Q161 side chains interact with A2 and G1, respectively, on the other strand. Dotted lines in green indicate hydrogen bonds between dsRBD and dsRNA, and between residues in the dsRBD.

RBM1-pb hydrogen bonds, and base functional group involvement, it is possible that the RBM1 plays a direct role in cleavage site selection in addition to providing binding energy and conferral of dsRNA selectivity. This project provides an analysis of the catalytic activities of Aa-RNase III containing mutations in the RBM1, and the processing reactivities of proximal box sequence variants of a cognate substrate. Evidence is presented that the proximal box-RBM1 interaction contributes to target site selection.

A crystal structure of the most-heavily studied ortholog, Ec-RNase III, has not been reported. Although the Aa-RNase III crystal structure can be used as a reference when studying the mechanisms of dsRNA processing by Ec-RNase III, enzymatic studies of Aa-RNase III can provide essential biochemical insight. It has been shown, using variants of an asymmetric substrate of Ec-RNase III (R1.1. RNA) that the single primary cleavage site is associated with the 5 nt segment of the internal loop (Figure 8) (Calin-Jageman and Nicholson, 2003). An Ec-RNase III heterodimer-based analysis of R1.1 RNA cleavage indicates that the dsRBD preferentially supports the action of the catalytic site of the same subunit (Meng and Nicholson, 2008). Therefore, a combination of additional asymmetric substrates and RNase III heterodimers can lead to additional insight on the pathway for substrate recognition by RNase III.

1.4.2 Objectives

The objective of this project was to use Aa-RNase III, for which there is atomic-level structural information, to determine how RNase III recognizes itssubstrates and selects the target site. The first objective was to define the conditions that support optimal *in vitro* catalytic activity of purified enzyme. The second objective was to identify cognate substrates for Aa-RNase III and characterize their

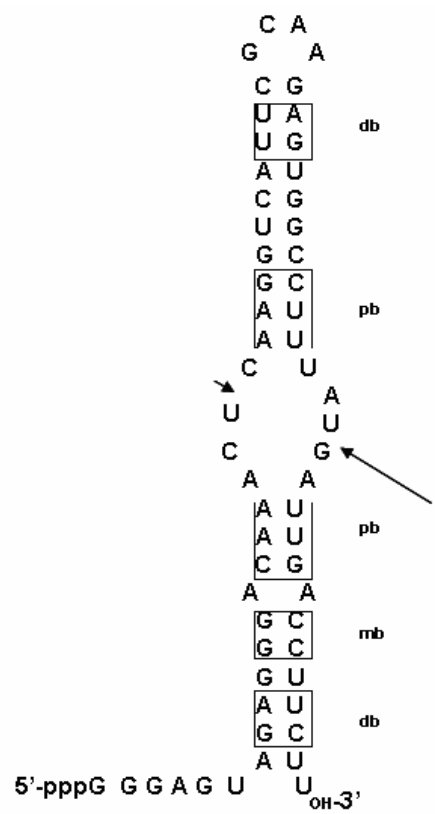

R1.1 RNA

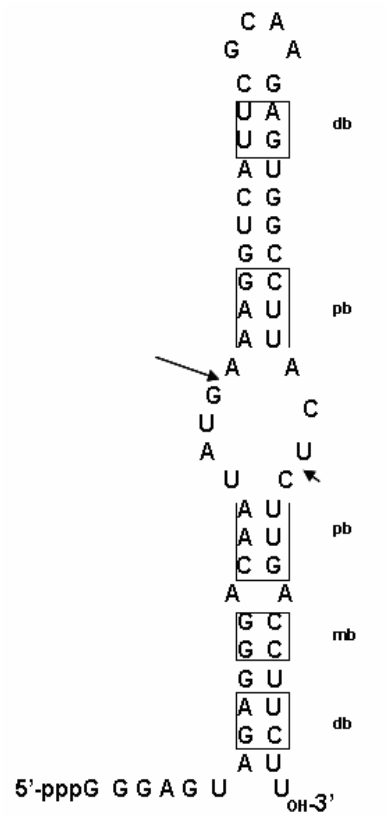

R1.1 [IL-Invert] RNA

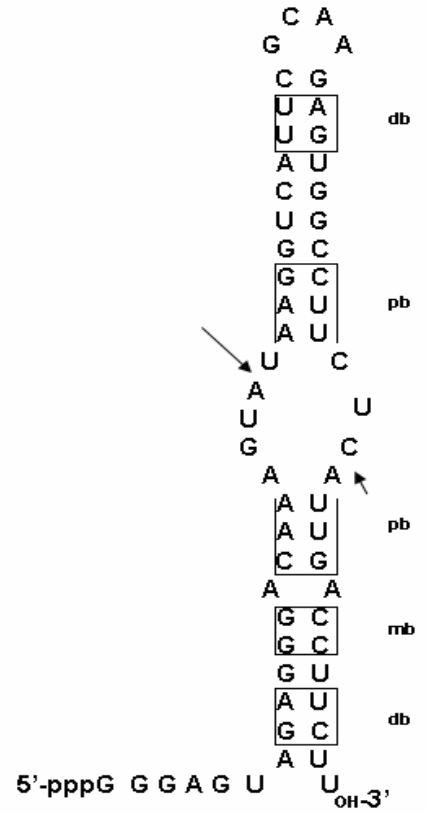

R1.1 [IL-Flip] RNA

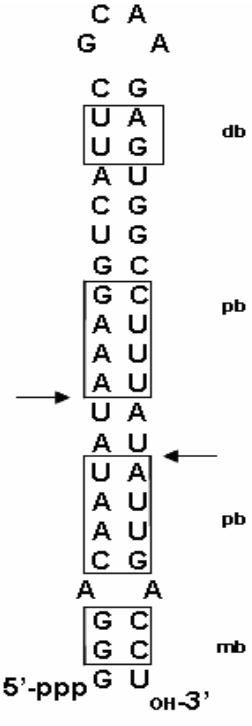

R1.1 [W C] RNA

Figure 8. *E. coli*-RNase III substrates.

Arrows indicate the Ec-RNase III cleavage sites. For R1.1 RNA, R1.1 internal loop (IL)-invert RNA (a vertical 180° rotation of IL), and R1.1 [IL-flip] RNA (a horizontal 180° flip of IL), the long arrow indicates the primary cleavage site, and the short arrow indicates the secondary cleavage site. The abbreviations db, mb, and pb refer to “distal box”, “middle box”, and “proximal box”, respectively (see also Results).

reactivity epitopes, including the identification of specific bp sequence elements that determine processing reactivity and selectivity. The third objective was to determine the role of the dsRBD in scissile bond selection by performing a mutational analysis of the conserved interactions of the RBM1 with substrate. The final objective was to further define and develop the cis-acting model for subunit involvement in substrate recognition by RNase III.

CHAPTER 2. MATERIALS AND METHODS

2.1. Materials and Reagents

2.1.1 Materials

Water was deionized and distilled. Chemicals and reagents were molecular biology grade and were purchased from Sigma-Aldrich (St. Louis, MO) or Fisher Scientific (Chicago, IL). Pipet tips and microcentrifuge tubes were purchased from ISC BioExpress (Kaysville, UT). Fuji Super RX film, Whatman 3M filter paper, and dialysis membranes (Spectra-Por CE, 3,500-5,000 MWCO and 8,000-10,000 MWCO) were purchased from Fisher Scientific. Amicon Centriprep units were purchased from Millipore (Billerica, MA). Glass electrophoresis plates, gel spacers, gel combs, and microelectroporation chambers were purchased from LabRepCo (Horsham, PA). Film developing solutions, nuclease P1, acrylamide, N,N'-methylene-bisacrylamide, and standardized aqueous 1M solutions of $MgCl_2$, $MnCl_2$, $CaCl_2$ were obtained from Sigma-Aldrich. Ni^{2+}-NTA affinity chromatography (His-Bind) resin and restriction grade thrombin were purchased from Novagen (Madison, WI). Calmodulin affinity chromatography resin and QuikChange Lightning site-directed mutagenesis kits were purchased from Stratagene (La Jolla, CA). Protein assay kits and protein MW standards (low MW range) for SDS-PAGE were purchased from Bio-Rad Laboratories (Hercules, CA). DH10B and BLR(DE3) electrocompetent *E. coli* cells, ultrapure buffer-saturated phenol, agarose, and low melting point agarose were obtained from Invitrogen (Carlsbad, CA). DNA ladder mix was purchased from MBI Fermentas (Amherst, NY). Plasmid mini- and midi-prep kits, QIAquick gel extraction kits, and QIAquick PCR purification kits were purchased from Qiagen (Valencia, CA). Ribonucleoside 5'-triphosphates (NTPs) were obtained from Amersham-Pharmacia Biotech (Piscataway, NJ). [α-^{32}P] UTP (3000 Ci/mmol), [γ-^{32}P] ATP (3000 Ci/mmol),

and [5'-^{32}P] cytidine 3',5'-bisphosphate (3000 Ci/mmol) were purchased from Perkin-Elmer (Boston, MA). *E. coli* bulk stripped tRNA was purchased from Sigma-Aldrich and was further purified by repeated phenol extraction followed by ethanol precipitation. T4 DNA ligase, T4 RNA ligase, Vent DNA polymerase, T4 polynucleotide kinase, and restriction enzymes (BamHI, NdeI, and BsrGI) were purchased from New England BioLabs (NEB) (Beverly, MA). Shrimp alkaline phosphatase and 2'-deoxyribonucleoside 5'-triphosphates (dNTPs) were obtained from Roche Molecular Biochemicals (Indianapolis, IN). T7 RNA polymerase was purified in-house as described (He *et al*., 1997). Superdex75 10/300GL gel filtration column and low molecular weight calibration kits for gel filtration columns were purchased from GE Healthcare (Piscataway, NJ). Oligodeoxynucleotide transcription templates and mutagenic oligodeoxynucleotides were synthesized by Invitrogen. Synthetic modified RNAs were purchased from Dharmacon-Thermo Scientific (Chicago, IL). The fully deprotected forms of the RNAs were further purified by denaturing gel electrophoresis, extracted using RNA/DNA extraction buffer (see below), ethanol precipitated, air dried, resuspended in TE buffer (pH 8.0), and stored at -20 °C.

2.1.2 Reagents

Tris buffers and salt solutions were autoclaved before use. Tris buffers were adjusted to the specified pH by concentrated HCl, and at the temperature corresponding to the reaction temperature. Polyacrylamide gel solutions were prepared in distilled and deionized water, filtered and stored in dark at 4 °C.

TBE Buffer (1×) (pH 8.0-8.2, adjustment not required)

89 mM	Tris base
89 mM	Boric acid
2 mM	EDTA (disodium salt)

TAE Buffer (1×) (pH 8.0-8.2, adjustment not required)

40 mM	Tris base
20 mM	Glacial acetic acid
1 mM	EDTA (disodium salt)

TE Buffer (1×)

10 mM	Tris•HCl (pH 8.0)
1 mM	EDTA (disodium salt)

RNA/DNA Extraction Buffer (adjusted to pH 8.0 with concentrated NH_4OH)

0.5 M	Ammonium acetate
10 mM	EDTA (disodium salt)

***E. coli* RNase III Dilution Buffer (1×)**

30 mM	Tris•HCl (pH 8.0)
0.1 mM	DTT
0.1 mM	EDTA (disodium salt)

T7 RNA Polymerase Transcription Buffer (1×) (for RNA synthesis)

40 mM	Tris•HCl (pH 8.0)
20 mM	$MgCl_2$
10 mM	Spermidine•3HCl
5 mM	DTT
0.01% (v/v)	Triton X-100
80 mg/ml	PEG 8000

Reaction Stop Mix / Denaturing Gel Loading Solution (2×)

89 mM	Tris base
89 mM	Boric acid
40 mM	EDTA (disodium salt)
10%(v/v)	Glycerol
7M	Urea
20% (w/v)	Sucrose (may be omitted)
0.04% (w/v)	Xylene cyanol
0.04% (w/v)	Bromophenol Blue

***E. coli* RNase III Substrate Cleavage Assay Buffer (1×)**

30 mM	Tris•HCl (pH 8.0)
160 mM	NaCl
10 mM	$MgCl_2$

***A. aeolicus* RNase III Substrate Cleavage Assay Buffer (1×)**

30 mM	Tris•HCl (pH 8.0)
50 mM	NaCl
10 mM	$MgCl_2$

***E. coli* RNase III Substrate Binding (Gel shift) Assay Buffer (1×)**

30 mM	Tris•HCl (pH 8.0)
0.1 mM	EDTA (disodium salt)
0.1 mM	DTT

10 µg/ml tRNA
5% (v/v) Glycerol
5 mM $CaCl_2$

***A. aeolicus* RNase III Substrate Binding (Gel shift) Assay Buffer (1×)**
30 mM Tris•HCl (pH 8.0)
250 mM Potassium Glutamate
5 mM Spermidine
0.1 mM EDTA (disodium salt)
0.1 mM DTT
5% (v/v) Glycerol
5 mM $CaCl_2$

30% Acrylamide Stock Solution (36.5:1 acrylamide: bisacrylamide)
(used for denaturing polyacrylamide gels)
29.2% (w/v) Acrylamide
0.8% (w/v) N,N'-methylene-bisacrylamide

30% Acrylamide Stock Solution (80:1 acrylamide: bisacrylamide)
(used for non-denaturing polyacrylamide gels)
29.63% (w/v) Acrylamide
0.375% (w/v) N,N'-methylene-bisacrylamide

15% Polyacrylamide Gel / 7M urea (used for substrate cleavage assays)
21 g Urea
5 ml 10×TBE
15 ml 30% Acrylamide Stock Solution (36.5:1)
0.5 ml 10% (w/v) Ammonium persulfate
0.05 ml TEMED
(50 ml total volume)

8% Non-denaturing Polyacrylamide Gel (for gel shift assays involving Ec-RNase III)
13.33 ml 30% Acrylamide Stock Solution (80:1)
0.25 ml 1M $CaCl_2$
2.5 ml 10×TBE
0.5 ml 10% (w/v) Ammonium persulfate
0.05 ml TEMED
(50 ml total volume)

8% Non-denaturing Polyacrylamide Gel (for gel shift assays involving Aa-RNase III)
13.33 ml 30% Acrylamide Stock Solution (80:1)
0.25 ml 1M $CaCl_2$
2.5 ml 10×TBE
0.5 ml 10% (w/v) Ammonium persulfate
0.05 ml TEMED
2.5% (v/v) Glycerol
(50 ml total volume)

SDS Gel Sample Buffer (1×)

50 mM	Tris•HCl (pH 6.8)
20 mM	EDTA (disodium salt)
10% (v/v)	Glycerol
1% (v/v)	2-mercaptoethanol
1% (w/v)	SDS

SDS Gel Loading Buffer (2×)

100 mM	Tris•HCl (pH 6.8)
4% (w/v)	SDS
0.2% (w/v)	Bromophenol Blue
20% (v/v)	Glycerol
200 mM	DTT (added separately each time before use)

12% SDS-PAGE Separation Gel

3.8 ml	Tris•HCl (1.5M, pH 8.8)
0.15 ml	10% (w/v) SDS
6.0 ml	30% Acrylamide Stock Solution (36.5:1)
0.15 ml	10% (w/v) Ammonium persulfate
0.006 ml	TEMED

(15 ml total volume)

Stacking Gel

1.25 ml	Tris•HCl (1M, pH 6.8)
0.1 ml	10% (w/v) SDS
6.0 ml	30% Acrylamide Stock Solution (36.5:1)
0.1 ml	10% (w/v) Ammonium persulfate
0.01 ml	TEMED

(10 ml total volume)

SDS-PAGE Electrophoresis Buffer (5×) (pH 8.3; adjustment not required)

72g	Glycine
15g	Tris base
5g	SDS

(1000 ml total volume)

Gel Staining Buffer

0.1% (w/v)	Coomassie Brilliant Blue R-250
45% (v/v)	Methanol
10% (v/v)	Glacial acetic acid

Gel Destaining Buffer

45% (v/v)	Methanol
10% (v/v)	Glacial acetic acid

Ni^{2+}-NTA column Binding Buffer

20 mM	Tris•HCl (pH 8.0)
500 mM	NaCl
5 mM	Imidazole

Ni^{2+}-NTA column Washing Buffer
20 mM Tris•HCl (pH 8.0)
500 mM NaCl
60 mM Imidazole

Ni^{2+}-NTA column Elution Buffer
20 mM Tris•HCl (pH 8.0)
1 M NaCl
400 mM Imidazole

Ni^{2+}-NTA column Dialysis Buffer (Buffer A)
60 mM Tris•HCl (pH 8.0)
1 mM NaCl
400 mM Imidazole

Ni^{2+}-NTA column Dialysis Buffer (or Ca^{2+}-CaM-column Dialysis Buffer, Buffer B)
60 mM Tris•HCl (pH 8.0)
1 M NaCl
1 mM EDTA (disodium salt)
1 mM DTT

Ca^{2+}-CaM column Protein Dilution Buffer (To be used at a ratio of one volume of sample eluted from Ni^{2+}-NTA column to two volumes of Dilution Buffer)
65 mM Tris•HCl (pH 8.0)
3 mM $CaCl_2$

Ca^{2+}-CaM column Binding Buffer
50 mM Tris•HCl (pH 8.0)
333 mM NaCl
2 mM $CaCl_2$

Ca^{2+}-CaM column Elution Buffer
50 mM Tris•HCl (pH 8.0)
1 M NaCl
2 mM EDTA (disodium salt)

Dialysis Buffer for fast protein liquid chromatography (FPLC) (Buffer C)
60 mM Tris•HCl (pH 7.5)
150 mM NaCl

2.2 Methods

Specific mutations in selected regions of the wild-type *A. aeolicus* (Aa) or *E. coli* (Ec) RNase III (*rnc*) gene were introduced to generate (i) single-site mutations in the RBM1 of Aa-RNase III; (ii) a truncated form of Aa-RNase III that lacks the dsRBD;

(iii) Ec-RNase III mutant heterodimers; and (iv) Aa-Ec RNase III chimeras (Table 2). Also constructed were asymmetric RNA substrates (Figure 8) for Ec-RNase III, derived from R1.1 RNA (Dunn and Studier, 1983; Saito and Richardson, 1981), as well as two cognate substrates of Aa-RNase III: Aa-16S[hp] RNA and Aa-23S[hp] RNA (Figure 6) (see also below). Optimal conditions for substrate cleavage were determined, which included temperature, pH, Na^+ and Mg^{2+} ion concentrations. Aa-RNase III cleavage sites were determined by gel electrophoresis-based assays that used reference ladders generated by alkaline hydrolysis, or P1 nuclease digestion of 5'- or 3'- ^{32}P- labeled RNAs. The catalytic actions of Aa- and Ec-RNase III mutants were compared with the original ("wild-type", WT) Aa- RNase III or Ec-RNase III by protein titration and time-course cleavage assays. Gel mobility shift assays were performed to assess whether target site selectivity and processing efficiency is a function of specific complex formation and stability.

2.2.1 Gene cloning

RNase III genes were cloned into a T7 expression plasmid, and *rnc* gene mutations were generated using the recombinant plasmids as templates. Specifically, the Aa or Ec *rnc* genes was cloned into plasmid pET-15b (Figure 9) or recombinant pACYC184 (Figure 10; Meng *et al*., 2008), using the NdeI and BamHI sites. Gene cloning included target gene amplification, purification, restriction enzyme digestion, ligation, and sequence verification.

2.2.1.1 Target gene amplification

rnc gene amplification

The Aa and Ec *rnc* genes were amplified from genomic DNA by PCR, using a 5' (forward) primer and 3' (reverse) primer (Table 1). The 5' primer contained an NdeI site, and the 3' primer contained a BamHI site. The reaction (100 μl) contained

pET-15b sequence landmarks	
T7 promoter	463-479
T7 transcription start	452
His•Tag coding sequence	362-380
Multiple cloning sites	
(*Nde* I - *Bam*H I)	319-335
T7 terminator	213-259
lacI coding sequence	(866-1945)
pBR322 origin	3882
bla coding sequence	4643-5500

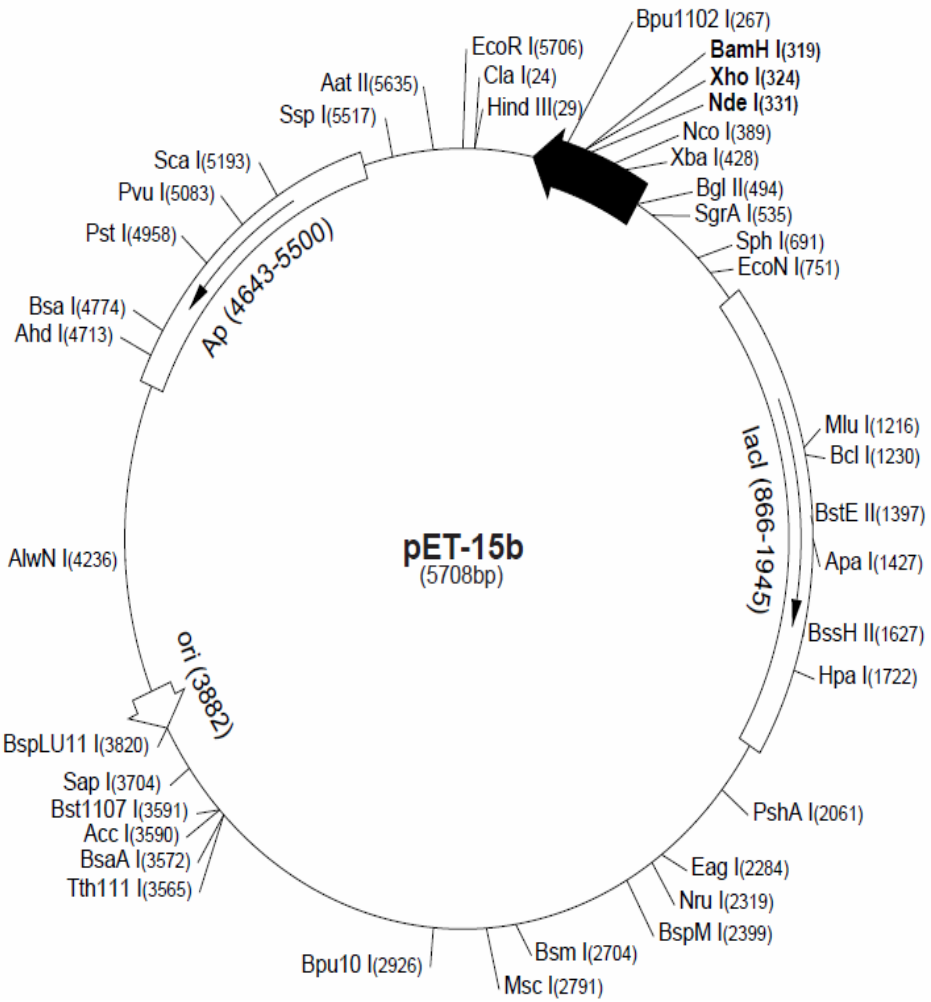

Figure 9. Plasmid pET-15b (Novagen).

The pET-15b plasmid encodes an N-terminal $(His)_6$-tag (~2 kDa) sequence, followed by a thrombin cleavage site, and also contains BamHI and NdeI sites for cloning purposes. The vector also carries a T7 promoter, under lacI control, a T7 transcription terminator sequence, and an ampicillin resistance gene. (http://depts.washington.edu/bakerpg/plasmid_maps/pet15bm.pdf).

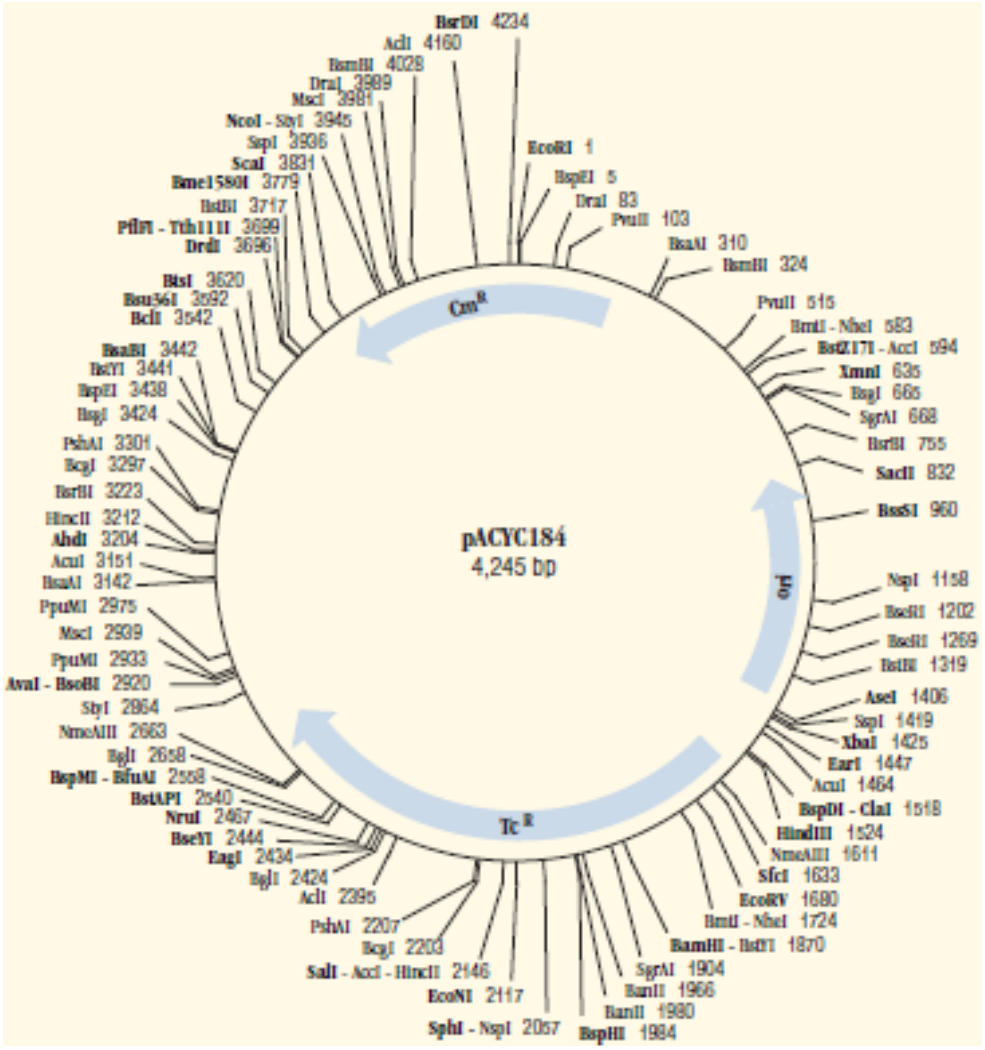
pACYC184
4,245 bp
Cm R
Tc R
Ori
BsrDI 4234
AclI 4160
BamHI 4028
DraI 3989
MscI 3981
NcoI - StyI 3945
SspI 3936
ScaI 3831
Bme1580I 3779
HstBI 3717
PflFI - Tth111 II 3699
DrdI 3696
BlsI 3620
Bsu36I 3592
BclI 3542
BsaBI 3442
HstYI 3441
BspEI 3438
BsgI 3424
PshAI 3301
BcgI 3297
BsrBI 3223
HincII 3212
AhdI 3204
AcuI 3151
BsaAI 3142
PpuMI 2975
MscI 2939
PpuMI 2933
AvaI - BsoBI 2920
StyI 2864
NmeAIII 2663
BglI 2658
BspMI - BfuAI 2558
BstAPI 2540
NruI 2467
BseYI 2444
EagI 2434
BglI 2424
AclI 2395
PshAI 2207
BcgI 2203
SalI - AccI - HincII 2146
EcoNI 2117
SphI - NspI 2057
BspHI 1984
BanII 1980
SgrAI 1904
BanII 1966
BamHI - HstYI 1870
BmtI - NheI 1724
EcoRV 1680
SfcI 1633
NmeAIII 1611
HindIII 1524
BspDI - ClaI 1518
AcuI 1464
EarI 1447
XbaI 1425
SspI 1419
AseI 1406
BstHI 1319
BseRI 1269
BseRI 1202
NspI 1158
BsaSI 960
SacII 832
HsrBI 755
SgrAI 668
BsgI 665
XmnI 635
BstZ17I - AccI 594
BmtI - NheI 583
PvuII 515
BsaAI 310
BamHI 324
PvuII 103
DraI 83
BspEI 5
EcoRI 1

Figure 10. Plasmid pACYC184 (http://www.neb.com/nebecomm/tech_reference/restriction_enzymes/maps/pACYC184_map.pdf).

The pACYC184 cloning vector (obtainable from New England Biolabs) contains the p15A origin of replication, and confers resistance both chloramphenicol (Cm) and tetracycline (Tc). The recombinant pACYC184-*rnc* plasmid contains the Ec-*rnc* gene, which was cloned into the BamHI and NdeI sites by disrupting the Tc^R gene (Meng and Nicholson, 2008)

1×PCR buffer (supplied by NEB), 2 mM $MgSO_4$, 100 ng DNA template, the four dNTPs (10 mM each), 50 pmol 5'-primer, 50 pmol 3'-primer, and 1 unit of Vent DNA polymerase. The PCR parameters were as follows. The initial template denaturing temperature was 94 °C (1 minute). This was followed by 30 cycles consisting of 94 °C for 30 seconds, (Tm-5) °C for 30 seconds (68.6 °C for Aa-*rnc*, and 70 °C for Ec-*rnc*; the lower of the two primers' Tm values was used), and 72 °C for 1 minute. The final extension temperature was 72 °C for 7 minutes. The PCR products were analyzed by electrophoresing an aliquot (5 µl) of the reaction in a 1% agarose gel (1×TBE buffer, 35-50 V, 1-2 hours), followed by staining in 0.5 µg/ml ethidium bromide (EB) for 10 minutes. Destained gel images (Figure 11A) were captured using an EpiChem Darkroom system (UVP, LLC), and using Labwork 4.0 software.

The PCR products were purified by electrophoresis in a 0.7% or 1.0% low-melting point agarose gel (1×TAE buffer, 4 °C, 35-50V, 1-2 hours). The gel was stained in 0.5 µg/ml EB for 10 minutes. Low-energy UV light (>320 nM) was used to locate the gel region containing the desired DNA, which was excised using a clean scalpel. The UV light exposure was kept to a minimum, to avoid damage to the DNA. The DNA was purified from the gel slice by the QIAquick gel extraction kit, according to the supplier's instructions.

2.2.1.2 Restriction enzyme digestion, DNA ligation, and E. coli cell electroporation

The *E. coli* pET-15b or pACYC184-*rnc* plasmid, and the gel-purified PCR products containing the Aa or Ec *rnc* gene were individually digested first by NdeI for 1 hour, followed by BamHI for 1 hour at 37 °C in 1× NEB Buffer 4 (supplied by NEB). The reactions contained 1 µg of DNA or plasmid, 20 units each of NdeI or BamHI, followed by heat inactivation (65 °C, 20 minutes). The digested products

A

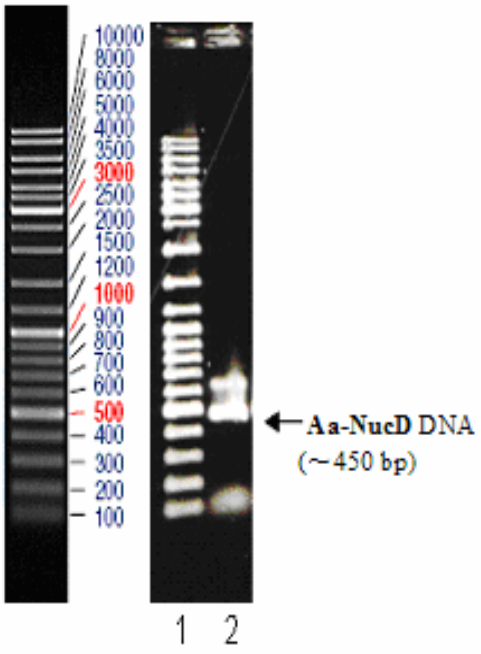
10000
8000
6000
5000
4000
3500
3000
2500
2000
1500
1200
1000
900
800
700
600
500
400
300
200
100
Aa-NucD DNA
(~450 bp)
1 2

B

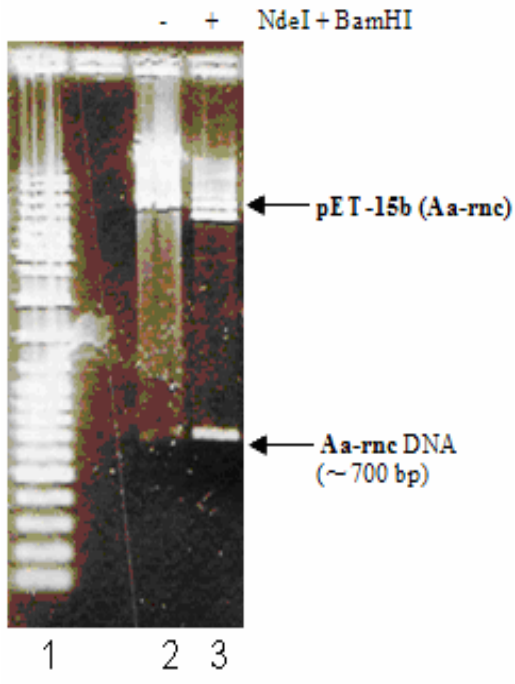
- + NdeI + BamHI
pET-15b (Aa-rnc)
Aa-rnc DNA
(~700 bp)
1 2 3

Figure 11. Recombinant plasmid construction.

A. Left, adapted DNA ladder image (http://www.fermentas.com/en/products/all/dna-electrophoresis/generuler-dna-ladders/sm0333-generuler-mix, unit in bp). Right, PCR product of Aa-*rnc* NucD (with NdeI and BamHI cleavage sites). Lane 1, 100 bp DNA ladder. Lane 2, PCR product. The arrow indicates the amplified DNA, migrating between the 400 and 500 bp marker.

B. Cleavage of the recombinant pET-15b plasmid containing the Aa-*rnc* gene by NdeI and BamHI. Lane 1, 100 bp DNA ladder. Lane 2, plasmid incubated in buffer without NdeI and BamHI. Lane 3, plasmid after NdeI and BamHI cleavage. The arrow indicates the full length Aa-*rnc* gene, mapping at ～700 bp.

(Figure 11B) were gel purified by low melting point agarose gel electrophoresis (note: prior to electrophoresis the digested vector was also treated with alkaline phosphatase, to minimize self-ligation). Ligation reactions (20 µl) contained ~0.02 µg of digested pET-15b or pACYC184 vector and ~0.18 µg Aa or Ec *rnc* DNA fragment, 1×T4 DNA ligase buffer (supplied by NEB) supplemented with ATP (1 mM) and 400 units of T4 DNA ligase. The reaction was incubated at 4 °C for 48 hours, and at 20 °C for an additional 24 hours, followed by heat inactivation (65 °C, 20 minutes).

Transformation of ligation reactions into *E. coli* cells was performed on ice, using pre-cooled microelectroporation chambers. An aliquot of the ligation reaction (1-4 µl) was electroporated into electrocompetent *E. coli* DH10B cells (Invitrogen, 15-20 µl). *E. coli* DH10B is derived from *E. coli* DH5, which is RecA- and exonuclease-deficient (Grant *et al*., 1990), and is preferred for plasmid purification since it provides plasmid that gives cleaner sequencing results. The *E. coli* Cell-porator pulser unit (Life Technologies) was used at the medium voltage setting (2.47 kV). After electroporation, cells were transferred into 1 ml LB medium and incubated at 37 °C (250 rpm shaker-incubator) for 1 hour. Cells were collected by low-speed centrifugation (6,000 rpm, 2 minutes), resuspended in 50 µl LB medium, and plated on LB Agar plates containing either ampicillin (Am, 100 µg /ml, for plasmid pET-15b-*rnc* containing cells) or chloramphenicol (Cm, 40 µg/ml, for plasmid pACYC184-*rnc* containing cells), followed by overnight incubation at 37°C. A single colony was picked and grown in 5 ml LB medium containing Am (100 µg/ml) or Cm (40 µg/ml) at 37 °C overnight. Cells were collected by low-speed centrifugation (6,000 rpm, 2 minutes), in preparation for plasmid purification (see below).

Electrocompetent cell preparation

E. coli cells [DH10B for plasmid preparation, BL21(DE3)*rnc*105*rec*A (laboratory stock) for RNase III homodimer preparation, and BLR(DE3) for RNase III heterodimer preparation] from -80°C freezer stocks were streaked on an LB agar plate (without antibiotic) followed by overnight incubation at 37 °C. A single colony was picked and grown in 5 ml LB medium (shaking at 250 rpm) at 37 °C overnight. The culture was diluted into 200-400 ml LB medium (without antibiotic) and grown at 37 °C (shaking at 250 rpm) to an optical density (OD) of 0.4-0.6 at 595 nM (0.4 corresponds to ~10^8-10^9 cells per ml culture), as measured by a Novaspec Plus visible spectrophotometer (GE Healthcare). Cells were harvested by low-speed centrifugation (6,000 rpm at 4 °C for 20 minutes in a Sorvall SLA-1500 rotor), then resuspended and washed twice with 50 ml of 10% (v/v) 4 °C glycerol, followed by a low-speed centrifugation (6,000 rpm at 4 °C for 20 minutes). Cell pellets were resuspended gently at 4 °C in 1-2 ml of 10% (v/v) glycerol, and divided into small aliquots (50-100 µl) in 0.65 ml microcentrifuge tubes at 4 °C, followed by a snap-freezing (5 minutes) in an ethanol/ dry ice bath before storage at -80 °C.

2.2.1.3 Target gene verification

Plasmids were purified from DH10B cell using a Qiagen plasmid mini kit according to the supplier's instructions. Recombinant plasmids were sequenced by DNA Sequencing Facility at University of Pennsylvania (http://www.med.upenn.edu/genetics/core-facs/dna-seq/) or by GeneWiz (http://www.genewiz.com/public/DNA-sequencing-services.aspx).

2.2.1.4 Site-directed mutagenesis

The sequence-confirmed Aa-and Ec-*rnc* genes, cloned in pET-15b or pACYC184, provided templates for site-directed mutagenesis using the QuikChange

Lightning site-directed mutagenesis kit. The Tm for each mutagenic oligonucleotide was calculated using Equation 1. The optimum primers should have a minimum GC content of 40%, between 25 and 45 bases in length, with a Tm of above 75°C.

Equation 1 $Tm=81.5+0.41\times(\%GC)-675/N-\%mismatch$

[where N= length of primer (nt), and %GC=(number of GC/length of primer) ×100]

2.2.1.5 Creation of truncated forms of Aa-RNase III and Aa-Ec RNase III chimeras

The truncated forms of RNase III included Aa-NucD, Ec-NucD, and Ec-NucD[E117A]. The truncated forms contain the N-terminal nuclease domain (NucD), but lack the C-terminal dsRBD. The Aa-Ec RNase III chimeras included $NucD^{Aa}$-$dsRBD^{Ec}$ and $NucD^{Ec}$-$dsRBD^{Aa}$, and were constructed by restriction fragment exchange using the NdeI or BamHI cleavage site at the 5' and 3' end, respectively, and an engineered BsrGI site within the linker region. The recombinant genes encoding the RNase III mutants listed above were prepared and purified as described in sections 2.2.1.1 and 2.2.1.2, using the primers listed in Table 1.

2.2.2 Protein overexpression and purification

RNase III homodimers were produced in *E. coli* BL21(DE3)*rnc*105*rec*A cells. The DE3 defective lambda lysogen encodes T7 RNA polymerase under control of the IPTG-inducible *lac* promoter. The rnc105 allele carries an inactivating mutation (G44D) (Nashimoto and Uchida, 1985) in the chromosomal RNase III gene, while the *rec*A allele serves to suppress plasmid recombination (Meng *et al*., 2008). RNase III heterodimers were produced in *E. coli* BLR(DE3) cells. BLR(DE3) is a derivative of BL21(DE3) that improves plasmid monomer yields, and does not express antibiotic

resistance, which allows it to serve as an expression host for two plasmids that carry separate antibiotic resistance markers (Meng and Nicholson, 2008).

2.2.2.1 Protein overexpression

For RNase III homodimer production, BL21(DE3)*rnc*105*rec*A cells were transformed with pET-15b-*rnc* [containing either the *E. coli rnc* gene (wild-type or mutant) or the *A. aeolicus rnc* gene (wild-type or mutant); the $NucD^{Aa}$-$dsRBD^{Ec}$ chimera gene; or the $NucD^{Ec}$-$dsRBD^{Aa}$ chimera gene] by electroporation at the low voltage (1.47 kV) setting. For RNase III heterodimer production, BLR(DE3) cells were co-transformed with pACYC184-*rnc* [containing either the *E. coli rnc* gene (wild-type or mutant) or the *A. aeolicus rnc* gene (wild-type or mutant)] and pET-15b-*rnc* [containing either the *E. coli rnc* gene (wild-type or mutant) or the *A. aeolicus rnc* gene (wild-type or mutant)] by electroporation at the low voltage (1.47 kV) setting. Transformants were plated on LB-agar plates containing ampicillin and chloramphenicol (40 μg/ml each). A single colony was picked and grown in 5 ml LB medium overnight at 37 °C containing Am (100 μg/ml) for homodimer expression, or Am and Cm (40 μg/ml each) for heterodimer expression. The culture was diluted into 200 ml LB medium containing Am and Cm, and incubation continued with aeration at 37°C. IPTG (1 mM) was added at an optical density of 0.4 (595 nm), and incubation continued with aeration for 4 hours. Cells were collected by low-speed centrifugation (4000 xg, 4 °C, 20 minutes in a Sorvall SLA-1500 rotor), and stored at -20 °C. An aliquot (1 ml) was removed immediately before IPTG addition, and compared by SDS-PAGE analysis with a second aliquot (1ml) taken 4 hours after IPTG addition. 12% SDS-PAGE was performed at 150 V until the bromophenol blue dye marker reached the bottom of the gel. The gel was stained using Coomassie Brilliant Blue, then destained as described in 2.1.2.

2.2.2.2 Protein purification

Two types of affinity chromatography columns were used for protein purification, according to the affinity tag affixed to the proteins: a Ni^{2+}-NTA column was used for His-tagged proteins, and a Ca^{2+}-Calmodulin (CaM) column was used for Calmodulin-binding-peptide (CBP)-tagged proteins.

Ni^{2+}-NTA affinity chromatography

E. coli cells obtained from a 200 ml culture were resuspended in 30 ml Ni^{2+}-column binding buffer and subjected to repeated sonication on ice. The ultrasonic cell disrupter (Misonix Inc) was used at setting 5, with 15 second bursts, followed by a 1 minute pause. The steps were repeated 20 times, or until the solution became viscous and without precipitant. The sonicate was clarified by low-speed centrifugation (4000 xg, 4 °C, 20 minutes) in a Sorvall SLA-1500 rotor. The supernatant was applied to the prepared purification column (see below). The pellet obtained from centrifugation was stored at -20 °C for future protein purification from inclusion bodies.

A Ni^{2+}-NTA column (His Bind resin, Novagen) was used for the first chromatographic step. A column containing ~1.5 ml resin was used to purify protein from a 200 ml culture. The column was prepared in a 20 ml disposable plastic pipette, with a small amount of sterile glass wool to support the resin; a short piece of Tygon tubing to direct the eluent; and a screw clamp to control the flow rate. The purification was performed in a 4-5 °C cabinet refrigerator. Prior to loading the sample, the resin was washed with 10 ml Ni^{2+}-NTA column binding buffer, then charged with 10 ml of 50 mM $NiSO_4$. The clarified supernatant of a sonicated cell pellet (30 ml) (see above) was loaded onto the column at a rate of ~1 ml/minute, followed by washing with 30 ml Ni^{2+}-NTA column binding buffer, followed by 20 ml Ni^{2+}-NTA column washing

buffer, or until no protein could be visualized by protein assay (Bio-Rad Laboratories). In this assay a blue color is generated in the presence of protein, reflecting a shift in the absorbance of the Coomassie Brilliant Blue R-250 dye upon binding to arginine or hydrophobic amino acid residues (Reinser *et al*., 1975). The target protein was eluted with 10×1 ml Ni^{2+}-NTA column elution buffer, and was present mainly in the first five eluted volumes.

If the protein contained only the $(His)_6$ tag, it was subjected to two serial dialyses at 4 °C using Spectra-Por CE dialysis tubing (10,000 MWCO). The first dialysis step used Ni^{2+}-NTA column dialysis buffer A (twice for two hours each), followed by an extensive overnight dialysis against one liter of Ni^{2+}-NTA column dialysis buffer B. Alternatively, dialysis buffer C was used for FPLC gel filtration analysis, or 50 mM NaH_2PO_4 for CD spectroscopic analysis. Proteins obtained from the latter two steps were kept at 4 °C without addition of glycerol, and were analyzed within 1 week of their preparation. For enzyme kinetic studies, the purified protein was stored at -20 °C in 50% (v/v) glycerol, 0.5 M NaCl, 30 mM Tris HCl (pH 8.0), 0.5 mM EDTA and 0.5 mM DTT. Protein concentrations were determined by the Bradford assay (Bio-Rad Laboratories) using bovine serum albumin (BSA) as a standard.

Ca^{2+}-CaM affinity chromatography

If the protein contained the $(His)_6$-tag and the CaM-tag as a heterodimer, it was further purified by Ca^{2+}-CaM column chromatography. Eluates from the Ni^{2+}-NTA column were diluted in Ca^{2+}-CaM column protein dilution buffer (1 volume sample: 2 volumes of buffer), and loaded onto a Ca^{2+}-CaM affinity column. The column was prepared using 1 ml CaM binding resin, and washed with 10 ml Ca^{2+}-CaM column binding buffer prior to adding the diluted sample. The protein was loaded at a rate of 1 ml/minute, and the column was washed with 20 ml of Ca^{2+}-CaM column binding

buffer, or until no protein could be visualized by protein assay. The protein was eluted using 10×1 ml of Ca^{2+}-CaM column elution buffer, and was contained mainly in the first five eluted volumes. The protein-containing eluent fractions were combined and dialyzed (using Spectra-Por CE dialysis tubing, 10,000 MWCO) against one liter of Ca^{2+}-CaM column dialysis buffer at 4 °C overnight. The purified protein was then stored at -20 °C in 50% (v/v) glycerol, 0.5 M NaCl, 30 mM Tris HCl (pH 8.0), 0.5 mM EDTA and 0.5 mM DTT. Protein concentrations were determined by the Bradford assay (Bio-Rad Laboratories) using bovine serum albumin (BSA) as a standard.

2.2.2.3 Thrombin-catalyzed removal of the $(His)_6$-tag

$(His)_6$-Aa-RNase III (~1 mg) was treated with recombinant bovine thrombin (Novagen, 20 units) for 48 h at 20°C in a 2 ml volume containing 150 mM NaCl and 20 mM Tris-HCl, pH 8.4, then purified by gel filtration on a Superdex75 10/300GL column using an Akta FPLC Explorer system (GE Healthcare). The buffer contained 150 mM NaCl and 60 mM Tris-HCl (pH 7.5). Removal of the $(His)_6$ tag was verified by SDS-PAGE (Figure 12). Thrombin cleavage leaves three additional amino acids (glycine, serine and histidine) on the Aa-RNase III N-terminus. The enzyme preparation was concentrated using an Amicon Centriprep unit (3,000 MWCO), then stored at -20 °C in 50% (v/v) glycerol, 0.5 M NaCl, 30 mM Tris HCl (pH 8.0), 0.5 mM EDTA and 0.5 mM DTT.

2.2.3 Enzyme assays

2.2.3.1 Substrate synthesis and purification

Purification of DNA and RNA oligonucleotides

Deprotected synthetic DNAs (Invitrogen, listed in Table 1) or RNAs (ThermoFisher Scientific, shown in Figure 28) were obtained in desiccated form, and

were resuspended in 200 µl TE buffer. An aliquot (50 µl) was mixed with an equal volume of denaturing gel loading solution and electrophoresed (25 V/cm) at room temperature in a 15% denaturing polyacrylamide gel (1.5 mm thick) containing 7 M urea in 1×TBE buffer. The oligodeoxynucleotides were visualized by UV shadowing (Hassur and Whitlock, 1974), which uses shortwave UV light (254 nm) and a fluor-coated TLC plate to locate the nucleic acid band in the gel, which appears as a dark band against the green fluorescent TLC plate background. Gel bands containing the DNA or RNA oligos were excised with a clean scalpel. Gel slices were crushed using 1 ml pipet tips into small (<1 mm) pieces and soaked in 0.5 ml RNA/DNA extraction buffer at room temperature overnight. After centrifugation at 14,000 rpm for 10 minutes, the supernatant was transferred to a clean tube and the DNA/RNA oligos were precipitated by adding 1/10 volume of 3 M NaOAc (pH 5.2) and 2.5 volumes of 95% ethanol. The sample was kept at -20 °C overnight, or -80 °C for at least four hours, followed by centrifugation at 14,000 rpm for 30 minutes. DNA/RNA pellets were washed with 70% ethanol at room temperature, and centrifuged at 14,000 rpm for 15 minutes. The pellets were dried using a Vacufuge Concentrator (Eppendorf) and resuspended in TE buffer (50 µl). The samples were stored at -20 °C. The DNA concentration was determined by a Beckman DU530 UV spectrophotometer (Beckman Coulter), and molar concentrations were calculated using Equation 2.

Equation 2

$$\text{Molarity}\ (\mu M) = \frac{OD_{260}(1\ \text{cm path length}) \times \text{dilution factor} \times 1000}{\text{Millimolar Extinction Coefficient}}$$

The millimolar extinction coefficients for oligodeoxynucleotides were obtained from the supplier's product manual (Invitrogen). Millimolar extinction coefficients for

nucleotides within long (>30 bases) oligodeoxynucleotides in units of OD_{260}•L/μmol•cm can be determined by the base composition: A, 15.4; C, 7.4; G, 11.5; T, 8.7. Millimolar extinction coefficients for nucleotides within long (>30 bases) RNA oligonucleotides (OD_{260}260•l/μmol•cm) is: A, 15.4; C, 7.2; G, 11.5; U, 9.9. The purity of nucleotides was assessed by OD_{260}/OD_{280}. The millimolar Extinction Coefficient of the oligo was the summation of the extinction coefficients of each base. A ratio of 2.0 represented pure RNA, 1.8 represented pure DNA, and less than 1.8 represented the presence of significant levels of contaminants.

Internal ^{32}P-labeling of RNA

In vitro transcription reactions used a oligodeoxynucleotide template encoding a T7 RNA polymerase Class III promoter (Milligan *et al*., 1987). The DNA (1.6 μM) and G18 start promoter oligonucleotide (1.8 μM, Table 1) were annealed in 100 μl of 10 mM Tris•HCl buffer (pH 8.2) by heating at 65 °C for 5 minutes, followed by cooling on ice for 15 minutes. 10 μl of the annealing mix was added to a transcription reaction (100 μl) containing 1×T7 transcription buffer, the four rNTPs (1 mM each), 15-30 μCi of [α-^{32}P] UTP, and 400 units of T7 RNA polymerase. Reactions were incubated at 37 °C for 4 hours, then stopped by adding 50 μl reaction stop solution. The sample was electrophoresed (25 V/cm) in a 15% denaturing polyacrylamide gel containing 7 M urea in 1×TBE buffer for 2 hours. The gel band corresponding to radioactive RNA substrate was visualized by a 15-20 minute exposure to x-ray film (Fuji RX). The film was developed in developing buffer (GBX, Sigma) for 2 minutes, stopped in stopping buffer (GBX, Sigma) for 30 seconds, and fixed in fixing buffer (GBX, Sigma) for 2 minutes. If the RNA was nonradioactive, the RNA in the gel was visualized by UV shadowing. The RNA-containing gel band was excised, crushed, and incubated in 500 μl RNA/DNA extraction buffer. RNA was recovered by ethanol

precipitation and resuspended in 50 µl TE buffer as described above. The amount of internally radiolabeled substrate was determined by counting a 1µl sample in Scintiverse E (5 ml) using an LS 6500 Liquid Scintillation Counter (Beckman Coulter). Equation 3 was used to convert cpm to mmol:

Equation 3

$$\frac{\text{cpm/counting efficiency (0.99)}}{\text{Number of U residues in RNA strand} \times \frac{\mu\text{Ci of hot UTP used} \times 2.2\times10^{6}\ \text{dpm/}\mu\text{Ci}}{\text{Total mmol of cold UTP used}}}$$

5'-^{32}P-labeling of RNA

To remove the 5' triphosphate group, enzymatically synthesized, gel-purified RNA (10 pmol) was treated with shrimp alkaline phosphatase (5 units) at 37 °C for 1 hour using the supplied buffer, followed by inactivation at 65 °C for 15 minutes. Dephosphorylated RNA (5 pmol) was incubated at 37 °C for 30 minutes with 10 pmol of [γ-^{32}P]ATP (3,000 Ci/mmol) and T4 polynucleotide kinase (10 units), using the supplied buffer. Radioactive RNA was purified by electrophoresis in a 15% denaturing polyacrylamide gel (1.5 mm thick) containing 7 M urea in 1×TBE buffer. The RNA was located by autoradiography, extracted from the gel slice, recovered by ethanol precipitation, then resuspended and stored at -20 °C in 50 µl TE buffer as described above. The amount of 5'-^{32}P-labeled RNA was determined by liquid scintillation counting a 1µl aliquot in 5 ml Scintiverse E. Equation 4 was used to calculate the amount in mmol:

Equation 4

$$\frac{\text{cpm/counting efficiency (0.99)}}{\text{Specific activity of isotope } (3\times10^{9}\ \mu\text{Ci/mmol}) \times 2.2\times10^{6}\ \text{dpm/}\mu\text{Ci}}$$

3'-^{32}P-labeling of RNA

Enzymatically synthesized, gel-purified RNA (100 pmol) was incubated at 4 °C overnight with 100 pmol of [^{32}P] pCp (3,000 Ci/mmol) and T4 RNA ligase (10 units) using the supplied buffer (20 µl reaction volume) (Peattie, 1979). Radioactive RNA was purified by electrophoresis in a 15% denaturing polyacrylamide gel (1.5 mm thick) containing 7 M urea in 1×TBE buffer. The RNA was recovered by ethanol precipitation, resuspended, and stored at -20 °C in 50 µl TE buffer. The amount (radioactivity) of 3'-^{32}P-labeled RNA substrate was determined by liquid scintillation counting a 1µl aliquot in 5 ml Scintiverse E.

2.2.3.2 Substrate cleavage assay

Assays of RNase III cleavage of substrate were performed primarily using internally ^{32}P-labeled RNA. To remove any intermolecular RNA complexes formed during storage at -20 °C, the RNA in TE buffer was first heated at 95-100 °C for 1.5-2 minutes, followed by snap-cooling on ice. Specific conditions of individual cleavage assays are given in the corresponding figure or table legends. Generally, assays were performed by incubating RNA (100 nM) at the specified temperature for 1 minute in cleavage assay buffer [for Aa-RNase III, the cleavage buffer consisted of 50 mM NaCl, and 30 mM Tris-HCl (pH 8.0); for Ec-RNase III, the cleavage buffer consisted of 160 mM NaCl, and 30 mM Tris-HCl (pH 8.0)] lacking Mg^{2+}. RNase III at the specified concentrations was also pre-incubated at the assay temperature for 1 minute prior to addition to the reaction. Either $MgCl_2$ (10 mM) or RNase III was then added to initiate the reaction. Reactions (20 µl) were stopped by adding an equal volume of reaction stop solution, followed by electrophoresis of aliquots in a 15% denaturing polyacrylamide gel containing 7 M urea in 1×TBE buffer. The gel was exposed to a phosphorimager screen overnight at 4 °C, and the reactions were visualized by

phosphorimaging (Typhoon 9400 System) and quantified by ImageQuant software (v.5.2). To count the pixels, a rectangle was placed over each band. The percentage of substrate cleaved was determined by the pixels of all cleaved bands divided by the pixels of both cleaved and uncleaved bands. Assays were performed in duplicate, with maximum error typically less than ~20%. Curve fitting for determination of the kinetic parameters was done by Kaleidagraph software V.4.0 (Synergy Software, Reading, PA).

Experimental determination of k_{cat} and K_m values

The kinetic parameters V_{max} and K_m were determined by a Michaelis-Menten plot of the initial velocity (V_0) as a function of substrate concentration, and using Kaleidagraph (v.4.0) software. The percentage of substrate cleaved was converted into nM/min at each corresponding substrate concentration that was integrated into the Michaelis-Menten plot. Under steady-state conditions, the relationship between V_{max} and K_m can be shown as Henri-Michaelis-Menten equation (Equation 5).

Equation 5

$$V_0 = \frac{V_{max}[S]}{K_m+[S]}$$

At the beginning of the reaction, due to the large excess of substrate over enzyme, the free (unreacted) substrate concentration is essentially the same as the total substrate concentration. Under these conditions, the K_m corresponds to the substrate concentration where the reaction velocity is half the maximal velocity. The turnover number k_{cat} can be calculated using Equation 6, where $[E]_T$ is the total enzyme concentration.

Equation 6

$$k_{cat} = \frac{V_{max}}{[E]_T}$$

2.2.3.3 RNase III cleavage site mapping

Aa-16S[hp] RNA and Aa-23S[hp] RNA were 5'-end or 3'-end labeled to determine 5'-end-proximal and 3'-end-proximal RNase III cleavage sites, respectively. Labeled RNA (~1,000 dpm) was incubated with Aa-RNase III (20 nM) for 1 min at 50 °C in the standard cleavage assay buffer. The control reaction was identical except that Aa-RNase III was omitted. Alkaline ladders were generated by incubating labeled RNA (6,000 dpm) for 6-10 min at 95°C in 1×alkaline cleavage buffer containing 10 mg/ml yeast RNA (15 µl reaction volume), both provided by Ambion. P1 nuclease ladders were generated by incubating 5'- or 3'-^{32}P-labeled Aa-23S[hp] RNA or Aa-16S[hp] RNA RNA (4,000 dpm) with 0.05 or 1 unit, respectively, of P1 nuclease in pH 9 buffer (Cruz-Reyes *et al*., 1998). Aliquots were electrophoresed at 1500 V for 3.5-4 hours in a 15% acrylamide gel (0.6 mm thick), containing 7 M urea in 1×TBE buffer. Reactions were visualized by phosphorimaging. For comparison of different Aa-RNase III mutant enzymes, the reaction time was lengthened to 30 minutes, and a higher concentration of enzyme was used (100 nM).

2.2.3.4 Gel mobility shift assay

Gel mobility shift assays were performed using 5'-^{32}P-labeled Aa-16S [hp] RNA or Aa-23S [hp] RNA. ^{32}P-labeled RNA in TE buffer was heated at 95 °C for 1.5-2 minutes, followed by snap-cooling on ice. RNA (8,000-10,000 cpm; 1-2 fmol) was combined with the indicated amount of enzyme in reactions (20 µl total volume) containing 5 mM $CaCl_2$, 250 mM potassium glutamate, 30 mM Tris-HCl (pH 8.0 at room temperature), 5 mM spermidine, 0.1 mM DTT, and 5% (v/v) glycerol. The reaction was kept at room temperature for 10-20 minutes. Gel electrophoresis was performed at room temperature for 3-4 hours in a 1.5-mm thick, 8% non-denaturing polyacrylamide gel (15 cm, 80:1 acrylamide:bisacrylamide) containing 0.5×TBE

buffer, 2.5% (v/v) glycerol, and 5 mM $CaCl_2$. The electrophoresis buffer was identical to the polyacrylamide gel buffer, and the gel was electrophoresed (10 V/cm) for 30 minutes prior to sample addition. To track the progress of electrophoresis, side lanes contained bromophenol blue (0.04% w/v) in binding reaction buffer. Reactions were visualized by phosphorimaging, and the fraction of substrate bound was determined as described (Carey *et al*., 1983). Some dissociation of RNA–protein complexes occurred during electrophoresis, causing a 'trail' of ^{32}P radioactivity extending up from the free (unbound) RNA. This behavior has been noted elsewhere (Carey, 1991), and was taken into account in determining the fraction of substrate bound. The fraction of substrate bound was determined by pixels from the initial appearance of bound substrate /pixels of bound and free substrate bands. The K'_D values were calculated using Equation 7 or Equation 8, where $[E]_f$ and $[S]_f$ are the concentrations of unbound (free) enzyme and substrate, respectively, and [ES] is the concentration of the enzyme-substrate complex.

Equation 7

$$K'_D = \frac{[E]_f \times [S]_f}{[ES]}$$

Equation 8 $$1/B = 1 + K'_D/[E]_T$$

The fraction of RNA bound (B) was determined using Equation 9, where $[S]_T$ is the concentration of total substrate, and [ES] is the concentration of the enzyme-substrate complex. Because the enzyme concentration (50-3,000 nM) is in large excess over the substrate (1-2 nM), the free enzyme concentration is essentially the same as the total enzyme concentration, $[E]_T$. The amount of free RNA is used to calculate the fraction of bound RNA, since dissociation of the RNA-protein complex was usually observed

during electrophoresis (see above). Assays were performed in duplicate, with maximum error less than ~20%.

Equation 9

$$B = \frac{[ES]}{[S]_T}$$

2.2.3.5 Assessment of protein secondary structure by CD spectroscopy

Aa-RNase III and mutants were overexpressed and purified by Ni^{2+} affinity chromatography. Following elution from the affinity column, proteins were dialyzed against 150 mM NaCl, 20 mM Tris-HCl (pH 7.5) buffer. The buffer was then changed to 50 mM sodium phosphate (pH 7) using an Amicon Ultra-15 centrifugal filter (3,000 MWCO). Spectra were taken at room temperature using a JASCO Model J-815 CD Spectrometer. Sample protein concentrations were ~15 μg/ml. Samples were scanned continuously at 25 °C, with sensitivity at 100 mdeg, data pitch at 0.1 nm, scanning speed at 50 nm/min, response at 1 second, and band width of 1 nm.

2.2.3.6 Charged *versus* polar bias

The Charged-*versus*-Polar bias (C*v*P-bias) of the amino acid compositions of thermophile proteins is larger than that for mesophile proteins (Cambillau and Claverie, 2000; Suhre and Claverie, 2003). C*v*P-bias is the difference between the percent charged residues [Asp (D), Glu (E), Arg (R), Lys (K)] and polar (non-charged) residues [Asn (N), Gln (Q), Thr (T), Ser (S)] in the polypeptide (Equation 10). The greater C*v*P-bias values reflect a preference for charged residues that can form salt bridges, as well as a preference for Glu/Asp instead of Gln/Asn, the side chains of which contain thermolabile carboxamide groups.

Equation 10 $C\nu P = [(N_{D+E+R+K} - N_{N+Q+T+S})/N_{total}] \times 100$

(where N represents the number of corresponding residues).

2.2.3.7 Contact order

Another potential contributor to protein thermostability is contact order (CO), which is a measure of structural compactness of a protein, due to an increased density of noncovalent, non-nearest neighbor interactions (Plaxco *et al*., 1998; Robinson-Rechavei and Godzik, 2006). The CO can be calculated online (http://depts.washington.edu/bakerpg/contact_order/) by inputting the corresponding PDB entry number for the protein.

Table 1. List of Oligodeoxynucleotides.

Name	Sequence (5' to 3')
G-18 (T7 promoter oligo) (18 nt)	TAA TAC GAC TCA CTA TAG
R1.1 DNA (77 nt)	AAG AAG GTC AA**T CAT A**AA GGC CAC TCT TGC GAA TGA CCT T**GA GT**T TGT CCC TCT ACT CCC TAT AGT GAG TCG TAT TA
R1.1 [IL-Flip] DNA (77 nt)	AAG AAG GTC AA**T GAG** AAG GCC ACT CTT GCG AAT GAC CTT **ATA CT**T TGT CCC TCT ACT CCC TAT AGT GAG TCG TAT TA
R1.1 [IL-invert] DNA (77 nt)	AAG AAG GTC AA**G AGT** AAG GCC ACT CTT GCG AAT GAC CTT **TCA TA**T TGT CCC TCT ACT CCC TAT AGT GAG TCG TAT TA
R1.1[WC] DNA (63 nt)	AGG TCA ATA TAA AGG CCA CTC TTG CGA ATG ACC TTT ATA TTG TCC CTA TAG TGA GTC GTA TTA
Aa-16S [hp] DNA (67 nt)	GCA ACT GAG TAG AGG GTG AGC TTG CGC TCA CCC TCT ATT CAG TTG CTC CCT ATA GTG AGT CGT ATT A
Aa-16S [μ-hp] DNA (53 nt)	ATA GAG GGT GAG CTT GCG CTC ACC CTC TAT TCT CCC TAT AGT GAG TCG TAT TA
Aa-23S [hp] DNA (75 nt)	GTC AAC AGA ATA AAG CCT GTA CCT CTT GCG AGG TAC AGG CTT TAT TCT GTT GAC TCC CTA TAG TGA GTC GTA TTA
Ec *rnc* gene 5' primer (Tm=75 °C)	GGG AAT TC<u>C ATA</u>* **<u>TG</u>**<u>A</u> ACC CCA TCG TAA TTA
Ec *rnc* gene 3' primer (Tm=74.8 °C)	CCC <u>G*GA TCC</u> **TCA** TTC CAG CTC
Ec *rnc* gene **E117A** mutagenic primer	ATT AAT GC**T GC**G ACG GTG TCG
Ec *rnc* gene **NucD** 3' primer (Tm=72.8 °C)	CCC <u>G*GA TCC</u> **TCA** TGG GCT AAT
Ec *rnc* gene **NucD** [**BsrG1**] 3' primer (Tm=82 °C)	GGG AAT TCC <u>T*GT ACA</u> CGT CCC TCT TTT ATA GCA CTC
Aa *rnc* gene 5' primer (Tm=77.3 °C)	GGG AAT TC<u>C ATA</u>* **<u>TG</u>**<u>A</u> AAA TGT TGG AGC AAC TTG A
Aa *rnc* gene 3' primer (Tm=73.6 °C)	CCC <u>G*GA TCC</u> **TCA** TTC TGA TTC CT
Aa *rnc* gene **NucD** 3' primer (Tm=73.2 °C)	CCC <u>G*GA TCC</u> **TCA** TCC CTC TTT T
Aa *rnc* gene **NucD** [**BsrG1**] 3' primer (Tm=79°C)	GTG CTA TAA AAG AGG GAA <u>GT*G TAC A</u>AA AAG ATT ACA AAA CG
Aa *rnc* gene **E110A** mutagenic primer	GGA GAC GTA TTT **AAA** GCT CTT TGG GCA GCG
Aa *rnc* gene **D151A** mutagenic primer	GAG GGA AGA GTA AAA AAA **GCT** TAC AAA ACG ATA CTT CAG GAG

Table 1. (continued)

Aa *rnc* gene **K153A** mutagenic primer	GAG GGA AGA GTA AAA AAA GAT TAC **GCA** ACG ATA CTT CAG GAG ATC
Aa *rnc* gene **T154A** mutagenic primer	GAT TAC AAA **GCG** ATA CTT CAG GAG ATC ACT CAA AAA CGA TGG
Aa *rnc* gene **Q157A** mutagenic primer	GAT TAC AAA ACG ATA CTT **GCG** GAG ATC ACT CAA AAA CGA TGG
Aa *rnc* gene **Q157N** mutagenic primer	GAT TAC AAA ACG ATA CTT **AAT** GAG ATC ACT CAA AAA CGA TGG
Aa *rnc* gene **E158A** mutagenic primer	C AAA ACG ATA CTT CAG **GCG** ATC ACT CAA AAA CGA TGG
Aa *rnc* gene **Q161A** mutagenic primer	CGA TAC TTC AGG AGA TCA CT**G CA**A AAC GAT GGA AGG AAA GAC GGG

For the R1.1 DNAs, the letters in bold-face represent the 4/5 asymmetric internal loop in the transcribed RNAs. For the 5'-primers, the underlined letters represent the NdeI site, with the cleavage site indicated by the asterisk, with the *rnc* AUG translation initiation codon indicated in bold-face. For the 3'-primers, the BamHI site is underlined, with the cleavage site indicated by the asterisk, directly adjacent to the sequence complementary to the *rnc* UGA translation stop codon, indicated in bold-face. The 3'-primers for NucD [BsrGI] are used to introduce an BsrGI site in the linker region for the construction of Aa-Ec chimera proteins. The site is underlined, with the cleavage site indicated by the asterisk. For single site mutagenic primers, the mutant residue codon is labeled in bold-face.

Table 2. Summary of RNase III mutants.

Bacteria	Region	
A. aeolicus	dsRBD (RBM1)	D151A, homodimer
		K153A, homodimer
		T154A, homodimer
		Q157A, homodimer
		Q157N, homodimer
		E158A, homodimer
		Q161A, homodimer
	(Truncated)	dsRBD, monomer
		NucD, homodimer
E. coli	(heterodimer)	WT/NucD, heterodimer
		WT/NucD[E117A], heterodimer
		WT[E117A]/NucD, heterodimer
A. aeolicus, E. coli	Chimera	$NucD^{Aa}$-$dsRBD^{Ec}$, homodimer
		$NucD^{Ec}$-$dsRBD^{Aa}$, homodimer

CHAPTER 3. RESULTS

3.1 Characterization of Aa-RNase III

3.1.1 Physical characteristics

The basic physical properties of purified recombinant Aa-RNase III were analyzed. This included determination of the polypeptide molecular mass, and subunit structure of the holoenzyme. In addition, comparative secondary structural differences between Aa-RNase III and selected mutants were assessed using circular dichroism spectroscopy.

3.1.1.1 Apparent molecular mass of the Ec- and Aa-RNase III polypeptides

As shown by SDS-PAGE, the two subunits of purified Ec-RNase III heterodimer [in which one subunit carries an N-terminal $(His)_6$ tag (~2 kDa) (expressed from plasmid pET-15b), and the other subunit carries an N-terminal CBP-tag (~4.1 kDa) (expressed from plasmid pACYC184)] exhibit molecular masses between 25 and 30 kDa. The molecular mass range is consistent with the predicted masses: 27.6 kDa for full-length RNase III subunit + $(His)_6$ tag, and 29.7 kDa for full-length RNase III subunit + CBP-tag (Figure 12A).

The Aa-RNase III holoenzyme, as eluted from the Ni^{2+}-NTA affinity column contains a $(His)_6$-tag on each subunit. The $(His)_6$-tag was removed by thrombin treatment, and the protein was purified from the $(His)_6$-tag and thrombin by gel filtration FPLC. The Aa-RNase III polypeptide lacking the $(His)_6$-tag has a calculated molecular mass of ~26.4 kDa (Figure 2C; Figure 9) and was verified by SDS-PAGE (Figure 12B). The sizes of the truncated Aa-RNase III mutant polypeptides are also shown in Figure 12C, with the $(His)_6$-NucD polypeptide having an apparent molecular mass of ~18-20 kDa (19.2 kDa by calculation; Figure 2C), and the $(His)_6$-dsRBD polypeptide, ~10 kDa (11.1 kDa by calculation; Figure 2C).

A

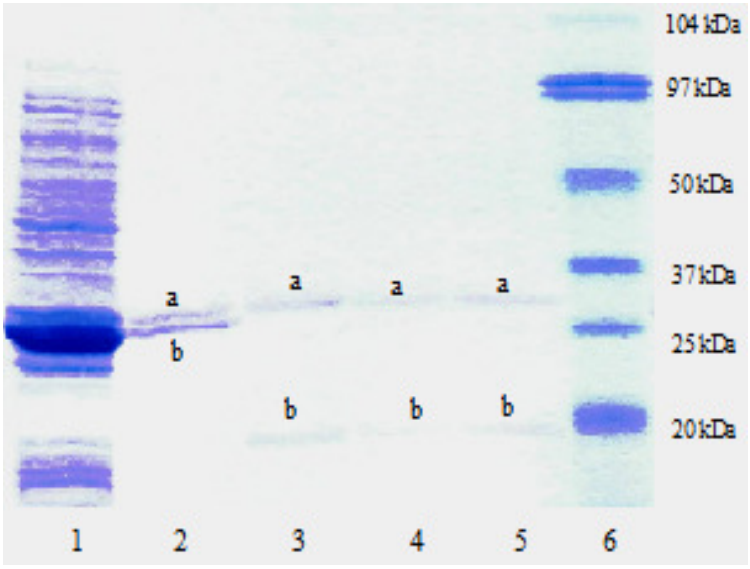
104 kDa
97kDa
50kDa
37kDa
25kDa
20kDa
a
b
1
2
3
4
5
6

B

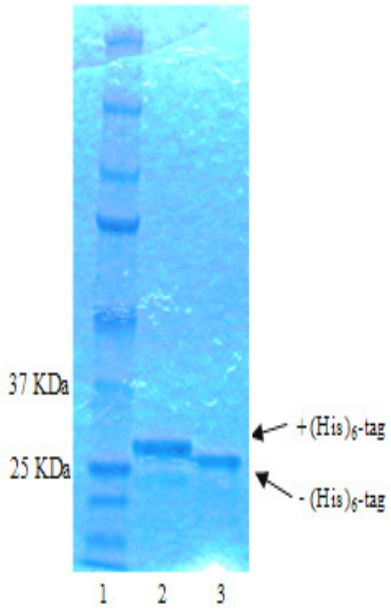
37 KDa
25 KDa
+(His)6-tag
-(His)6-tag
1
2
3

C

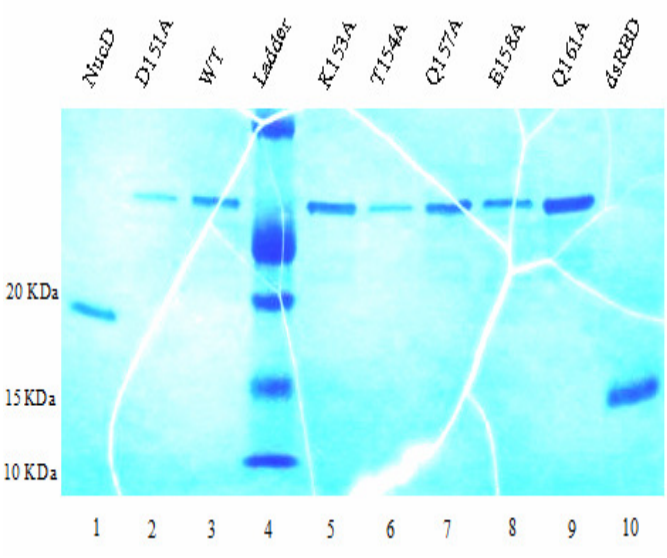
NtoD
D151A
WT
Ladder
K153A
T154A
Q157A
E158A
Q161A
dsRBD
20 KDa
15 KDa
10 KDa
1
2
3
4
5
6
7
8
9
10

Figure 12. Overexpression and purification of Aa-RNase III and specific mutant forms.

A. SDS-PAGE analysis of Ec-RNase III, purified from the soluble portion of sonicated cell extracts, with one subunit carrying a $(His)_6$-tag, and the other subunit carrying a CBP-tag. Lane 1, total cell extracts containing Ec-RNase III [$(His)_6$-tagged]/CBP-tagged] polypeptide, before purification. Lane 2, Ec-RNase III heterodimer after Ni^{2+}-NTA column chromatography (first step) and Ca^{2+}-CBP column chromatography (second step). Lane 3, Ec-RNase III [WT/NucD] heterodimer. Lane 4, Ec-RNase III [E117A]/NucD] heterodimer. Lane 5, Ec-RNase III [NucD/E117A] heterodimer. Lane 6, protein ladder. Band "a" is CBP-tagged Ec-RNase III monomer; band "b" is $(His)_6$-tagged Ec-RNase III monomer (or truncated mutant).

B. SDS-PAGE analysis of Aa-RNase III, before and after thrombin treatment to remove the $(His)_6$-tag. Lane 1, protein ladder. Lane 2, $(His)_6$-tagged RNase III. Lane 3, RNase III without the $(His)_6$-tag.

C. SDS-PAGE of Aa-RNase III mutants (all containing the $(His)_6$-tag). Lane 1, Aa-NucD. Lane 2, Aa-RNase III[D151A]. Lane 3, Aa-RNase III. Lane 4, protein ladder. Lane 5, Aa-RNase III[K153A]. Lane 6, Aa-RNase III[T154A]. Lane 7, Aa-RNase III[Q157A]. Lane 8, Aa-RNase III[E158A]. Lane 9, Aa-RNase III[Q161A]. Lane 10, Aa-RNase III dsRBD.

3.1.1.2 Dimeric behavior of Aa-RNase III

Purified Aa-RNase III was analyzed by gel filtration FPLC (Figure 13). The time of elution of the protein (detected by absorbance at 280 nm) was compared with those of protein standards. Aa-RNase III elutes at 10.78 minutes after column loading, and is positioned between the 75 kD (9.52 minutes) and 29 kD (11.69 minutes) protein markers, demonstrating that it has a homodimeric structure. Thus, the reported concentrations refer to the concentration of the homodimer.

3.1.1.3 CD-based secondary structure analysis of Aa-RNase III mutants

Circular Dichroism was used to determine whether specific point mutations in the RBM1 caused significant secondary structural changes. The CD spectra of the mutants revealed closely similar spectra to that of wild-type enzyme, including overall shape and inflection points. (Figure 14). This indicates that the point mutants do not alter the overall secondary structure of Aa-RNase III.

3.1.2 Functional analysis of Aa-RNase III

Functional analyses of Aa-RNase III included assays of binding and cleavage of cognate substrates, as well as a Michaelis-Menten kinetic analysis, from which the kinetic parameters K_m and k_{cat} were determined.

3.1.2.1 Effect of $(His)_6$-tag on Aa-RNase III catalytic behavior

To determine whether the N-terminal $(His)_6$-tag influences the catalytic activity of Aa-RNase III, time-course assays of cleavage of a modified cognate substrate were performed, and the initial rates of cleavage measured. There was no significant difference in the kinetic behaviors of the two forms of enzyme (Figure 15). Therefore, unless otherwise stated, experiments in subsequent studies used $(His)_6$-tagged Aa-RNase III.

A

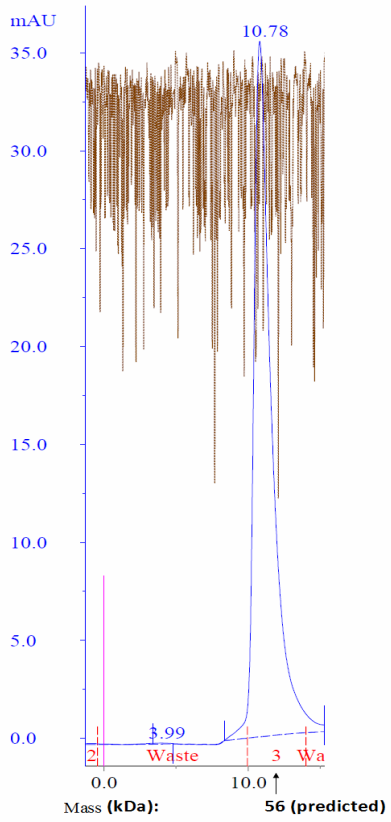
mAU
35.0
30.0
25.0
20.0
15.0
10.0
5.0
0.0
10.78
$.99
2
Waste
3
Wa
0.0
10.0
Mass (kDa):
56 (predicted)

B

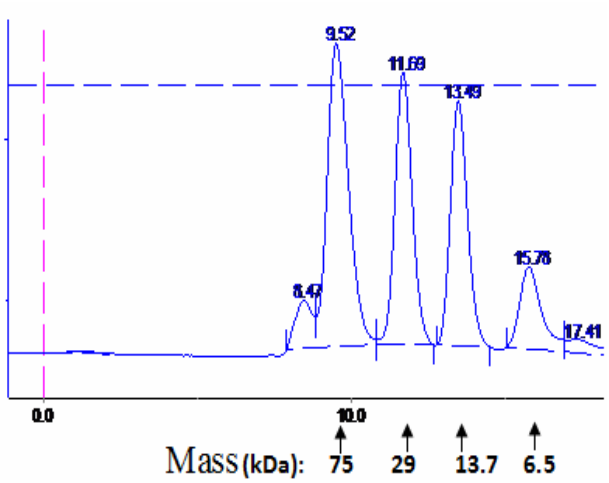
9.52
11.69
13.49
15.76
17.41
0.0
10.0
Mass (kDa):
75
29
13.7
6.5

C

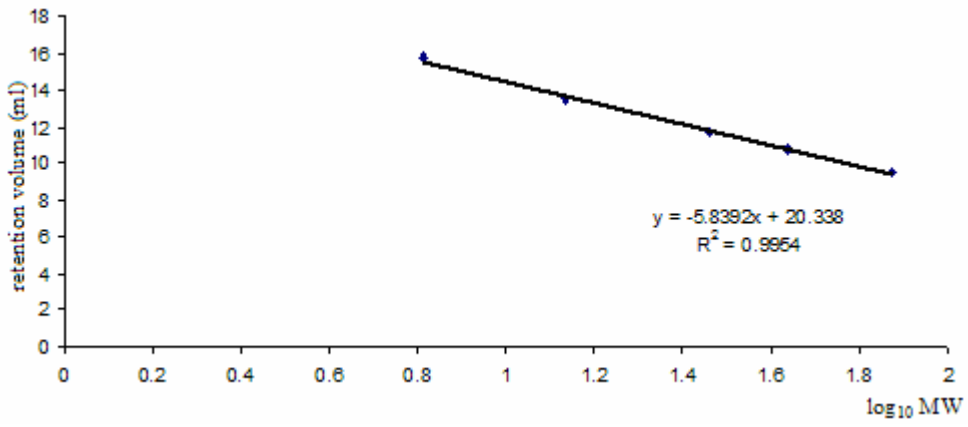
retention volume (ml)
18
16
14
12
10
8
6
4
2
0
0
0.2
0.4
0.6
0.8
1
1.2
1.4
1.6
1.8
2
log10 MW
y = -5.8392x + 20.338
R2 = 0.9954

Figure 13. Homodimeric structure of Aa-RNase III as determined by gel filtration (FPLC).

A. Profile of Aa-RNase III elution from a Superdex 75 column. Arrows show the corresponding molecular weight (kDa). The pink vertical line indicates when the sample was loaded. Aa-RNase III eluted at 10.78 min.

B. Elution profile of protein molecular weight standards. X-axis: elution volume (ml) or time (minutes); Y-axis: absorbance at 280 nm; peaks represent proteins of different sizes. Peaks at 9.52, 11.69, 13.49, and 15.78 minutes correspond to conalbumin, carbonic anhydrase, ribonuclease A, and aprotinin, respectively. The pink vertical line indicates when the sample was loaded.

C. Determination of MW of Aa-RNase III by curve fitting (Akta FPLC UNICORN Software Analysis Module). X-axis: $\log_{10}$ MW; Y-axis: retention volume (ml). The graph and equation were based on panel B. The calculated value for Aa-RNase III is 43.3 kDa.

A

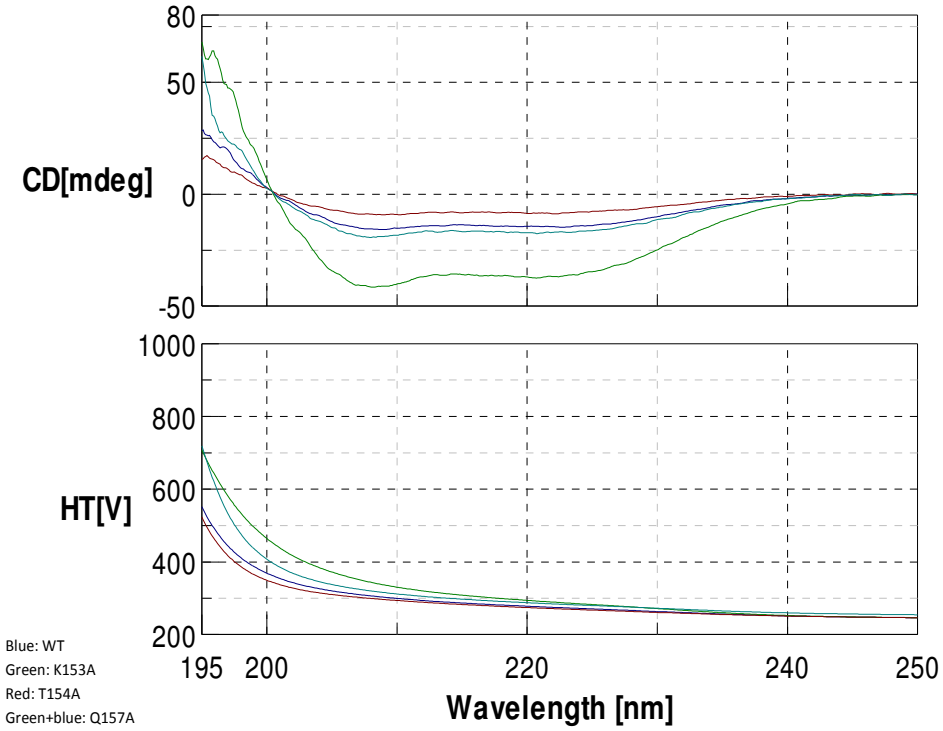
80
50
0
-50
CD[mdeg]
1000
800
600
400
200
HT[V]
195
200
220
240
250
Wavelength [nm]
Blue: WT
Green: K153A
Red: T154A
Green+blue: Q157A

B

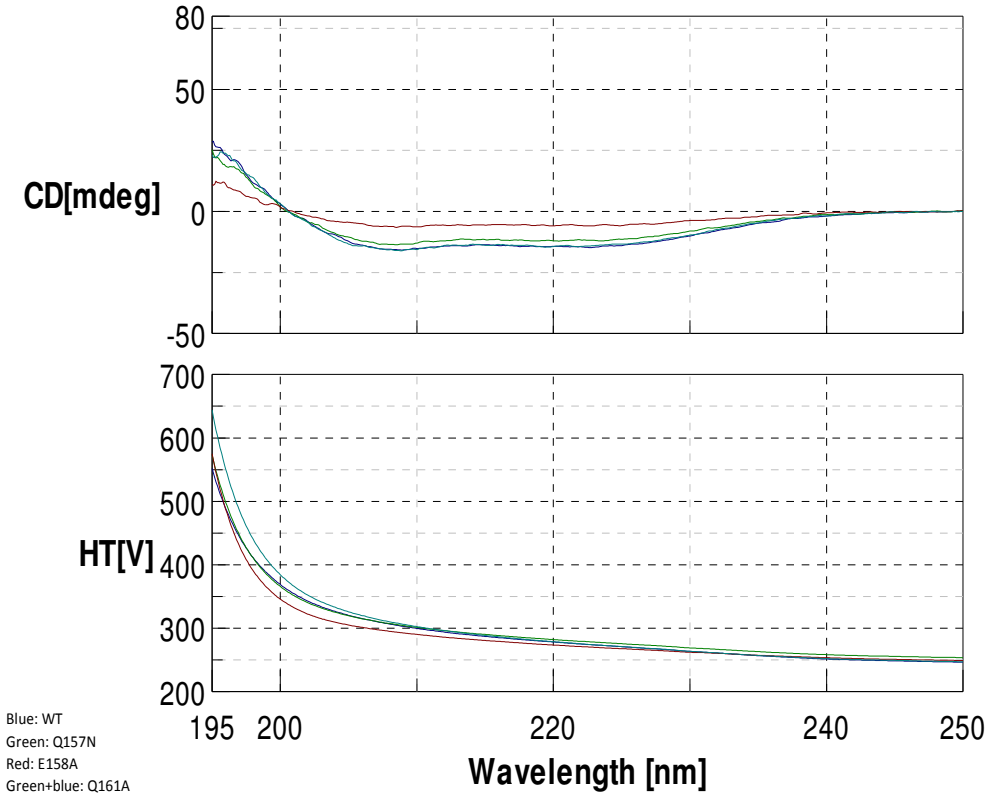
80
50
0
-50
CD[mdeg]
700
600
500
400
300
200
HT[V]
195
200
220
240
250
Wavelength [nm]
Blue: WT
Green: Q157N
Red: E158A
Green+blue: Q161A

C

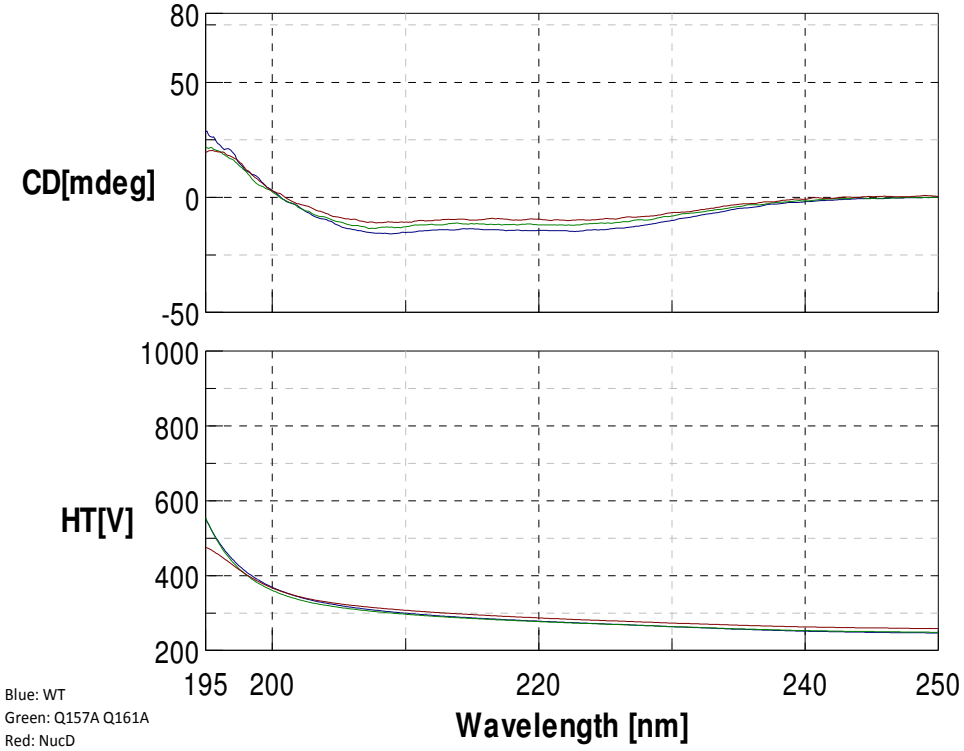

Blue: WT
Green: Q157A Q161A
Red: NucD

D

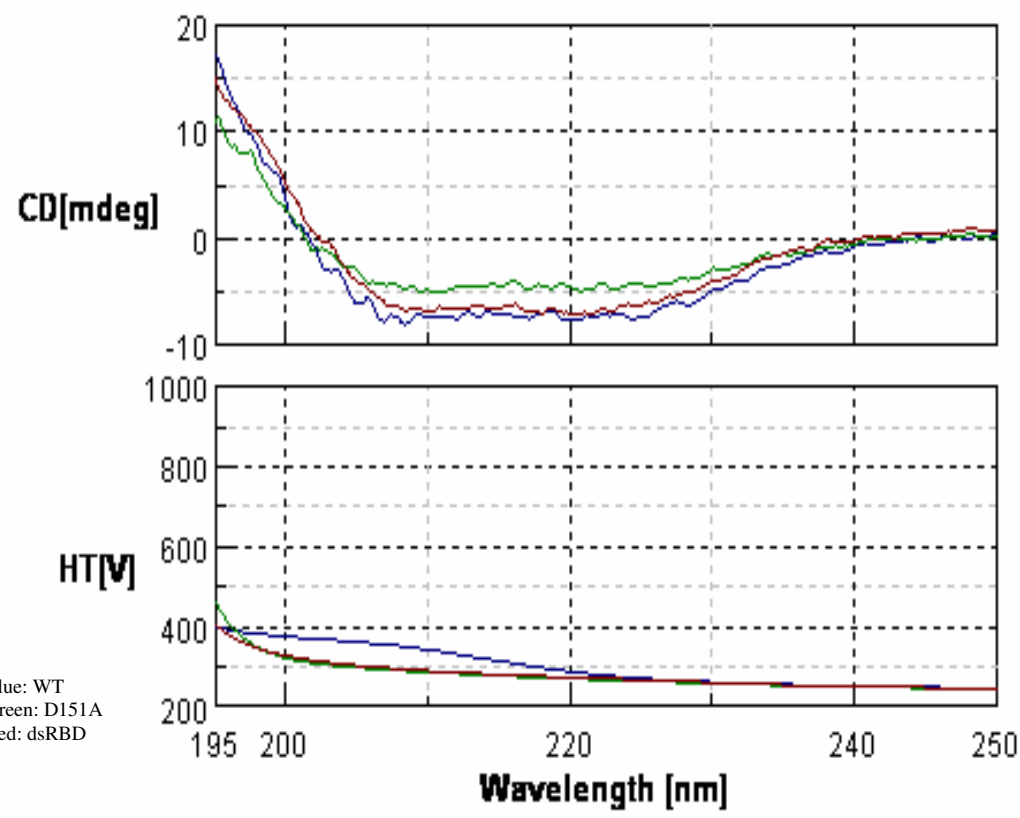

Blue: WT
Green: D151A
Red: dsRBD

E

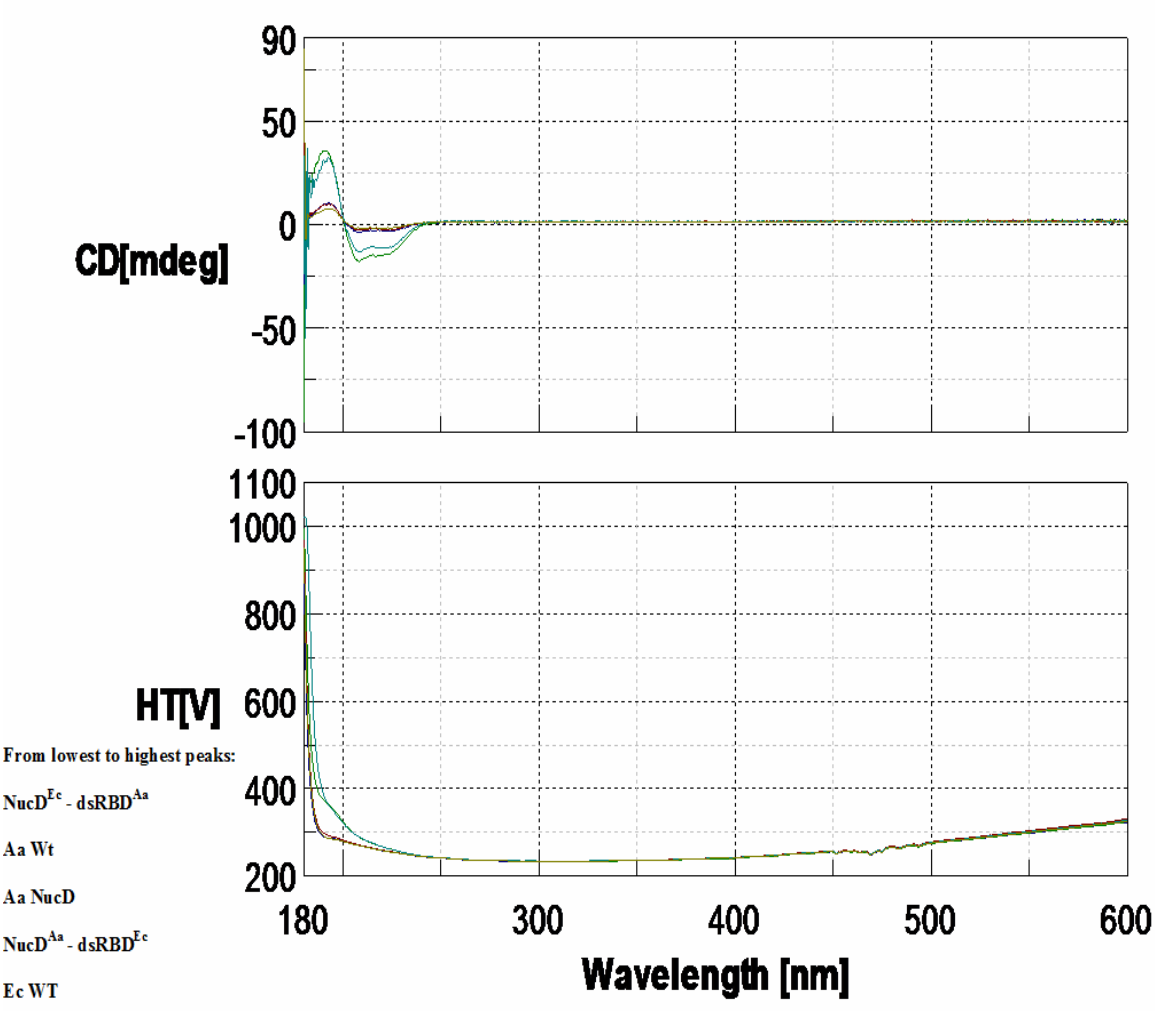
90
50
0
-50
-100
CD[mdeg]
1100
1000
800
600
400
200
HT[V]
180
300
400
500
600
Wavelength [nm]
From lowest to highest peaks:
NucD^Ec - dsRBD^Aa
Aa Wt
Aa NucD
NucD^Aa - dsRBD^Ec
Ec WT

Figure 14. CD spectra of Aa-RNase III and specific point mutants.

A. Blue: WT; Green: K153A; Red: T154A; Green/Blue: Q157A.

B. Blue: WT; Green: Q157N; Red: E158A; Green/Blue: Q161A.

C. Blue: WT; Green: Q157A+Q161A; Red: NucD.

D. Blue: WT; Green: D151A; Red: dsRBD.

E. From the lowest to highest peaks, the proteins are: $NucD^{Ec}$-$dsRBD^{Aa}$; Aa WT; Aa NucD; $NucD^{Aa}$-$dsRBD^{Ec}$; Ec WT.

A

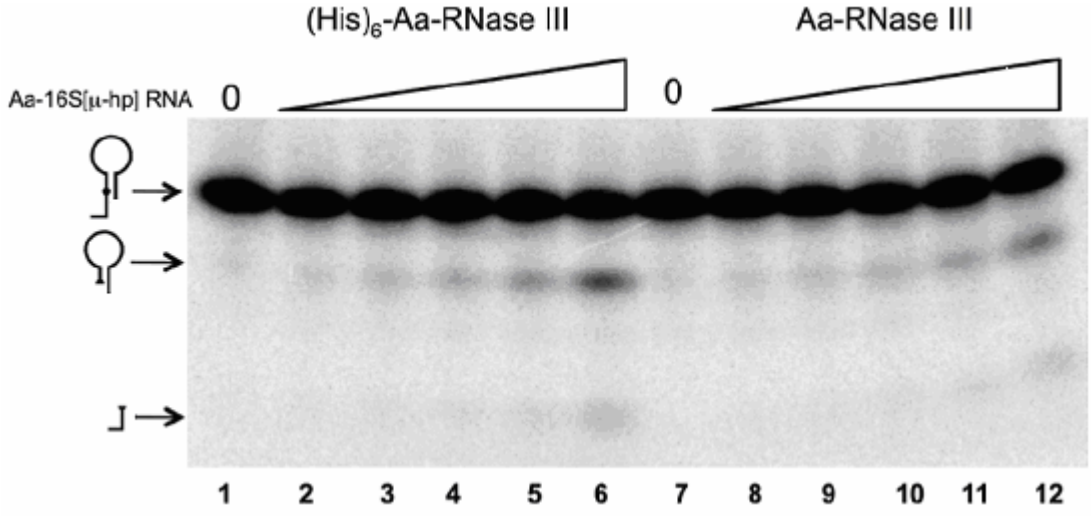
(His)6-Aa-RNase III
Aa-RNase III
Aa-16S[μ-hp] RNA
0
0
1 2 3 4 5 6 7 8 9 10 11 12

B

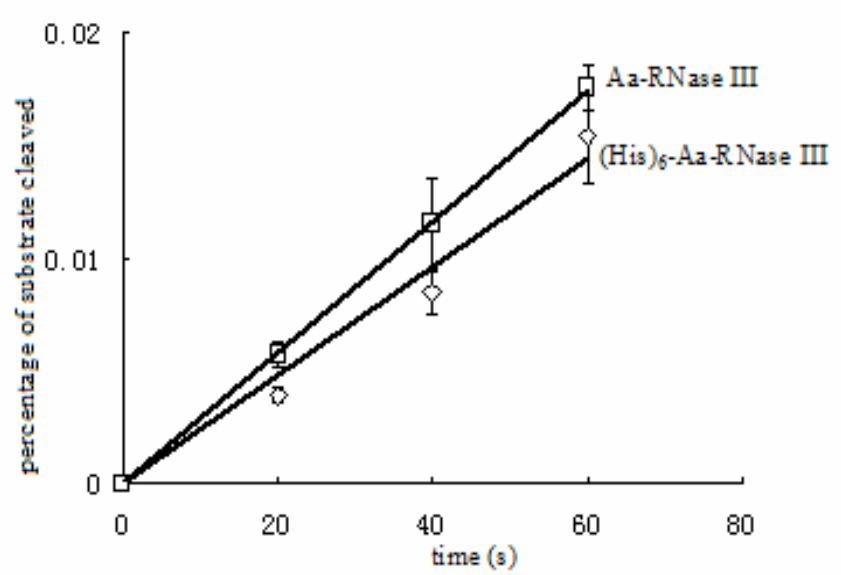
0.02
0.01
0
percentage of substrate cleaved
Aa-RNase III
(His)6-Aa-RNase III
0
20
40
60
80
time (s)

Figure 15. The presence of an N-terminal Hexahistidine [$(His)_6$] tag does not significantly affect the catalytic activity of Aa-RNase III (Shi *et al*., 2011).

A. Time course for cleavage of internally ^{32}P-labeled Aa-16S[μ-hp] RNA by $(His)_6$-Aa-RNase III and Aa-RNase III. Reaction conditions were as described in Materials and Methods. The enzyme concentration was 20 nM, and the RNA concentration was 360 nM .The reaction temperature was 55°C. Lanes 1-6 display a time course reaction using $(His)_6$-Aa-RNase III. Lanes 7-12 display a time course reaction using thrombin-treated Aa-RNase III (see text). Lanes 2-6, and 8-12 exhibit reaction times of 20 sec, 40s, 60 sec, 90 sec and 180 sec. Reactions were pre-incubated at 55°C for 1 minute, and $MgCl_2$ was added last to initiate the reaction. Lanes 1 and 7 represent otherwise complete reactions that lacked enzyme (1 minute incubation).

B. Comparison of initial cleavage rates based on duplicate experiments. Open diamonds, $(His)_6$-Aa-RNase III ($y=0.0002x$, $R^2=0.9768$); Open squares, Aa-RNase III ($y=0.0003x$, $R^2=0.9999$). The difference in slope [0.0002 for $(His)_6$-Aa-RNase III *vs*. 0.0003 for Aa-RNase III] is 33%. X-axis: time (sec); Y-axis: percentage of substrate cleaved.

3.1.2.2 Substrate cleavage by Aa-RNase III

3.1.2.2.1 Cleavage site mapping

The cleavage sites in Aa-16S[hp] and Aa-23S[hp] RNA were mapped by comparison of the gel electrophoretic mobilities of the products of Aa-RNase III cleavage of 5'-^{32}P or 3'-^{32}P-labeled RNA with the products of partial cleavage by P1 nuclease, or incubation at alkaline pH. The results show that the cleavage sites occupy equivalent positions in each substrate with respect to specific sequence elements (Figure 16). The positions of the target sites are consistent with a role of Aa-RNase III in creating the immediate precursors to the mature 16S and 23S rRNAs (Figure 6).

3.1.2.2.2 Salt and pH dependence of Aa-RNase III catalytic activity

Monovalent cations influence Ec-RNase III catalytic activity in vitro. Ec-RNase III exhibits optimal activity and specificity at salt concentrations of ~100–150 mM, while at lower salt concentrations, additional secondary sites are cleaved that are not utilized *in vivo* (Dunn, 1976). The salt dependencies of RNase III orthologs may exhibit significant differences from that of Ec-RNase III. To assess the effect of salt type and concentration on Aa-RNase III activity, substrate cleavage assays were performed using a range of concentrations of Na^+, K^+, or NH_4^+ ions (as the chloride salts), using Aa-16S[hp] RNA as substrate. In these experiments the Mg^{2+} concentration was 10 mM. Aa-RNase III catalytic activity exhibits a maximum at ~50 mM Na^+, ~50 mM K^+ or ~25 mM NH_4^+, while higher concentrations of each species causes a progressive reduction in activity (Figure 17A). There also is no evidence for cleavage of secondary sites at any salt concentration. These results demonstrate the absence of a strong preference for a specific salt species, and that the pattern of cleavage is insensitive to the salt type or concentration.

The pH dependence of Aa-RNase III catalytic activity was determined by

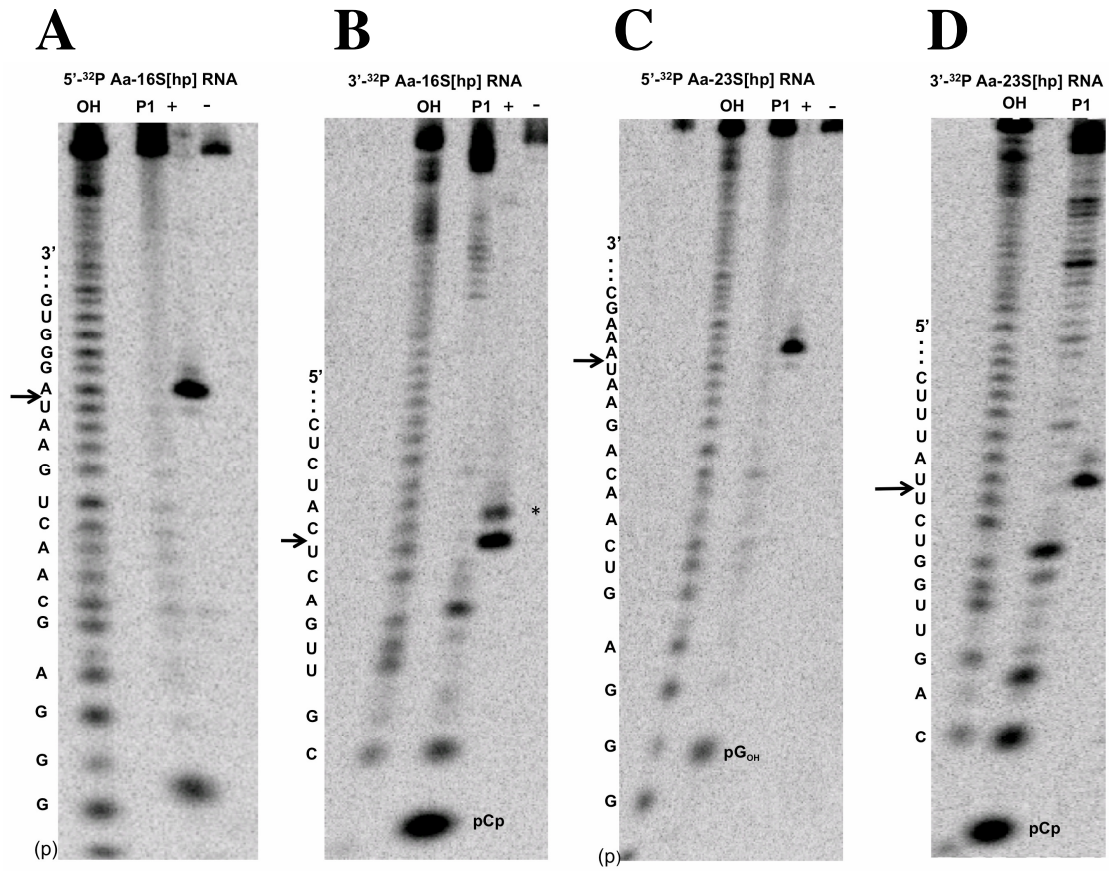
A
B
C
D
5'-32P Aa-16S[hp] RNA
3'-32P Aa-16S[hp] RNA
5'-32P Aa-23S[hp] RNA
3'-32P Aa-23S[hp] RNA
OH
P1
+
-
pCp
pG
(p)

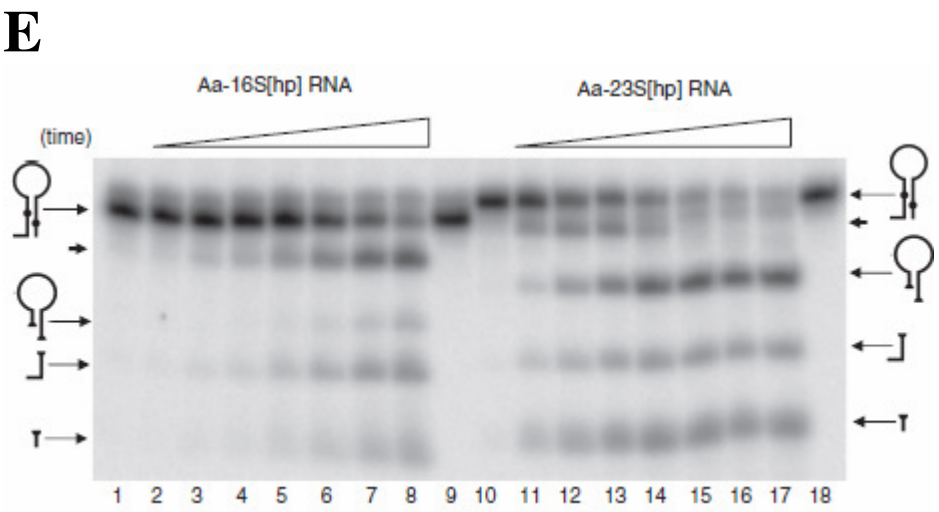
E
Aa-16S[hp] RNA
Aa-23S[hp] RNA
(time)
1 2 3 4 5 6 7 8 9 10 11 12 13 14 15 16 17 18

Figure 16. Determination of the Aa-RNase III cleavage sites in Aa-16S[hp] RNA and Aa-23S[hp] RNA (Shi *et al*., 2011).

A. Mapping the 5'-end-proximal RNase III cleavage site in 5'-^{32}P labeled Aa-16S[hp] RNA. "OH", alkaline cleavage reaction; "P1", P1 nuclease reaction; "+", Aa-RNase III reaction; "-" control reaction that lacked enzyme. The predominant product in the P1 reaction is [5'-^{32}P]p**G$_{OH}$**, and was used to establish the 5'-end nucleotide in the alkaline ladder. The cleavage site is indicated by an arrow. "p", ^{32}P-phosphate.

B. Mapping the 3'-end-proximal RNase III cleavage site in 3'-^{32}P-labeled Aa-16S[hp] RNA. The main P1 nuclease product seen at the bottom of the gel lane is [5'-^{32}P]pCp, and was used to identify the 3'-end-proximal nucleotides in the alkaline ladder. The Aa-RNase III cleavage site is indicated by the arrow. The asterisk in the RNase III reaction lane probably represents the product of cleavage of RNA carrying an extra, non-templated nucleotide at the 3'-end, which was incorporated during T7 RNA polymerase transcription, and which was 3'-^{32}P-labeled.

C. Mapping the 5'-end-proximal cleavage site in 5'-^{32}P-labeled Aa-23S[hp] RNA. In the P1 nuclease lane, the species with the greatest electrophoretic mobility is [5'-^{32}P]pG$_{OH}$. The species in the adjacent alkaline cleavage lane with slightly greater mobility is [5'-^{32}P]pGp, and which migrates at a slightly slower rate than ^{32}P-phosphate (p). These products were used to identify the RNA 5'-end nucleotides, therefore allowing mapping of the cleavage site (indicated by the arrow).

D. Mapping the 3'-end-proximal RNase III cleavage site in 3'-^{32}P-labeled Aa-23S[hp] RNA. The fastest-moving species in the P1 nuclease lane is [5'-^{32}P]pCp. The corresponding alkaline cleavage product, Cp, is not visible since it is not radiolabeled. However, the next-larger dinucleotide cleavage product, UpCp, is visible, and was used to identify the 3'-end, and by inference the Aa-RNase III cleavage site (indicated by the arrow). The control reaction lacking Aa-RNase III is not included in the image.

E. Time course for Aa-RNase III cleavage of Aa-16S[hp] RNA and Aa-23S[hp] RNA. Internally ^{32}P-labeled Aa-16S[hp] RNA (400 nM) or Aa-23S[hp] RNA (200 nM) were combined with Aa-RNase III (30 nM) and incubated at 45°C in buffer consisting of 200 mM NaCl, 2 mM $MgCl_2$, and 30 mM Tris–HCl (pH 8). Lanes 2–8 and lanes 11–17 show reaction times of 0, 0.5, 1, 2, 4, 8 and 16 min for Aa-16S[hp] RNA and Aa-23S[hp] RNA, respectively. Lanes 1 and 10 represent complete reactions that were assembled, then immediately quenched with excess EDTA. Lanes 9 and 18 represent 16-min reactions with Aa-16S[hp] RNA and Aa-23S[hp] RNA, respectively, that lacked Mg^{2+}. Icons indicate the identities of the specific products. The short arrow indicates the product of cleavage of one of the two scissile bonds.

A

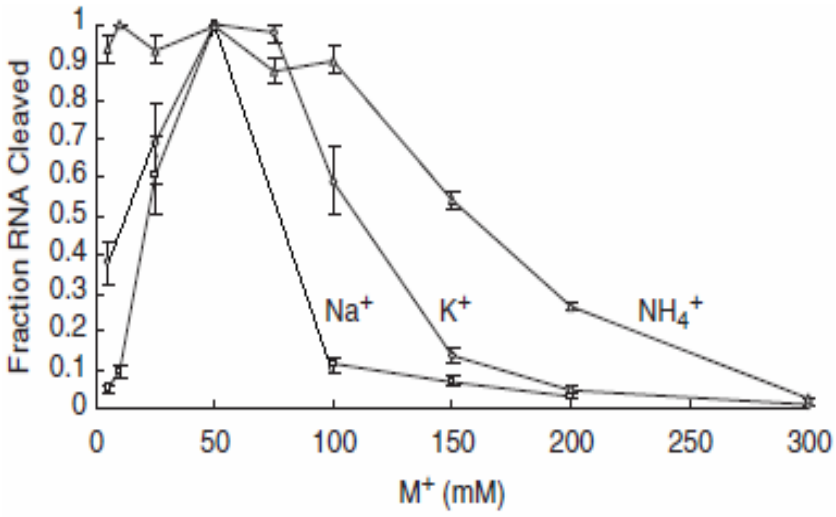
Fraction RNA Cleaved
1
0.9
0.8
0.7
0.6
0.5
0.4
0.3
0.2
0.1
0
0
50
100
150
200
250
300
M+ (mM)
Na+
K+
NH4+

B

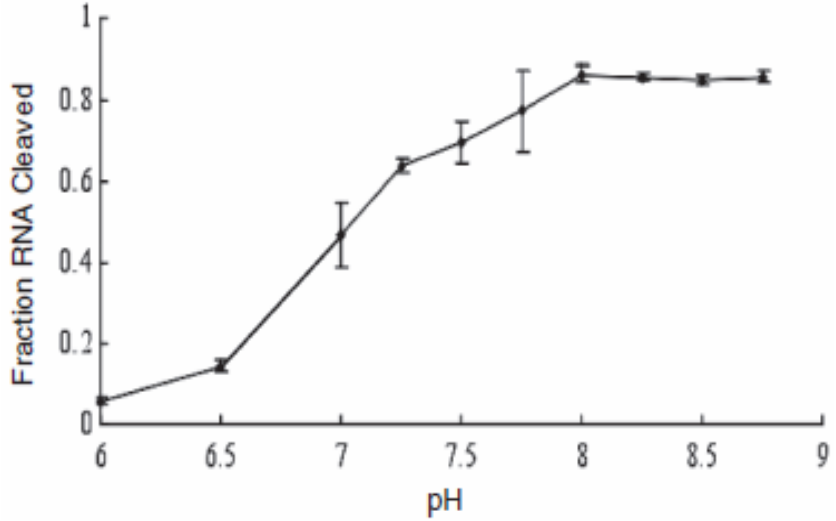
Fraction RNA Cleaved
1
0.8
0.6
0.4
0.2
0
6
6.5
7
7.5
8
8.5
9
pH

Figure 17. Salt and pH dependence of Aa-RNase III catalytic activity (Shi *et al*., 2011).

A. Salt dependence of catalytic activity. Cleavage reactions were performed in duplicate using internally ^{32}P-labeled Aa-16S[hp] RNA (100 nM) and Aa-RNase III (20 nM), in buffer containing 10 mM $MgCl_2$, 30 mM Tris–HCl (pH 8.0) and the specified salt at the indicated concentration. Reactions were incubated at 40°C for 1 min. The fraction of substrate cleaved was plotted as a function of salt concentration. Symbols represent the average values, with maximum errors shown. Open triangles represent NH_4^+, open squares represent Na^+, and open diamonds represent K^+.

B. pH dependence of catalytic activity. Reactions were performed in duplicate, using internally ^{32}P-labeled Aa-16S[hp] RNA (100 nM), Aa-RNase III (20 nM), 50 mM NaCl, 10 mM $MgCl_2$, and 30 mM Tris–HCl adjusted to the indicated pH. Reactions were incubated for 1 min at 40°C. The fraction of substrate cleaved was plotted as a function of pH. Maximum errors are shown for the averaged data points.

measuring the extent of Aa-16S[hp] RNA cleavage at pH values between 6 and 9, and in the presence of 30 mM Tris, 10 mM Mg^{2+} and 50 mM Na^{+}. The fraction of substrate cleaved as a function of pH is shown in Figure 17B, which reveals a transition to maximal activity between pH 6 and 9. The shape of the transition suggests the generation of a more active form of the enzyme by deprotonation of one or more groups with an average apparent pK_a of ~7.0. Based on these results, NaCl (50mM) and a pH of 8 were incorporated as features of the standard reaction.

3.1.2.2.3 Thermostability of Aa-RNase III catalytic activity

We determined the temperature dependence of Aa-RNase III catalytic activity using Aa-16S[hp] RNA as substrate. Ec-RNase III was included for comparison, and the same substrate was used in order to avoid any substrate-dependence of the temperature-reactivity profile. Reactions were initiated by adding RNase III at the specified temperature, then quenched with excess EDTA, and aliquots subjected to polyacrylamide gel electrophoresis, followed by phosphorimaging. The fraction of substrate cleaved was determined by ImageQuant analysis of the phosphorimages. To minimize any temperature-dependent changes in buffer pK, the pH was adjusted to 8.0 at each temperature used in the assay. Figures 18A and B show phosphorimages of the experiments with Aa-RNase III and Ec-RNase III, respectively. The data are graphically summarized in Figure 18C. Aa-RNase III activity increased from 35°C, reaching a maximum at ~70°C, and with significant activity exhibited up to ~85°C. In contrast, Ec-RNase III exhibited a lower temperature range for optimal activity, with essentially all activity lost by ~60–65°C. We conclude that Aa-RNase III catalytic activity exhibits substantial thermostability compared to that of Ec-RNase III. The possible origins of thermostability are considered below (see Discussion).

A

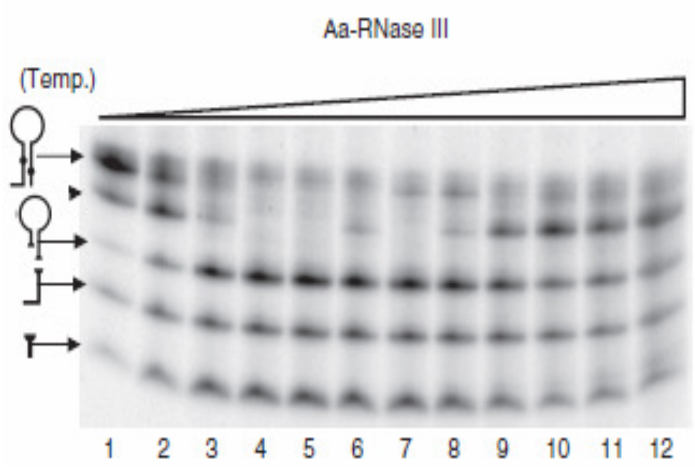
Aa-RNase III
(Temp.)
1 2 3 4 5 6 7 8 9 10 11 12

B

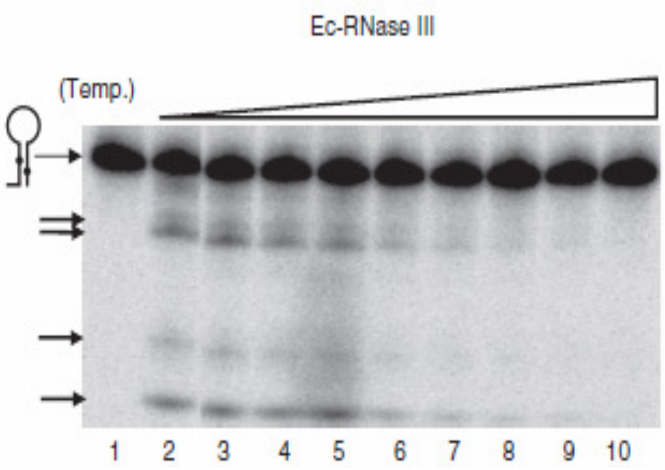
Ec-RNase III
(Temp.)
1 2 3 4 5 6 7 8 9 10

C

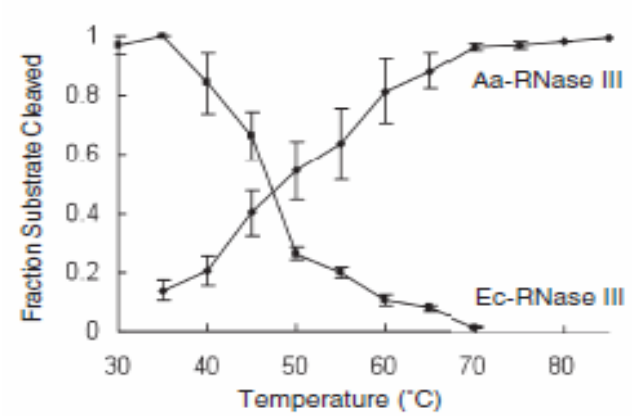
Fraction Substrate Cleaved
1
0.8
0.6
0.4
0.2
0
30 40 50 60 70 80
Temperature (˚C)
Aa-RNase III
Ec-RNase III

Figure 18. Temperature dependence of Aa-RNase III catalytic activity (Shi *et al.*, 2011).

A. Temperature dependence of Aa-RNase III cleavage of Aa-16S[hp] RNA. Reactions were performed in duplicate, and involved internally ^{32}P-labeled Aa-16S[hp] RNA (100 nM) and Aa-RNase III (20 nM) in 50 mM NaCl, 10mM $MgCl_2$ and 30 mM Tris–HCl (pH 8.0). The Tris buffer was adjusted to pH 8 at each temperature used in the experiment. Reactions were incubated for 1 min at the specified temperature. Lanes 1–12 show reactions performed at temperatures of 30, 35, 40, 45, 50, 55, 60, 65, 70, 75, 80 and 85°C, respectively. The figures on the left indicate the positions of the substrate and the three products. The arrowhead indicates the product of cleavage of only one of the two scissile phosphodiesters.

B. Temperature dependence of Ec-RNase III cleavage of Aa-16S[hp] RNA. Experimental conditions were the same as in Figure 17A. Lanes 2–10 show reactions carried out at 30, 35, 40, 45, 50, 55, 60, 65 and 70°C, respectively. Lane 1 represents RNA directly subjected to electrophoresis without prior incubation. The position of Aa-16S[hp] RNA is indicated, along with those cleavage products that differ in size from the ones produced by Aa-RNase III, as shown in Figure 17A.

C. Graphic comparison of the temperature dependence of the catalytic activities of Aa-RNase III and Ec-RNase III. Points represent average values of duplicate experiments, and maximum errors are shown.

3.1.2.2.4 Divalent metal ion dependence of Aa-RNase III catalytic activity

Structural (Gan *et al*., 2008) and biochemical (Sun *et al*., 2005) studies of Aa-RNase III and Ec-RNase III, respectively, have identified a two-metal-ion catalytic mechanism. Ec-RNase III can use several different divalent metal ions, with Mg^{2+} supporting optimal activity (Dunn, 1982). We examined the ability of Mg^{2+}, Mn^{2+}, Ni^{2+}, Co^{2+} and Ca^{2+} to support Aa-RNase III catalytic activity, using Aa-23S[hp] RNA as substrate. Short reaction times were applied to limit the extent of the reaction, thus allowing a more accurate assessment of the metal ion dependence. Cleavage assays (Figures 19A and B) show that both Mg^{2+} and Mn^{2+} support catalytic activity to comparable extents. In addition, the similar pattern of cleavage of the internally ^{32}P-labeled RNA indicates that the same target site is recognized in the presence of either metal. However, higher Mn^{2+} concentrations caused the appearance of several additional products (Figure 19B). Quantitative analysis (Figure 19C) shows that maximal activity is achieved at a ~4 mM concentration of either Mg^{2+} or Mn^{2+}, while Co^{2+} supports only a minor level of activity. Neither Ni^{2+} nor Ca^{2+} support catalytic activity over the concentration range examined (data not shown). Based on these results, Mg^{2+} at a 10 mM concentration was selected as a standard reaction component.

3.1.2.2.5 Determination of Aa-RNase III•substrate complex stability

Gel mobility shift assays were performed to assess whether target site selectivity and processing efficiency are related to formation and stability of a specific enzyme-substrate complex. Ca^{2+} was substituted for Mg^{2+}, which for Ec-RNase III was shown to stabilize the enzyme–substrate complexes (Li and Nicholson, 1996). Ca^{2+} moreover does not support Aa-RNase III catalytic activity (see above). Figures 20A and B show that 5'-^{32}P-labeled Aa-16S[hp] and Aa-23S[hp] RNA each bind

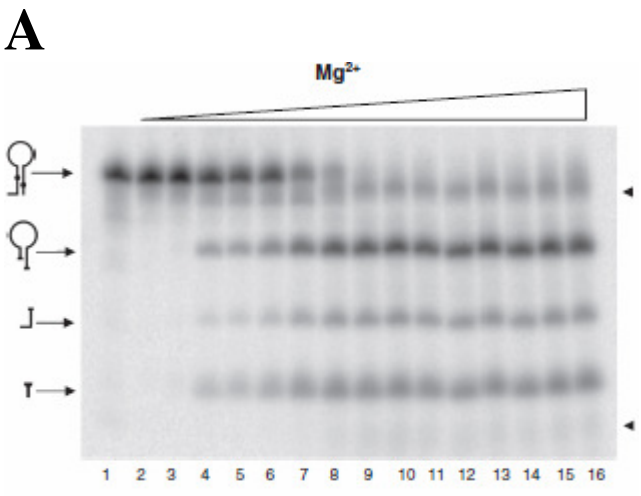
A
Mg2+
1 2 3 4 5 6 7 8 9 10 11 12 13 14 15 16

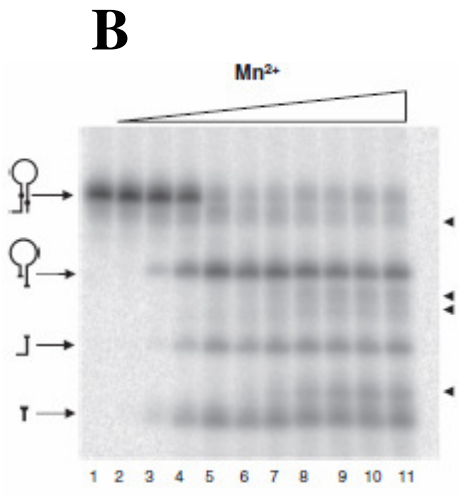
B
Mn2+
1 2 3 4 5 6 7 8 9 10 11

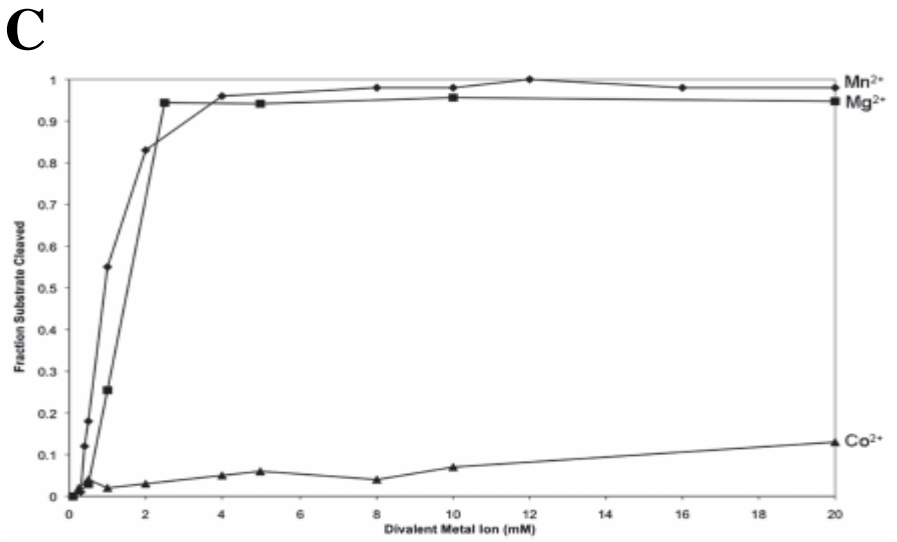
C
Fraction Substrate Cleaved
Divalent Metal Ion (mM)
Mn2+
Mg2+
Co2+
0 0.1 0.2 0.3 0.4 0.5 0.6 0.7 0.8 0.9 1
0 2 4 6 8 10 12 14 16 18 20

Figure 19. Divalent metal ion dependence of Aa-RNase III catalytic activity (Shi *et al*., 2011).

Internally ^{32}P-labeled Aa-23S[hp] RNA (100 nM) was incubated with Aa-RNase III (30 nM) at 45°C for 2 min in the standard reaction buffer, containing the specified divalent metal ion at the indicated concentration. Reactions were stopped with EDTA and aliquots electrophoresed in a denaturing 15% polyacrylamide gel as described in Materials and Methods.

A. Dependence of catalytic activity on the Mg^{2+} concentration. Lanes 2–16 show reactions using $MgCl_2$ concentrations of 0.1, 0.2, 0.3, 0.4, 0.5, 1, 2, 4, 8, 10, 12, 16, 20, 30 and 50 mM, respectively. Lane 1 shows a 2 min reaction in the absence of Mg^{2+}. The positions of the substrate and the three products of cleavage are indicated by the the figures on the left. The arrowhead on the upper right indicates a cleavage-resistant species, most likely an unreactive conformation of substrate. The arrowhead on the lower right indicates a low-level product appearing at higher Mg^{2+} concentrations.

B. Dependence of catalytic activity on the Mn^{2+} concentration. Lanes 2–11 show reactions using $MnCl_2$ concentrations of 0.1, 0.5, 1.0, 2.5, 5, 10, 20, 40, 80, and 100 mM, respectively. Lane 1 represents a 2 min reaction in the absence of Mn^{2+}. The figures on the left indicate the positions of substrate and the three products. The arrowheads on the right side of the gel indicate low-level cleavage products generated at higher Mn^{2+} concentrations.

C. Graphic analysis of the divalent metal ion dependence. The fraction of Aa-23S[hp] RNA cleaved was plotted as a function of divalent metal ion concentration. The Mg^{2+} dependence is indicated by squares, Mn^{2+} by diamonds, and Co^{2+} by triangles.

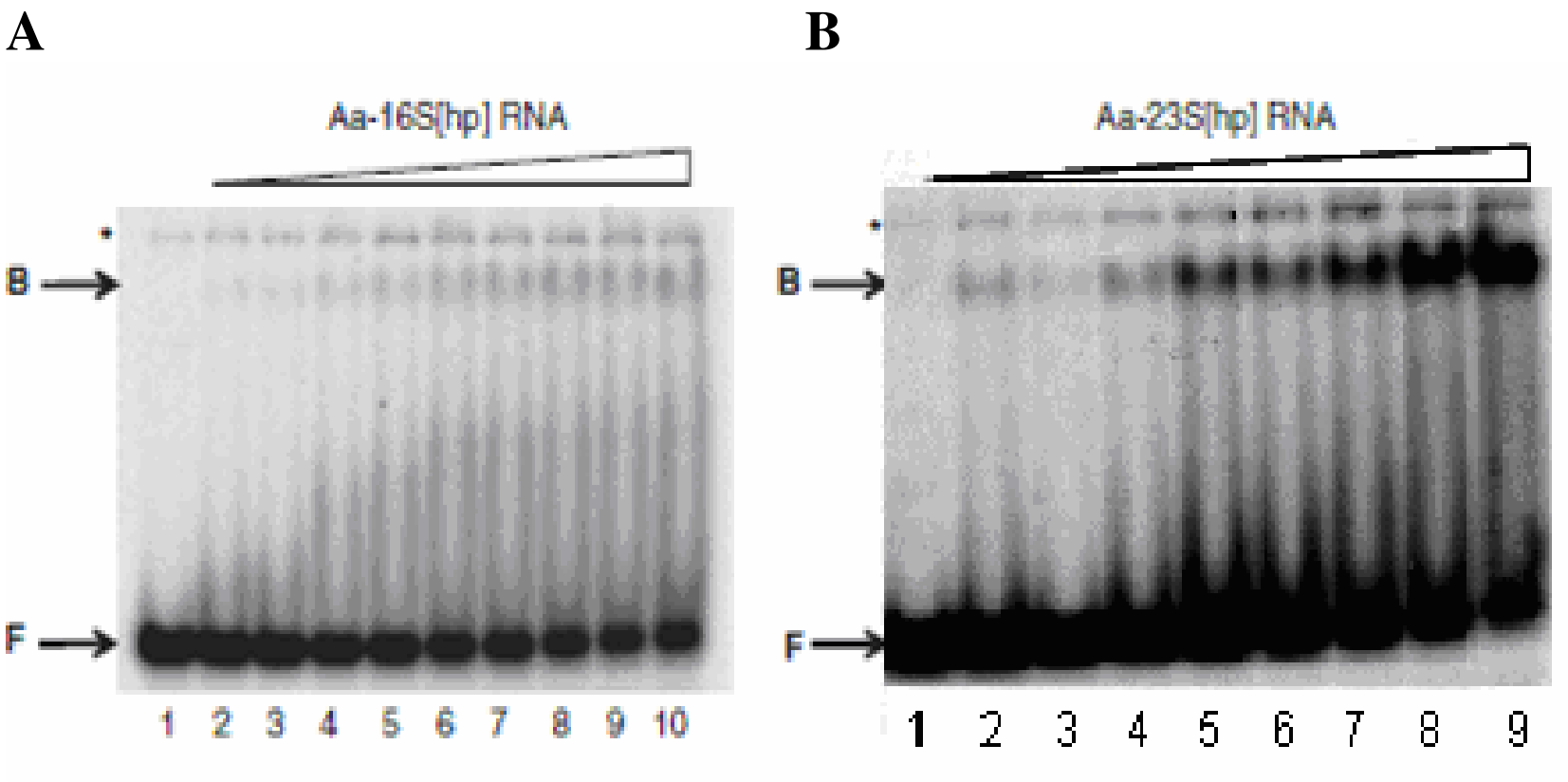
A
Aa-16S[hp] RNA
B
F
1 2 3 4 5 6 7 8 9 10
B
Aa-23S[hp] RNA
B
F
1 2 3 4 5 6 7 8 9

C

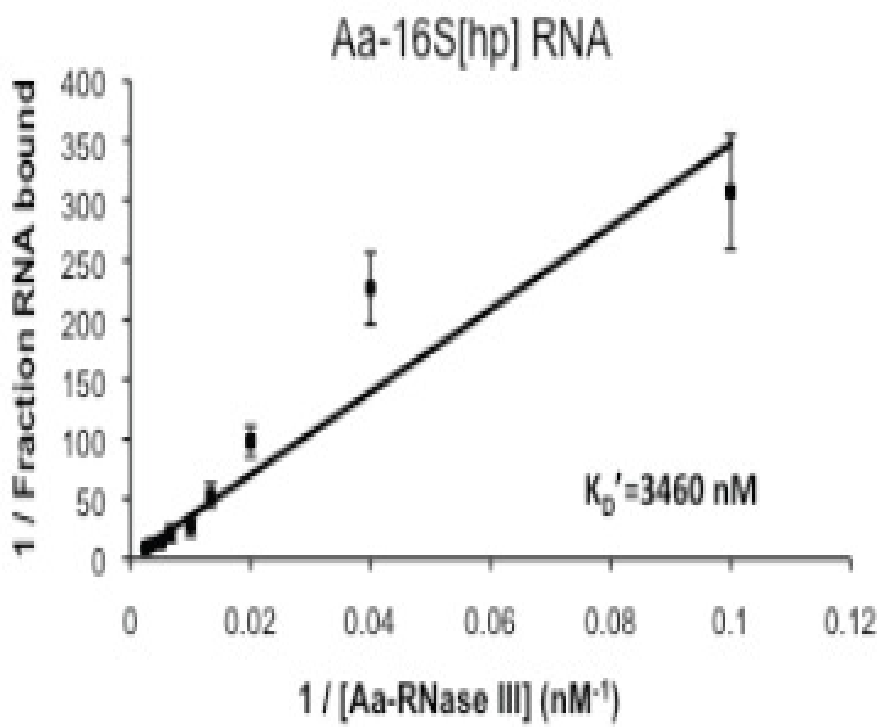
Aa-16S[hp] RNA
1 / Fraction RNA bound
400
350
300
250
200
150
100
50
0
0
0.02
0.04
0.06
0.08
0.1
0.12
K_D'=3460 nM
1 / [Aa-RNase III] (nM^{-1})

D

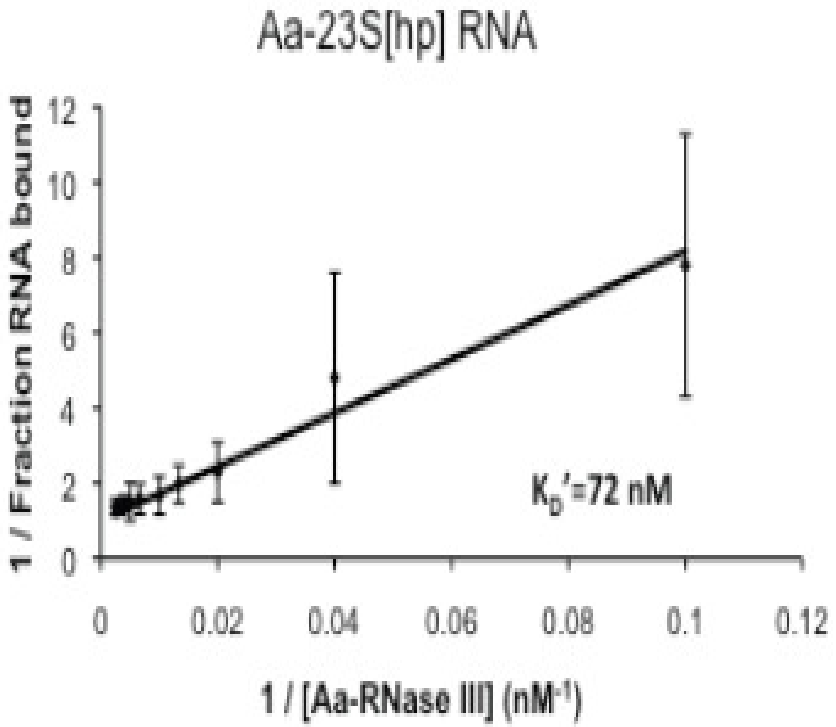
Aa-23S[hp] RNA
1 / Fraction RNA bound
12
10
8
6
4
2
0
0
0.02
0.04
0.06
0.08
0.1
0.12
K_D'=72 nM
1 / [Aa-RNase III] (nM^{-1})

Figure 20. Aa-RNase III binding affinities of small hairpin RNAs based on the Aquifex pre-16S and pre-23S rRNA processing stems (Shi *et al*., 2011).

A. Gel shift assay of Aa-RNase III binding to Aa-16S[hp] RNA. 5'-^{32}P-labeled RNA (10^4 dpm) was incubated with the specified amount of Aa-RNase III in binding buffer and electrophoresed in an 8% polyacrylamide gel containing 0.5×TBE buffer, 5 mM $CaCl_2$ and 2.5% (v/v) glycerol. Lanes 1–10 represent binding reactions containing 0, 10, 25, 50, 75, 100, 150, 200, 300 and 400 nM of Aa-RNase III (dimer concentration), respectively. 'F' and 'B' indicate the positions of free and protein-bound forms of the RNA, respectively. The asterisk indicates the origin of electrophoresis.

B. Gel shift assay of Aa-RNase III binding to 5'-^{32}P-labeled Aa-23S[hp] RNA. Lanes 1–9 show reactions containing 0, 3, 5, 10, 25, 50, 100, 200 and 400 nM Aa-RNase III, respectively. 'F' and 'B' indicate positions of free and bound forms of the RNA, respectively. The asterisk indicates the origin of electrophoresis

C. Quantitative analysis of Aa-RNase III binding to Aa-16S[hp] RNA. The fraction of substrate bound by Aa-RNase III was determined by taking into account the partial dissociation of the enzyme-RNA complex during electrophoresis. The reciprocal of the fraction of substrate bound was plotted as a function of the reciprocal of the protein concentration, and the slope (K'_D) determined according to Equation 8. The K'_D is 3.5 ± 0.5 μM.

D. Quantitative analysis of Aa-23S[hp] RNA binding to Aa-RNase III. The K'_D is 72 ± 40 nM.

Aa-RNase III, forming complexes with reduced electrophoretic mobility. The observation of a single complex is in accord with a single target site for each RNA. The K'_D value for each complex was determined by quantitative analysis of the gel shift assays. The values are 3.5 μM for the Aa-RNase III•16S[hp] RNA complex, and 72 nM for the Aa-RNase III•23S[hp] RNA complex (Figures 20 C and D). The larger K'_D value for the Aa-16S[hp] RNA complex is reflected in the comparatively lower reactivity of the RNA (Figure 16E).

3.1.2.2.6 A minimum substrate, based on Aa-16S[hp] RNA, used for K_m and k_{cat} determination

The reactivities of Ec-RNase III substrates are determined in part by sequences within the proximal box (pb) and distal box (db) (Zhang and Nicholson, 1997; Pertzev and Nicholson, 2006). Crystallographic studies of Aa-RNase III bound to cleaved hairpin RNAs (Gan *et al*., 2006; Gan *et al*., 2008) showed that the pb and db, as well as an additional 2-bp segment termed the middle box (mb), are sites of protein contact (Figure 3). The structural data therefore suggest that the bp sequences within the three boxes may influence reactivity of Aa-RNase III substrates. To examine this possibility, a minimal hairpin substrate (Aa-16S[μ-hp] RNA; Figure 21A) was designed, according to a previous strategy (Pertzev and Nicholson, 2006). The utilization of a single scissile bond in this substrate would simplify K_m and k_{cat} determine, since only one chemical step would occur. The 3'-end of Aa-16S[μ-hp] RNA corresponds to the 3'-end-proximal cleavage site of Aa-16S[hp] RNA, and retains the 5'-end-proximal cleavage site. Although full-length Aa-16S[hp] RNA (Figure 6B) containing an A–C pair adjacent to the 3' cleavage site is reactive, the presence of the A–C pair in Aa-16S[μ-hp] RNA inhibited cleavage (data not shown). Therefore, the A–C pair was changed to an A–U pair, in order to provide a reactive version of Aa-16S[μ-hp] RNA.

A

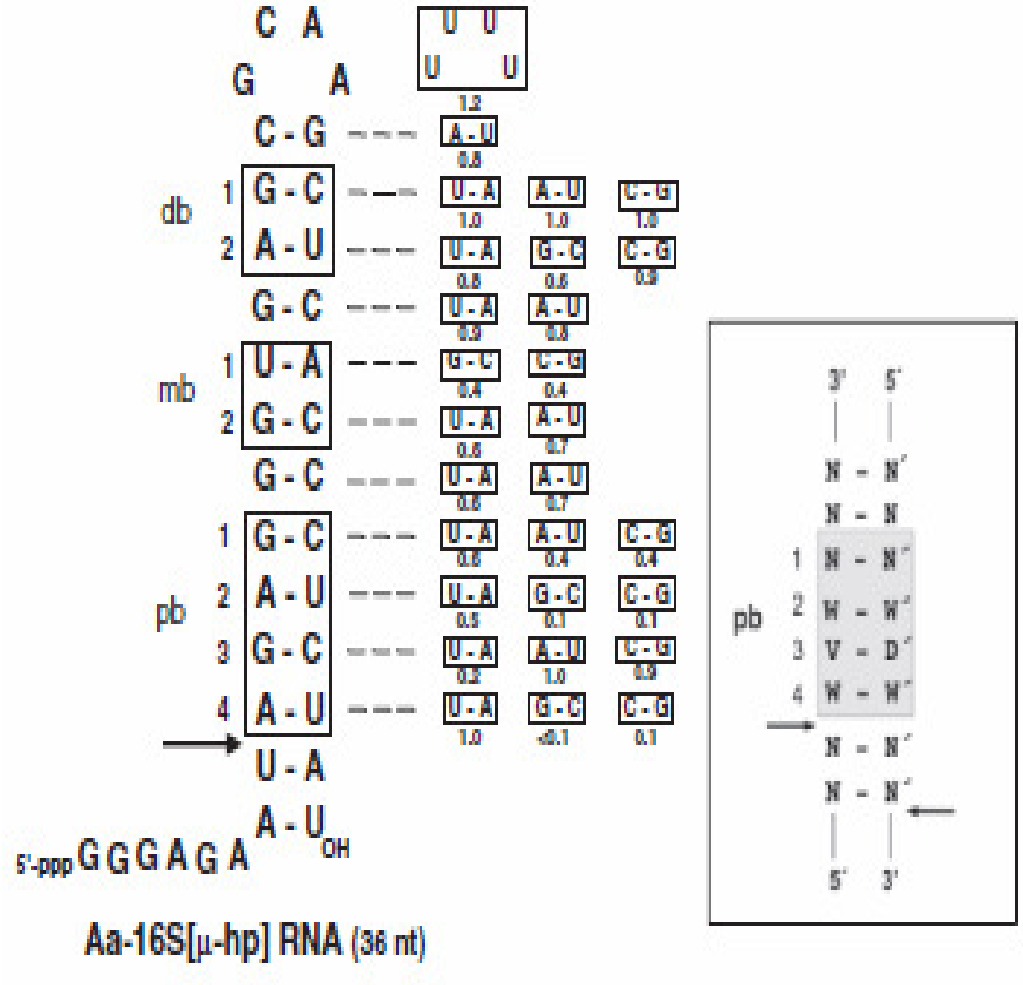
C A
U U
U U
G A
C - G
A - U
db
1 G - C
2 A - U
G - C
mb
1 U - A
2 G - C
G - C
pb
1 G - C
2 A - U
3 G - C
4 A - U
U - A
A - U
5'-ppp G G G A G A
OH
Aa-16S[μ-hp] RNA (36 nt)
3' 5'
N - N'
N - N
pb
1 N - N'
2 N - N'
3 V - D'
4 W - W'
N - N'
N - N'
5' 3'

B

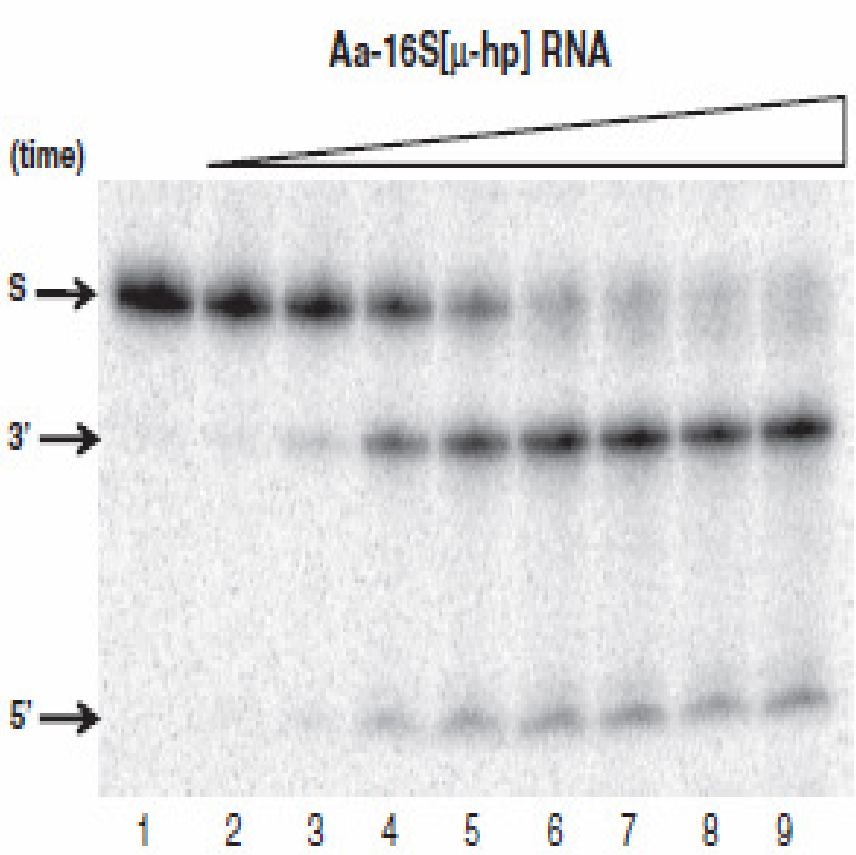
Aa-16S[μ-hp] RNA
(time)
S
3'
5'
1 2 3 4 5 6 7 8 9

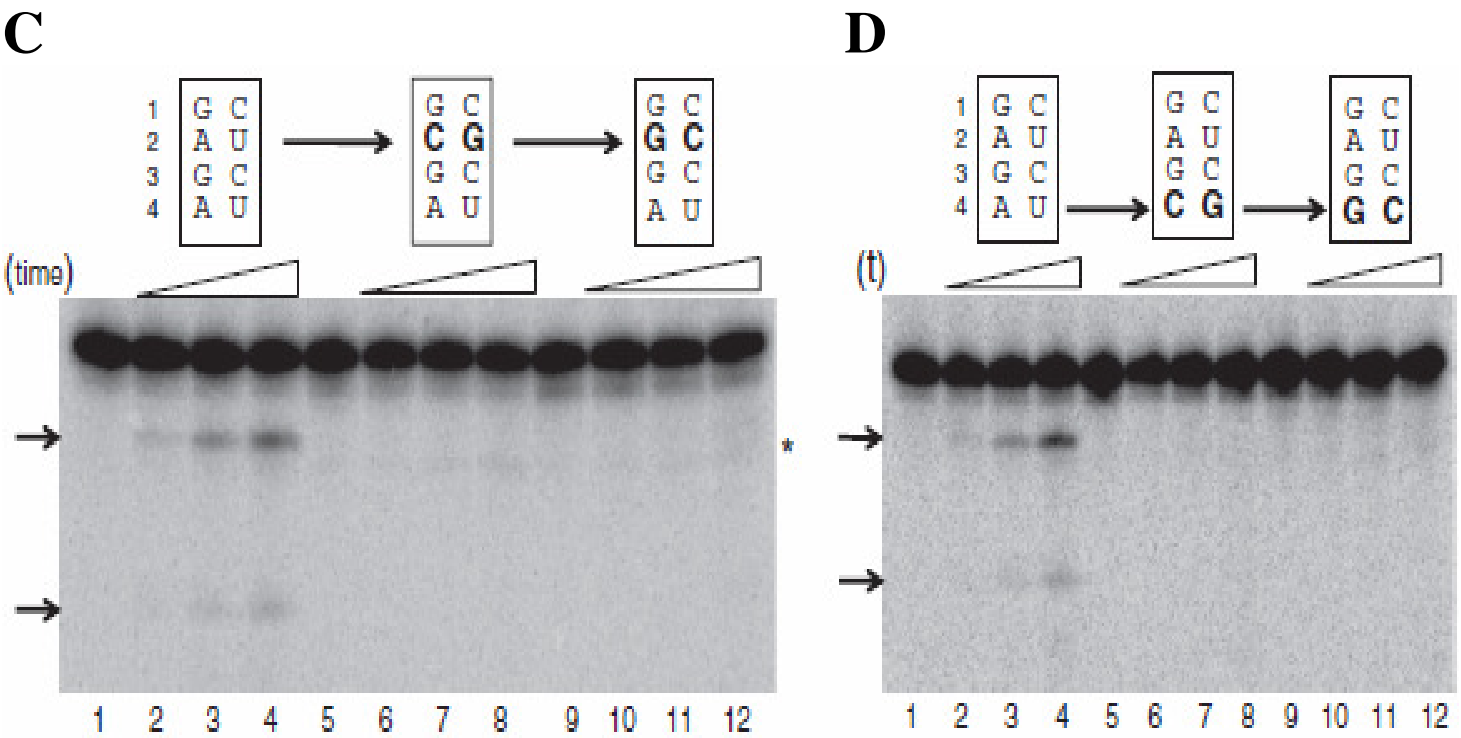
C
D
1 G C
2 A U
3 G C
4 A U
(time)
(t)
*
1 2 3 4 5 6 7 8 9 10 11 12

Figure 21. Base-pair sequence dependence of reactivity of a minimal substrate of Aa-RNase III (Shi *et al*., 2011).

A. Structure of Aa-16S[μ-hp] RNA. The arrow indicates the site of cleavage by Aa-RNase III. Also shown are the positions of the distal box (db), middle box (mb) and proximal box (pb). The base pair substitutions in the variants and the corresponding relative reactivities are displayed to the right. Inset: Proposed preferred sequence for the proximal box**.** N-N', any of the 4 standard Watson-Crick (WC) bp; W-W', AU or UA bp; V, G/C/A; D', G/U/A which can form a WC bp with V.

B. Time courses of cleavage of Aa-16S[μ-hp] RNA by Aa-RNase III (internally ^{32}P-labeled RNA, 100 nM; Aa-RNase III, 30 nM; reaction temperature, 65°C). Lanes 2–9 represent 0.5, 1, 2, 3, 5, 7.5 10 and 20 min time points, respectively. Lane 1 represents incubation of RNA in reaction buffer without enzyme for 20 min. 'S' represents substrate, and 3' and 5' denote the cleavage products containing the substrate 3' end and 5' end, respectively.

C. Time courses of cleavage of Aa-16S[μ-hp] RNA variants with a CG or GC bp substitution at pb position 2. Reactions involved internally ^{32}P-labeled RNA (500 nM) and Aa-RNase III (10 nM), in 50 mM NaCl, 10 mM $MgCl_2$, 30 mM Tris–HCl (pH 8.0), and were incubated at 30°C. Lanes 2–4, 6–8 and 10–12 represent 1, 2 and 5 min reaction times for Aa-16S[μ-hp] RNA and the 2-bp variants (sequences of the respective proximal boxes are shown above the image). In lanes 1, 5 and 9, RNA was combined with reaction buffer without enzyme, then immediately followed by addition of excess EDTA. Arrows indicate the two cleavage products. The asterisk indicates a minor product of nonenzymatic cleavage, observed in lanes 5–12.

D. Time courses of cleavage of Aa-16S[μ-hp] RNA variants with a CG or GC bp substitution at pb position 4. The proximal box sequences of the Aa-16S[μ-hp] RNA variants are shown above the gel images.

A time course assay of cleavage (Figure 21B) reveals that the RNA is cleaved at a single site, as predicted. Since the longer product comigrates with the largest product of Aa-16S[hp] RNA cleavage, which is a shortened hairpin, the Aa-16S[μ-hp] RNA cleavage site corresponds to the 5'-end-proximal cleavage site of Aa-16S[hp] RNA. The K_m and k_{cat} values were determined by measuring the initial rate as a function of substrate concentration, and fitting the observed dependence to a Michaelis–Menten kinetic scheme (Figure 22). For Aa-[16Sμ-hp] RNA, the K_m is 98 nM and the k_{cat} is 2.7 min^{-1}, thereby providing a catalytic efficiency (k_{cat}/K_m) of 2.8×10^7 min^{-1} M^{-1} (at 40°C).

3. 2 Assessing Aa-RNase III-substrate interactions

3.2.1 Base-pair sequence control of Aa-RNase III substrate reactivity

Single, standard (Watson-Crick [WC]) base-pair substitutions were introduced in Aa-16S[μ-hp] RNA at each position between the cleavage site and the terminal tetraloop. An additional variant possessed an altered tetraloop sequence (GCAA → UUUU). The initial rates of cleavage were measured using a high substrate/enzyme ratio (multiple-turnover conditions), and the relative reactivities were calculated as the ratio of the initial rate of cleavage of a given variant to that of Aa-16S[μ-hp] RNA. The relative reactivities are provided below the bp substitutions in Figure 21A. Substitutions having significant effects were identified as those that reduced the relative reactivity to <0.5. Based on this criterion, the greatest inhibitory effects were seen with specific bp substitutions within the proximal box. Thus, an AU→CG or GC bp change at pb position 2 or 4 caused a 10-fold reduction in reactivity (Figures 21C and D, respectively), while a GC→UA substitution at pb position 3 caused a 5-fold reduction in reactivity (Figure 21A). In contrast, substitutions in the db had negligible effects on reactivity, while substitutions within the mb had only moderate effects

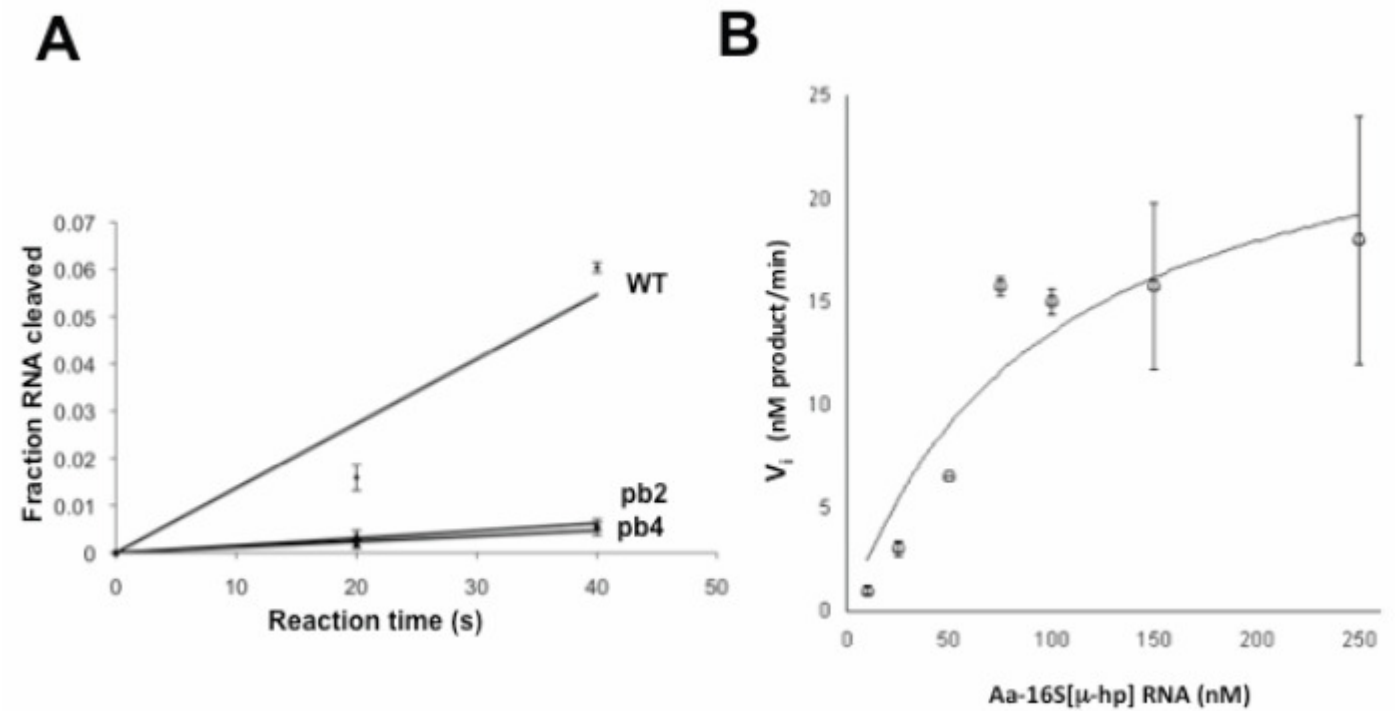
A
Fraction RNA cleaved
0.07
0.06
0.05
0.04
0.03
0.02
0.01
0
0
10
20
30
40
50
Reaction time (s)
WT
pb2
pb4
B
V_i (nM product/min)
25
20
15
10
5
0
0
50
100
150
200
250
Aa-16S[μ-hp] RNA (nM)

Figure 22. Determination of initial velocities of cleavage of Aa-16S[μ-hp] RNA and specific sequence variants, and determination of K_m and V_{max} (Shi *et al.*, 2011).

A. Initial rates of cleavage of Aa-16S[μ-hp] RNA ("WT") and two variants: (i) AU→GC at pb position 2 ("pb2") and (ii) AU→GC substitution at pb position 4 ("pb4"). Reactions were carried out in duplicate at 40°C in buffer consisting of 50 mM NaCl, 10 mM $MgCl_2$, 30 mM Tris-HCl (pH 8.0), Aa-RNase III (10 nM), and internally ^{32}P-labeled RNA (500 nM). At least three time points were taken; the graph shows the two shortest of the three time points taken for wt substrate and two variants, within which <20% of the substrate was converted to product.

B. Plot of initial rate (Vi) of Aa-16S[μ-hp] RNA cleavage as a function of RNA concentration. The initial rate of Aa-16S[μ-hp] RNA cleavage was determined in duplicate as shown in panel A, using the experimental conditions described in the text.

(Figure 21A). There also is no strict dependence of reactivity on the tetraloop sequence (Figure 21A). We conclude that the pb is the primary determinant of reactivity for the Aa-RNase III pre-rRNA substrate, with pb positions 2, 3 and 4 playing a dominant role. The sequences in the pb which confer optimal reactivity are summarized in the inset in Figure 21. The origin of the bp dependence at pb position 2 is investigated further below.

3.2.2 Interaction of the Aa-RNase III dsRBD α_1 helix with the substrate proximal box

The consensus sequence for RBM1 is Dx**K**(T/S)x**LQ**ExxQ (Figure 7B) [residues that are invariant in ~300 bacterial Class 1 RNases III (Gan *et al*., 2006) are shown in bold-face]. A key interaction of Aa-RNase III with its cognate substrates involves a network of hydrogen bonds between conserved residues in the N-terminal region of the α_1 helix of the dsRBD and the substrate proximal box (pb) (Figure 7D) (Gan *et al*., 2006; Gan *et al*. 2008). To assess the contribution of each hydrogen bond towards substrate binding affinity and selectivity, a set of Aa-RNase III point mutants was created in which each potentially interacting residue was changed to alanine (Table 2). Alanine substitution allows assessment of the contribution of individual hydrogen bonds by a "loss-of-contact" approach (Ebright, 1985), while minimizing potential disruption of protein secondary structures (Wells, 1991). The Aa-RNase III mutants D151A, K153A, T154A, Q157A, E158A and Q161A were purified from an *E. coli* expression host as described (Shi *et al*., 2011). None of the mutations affect folding or stability in a significant manner, since (i) all the mutant proteins were efficiently overexpressed in soluble form, and (ii) the circular dichroism spectrum of each mutant was essentially identical with that of Aa-RNase III (Figure 14). Two cognate substrates, Aa-16S[hp] RNA and Aa-23S[hp] RNA (Figure 6) were used to assess the

catalytic activities of the Aa-RNase III mutants. Both substrates are cleaved at single target sites, but Aa-16S[hp] RNA is less reactive than Aa-23S[hp] RNA, presumably reflecting the absence of a full complement of RNase III contact sites (Figure 16E; Figure 20A,B). Using two substrates of differing reactivity could therefore provide complementary information on the functional consequences of mutational alteration of RBM1-substrate contacts. To evaluate RNA functional group contributions to substrate binding, site-specific 2'-deoxyribose or nucleobase mutations were introduced in the proximal box of the minimal substrate, Aa-16S[μ-hp] RNA.

3.2.2.1 Functional analysis of a highly conserved glutamine in the α_1 helix

The residue Q157 within the N-terminal portion of the α_1-helix of the dsRBD of Aa-RNase III (Figure 7B) is invariant among 100 examined bacterial RNase III sequences (Gan *et al.*, 2008). This high conservation appears to be restricted to bacterial Class 1 RNase III family members, as it is not conserved in the fungal Class 1 RNase III orthologs (Wu *et al*., 2004; Leulliot *et al*., 2004; Figure 7C), and suggests a specific conserved role in recognition of cognate bacterial substrates. A crystallographic analysis of Aa-RNase III bound to a cleaved dsRNA (thus formally resembling a post-catalytic complex) (Gan *et al.*, 2006) showed that the Q157 side chain is engaged in two hydrogen bonds with the U of the UA bp at pb position 2 (Figure 23C, left). One hydrogen bond connects the Q157 carboxamide oxygen atom and the uridine 2'-OH group, while the second hydrogen bond involves the carboxamide amino group and the uracil O2 atom (Figure 23C, left). The strong conservation of the glutamine and the dependence of substrate reactivity on the bp identity at pb position 2 together suggest a functionally important interaction. To assess the functional importance, Q157 was changed to alanine. Time-course cleavage assays (Figure 23A) show that the Q157A mutant does not exhibit detectable catalytic

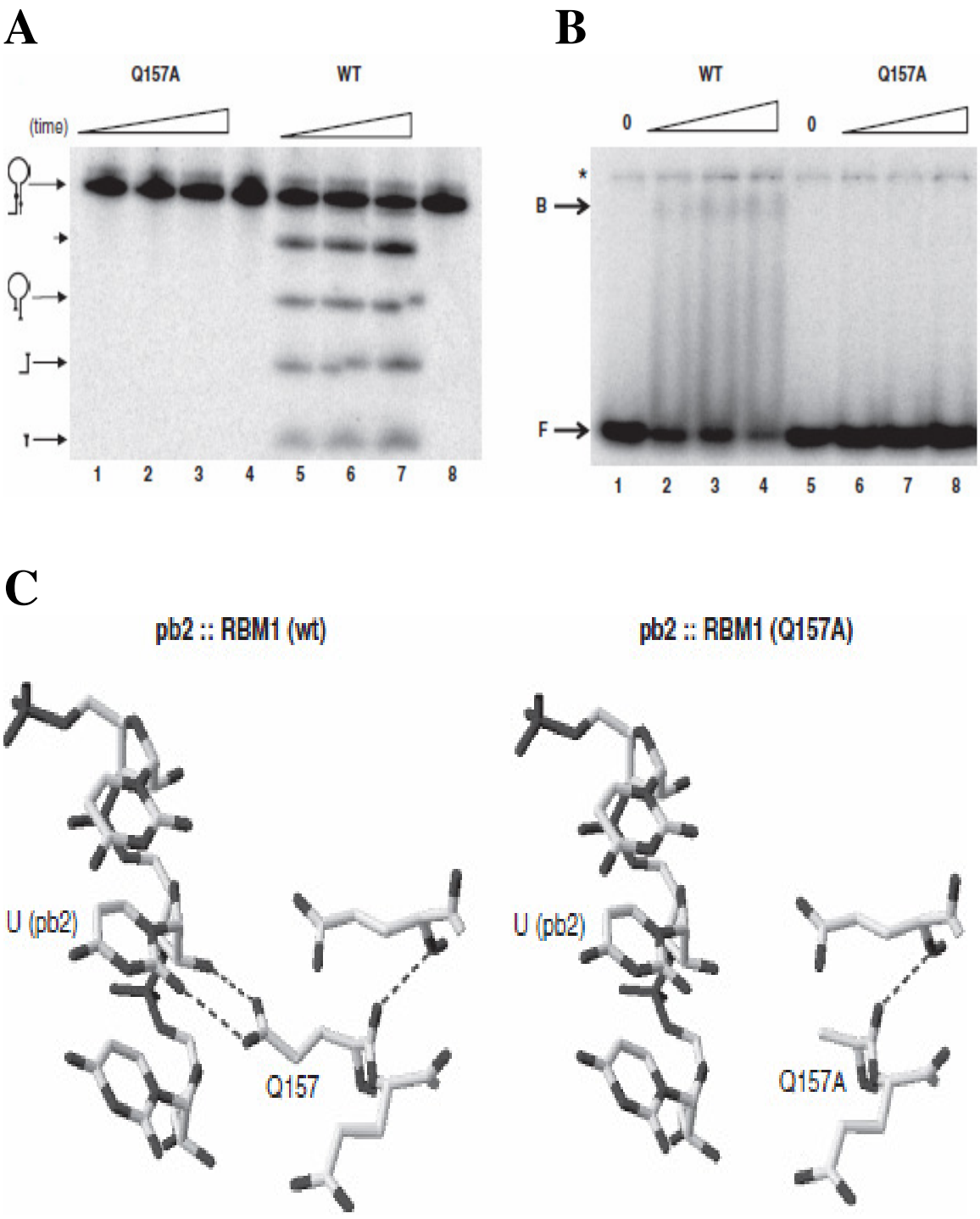
A
Q157A
WT
(time)
1 2 3 4 5 6 7 8
B
WT
Q157A
0
0
*
B
F
1 2 3 4 5 6 7 8
C
pb2 :: RBM1 (wt)
U (pb2)
Q157
pb2 :: RBM1 (Q157A)
U (pb2)
Q157A

Figure 23. The Q157 side chain has an important function in substrate binding (Shi *et al*., 2011).

A. Substrate cleavage time course assays of the Aa-RNase III Q157A mutant. Internally ^{32}P-labeled Aa-16S[hp] RNA (400 nM) was combined with the Q157A mutant or Aa-RNase III (10 nM) in reaction buffer consisting of 50 mM NaCl, 10 mM $MgCl_2$ and 30 mM Tris–HCl (pH 8.0). The reaction temperature was 30°C. Lanes 1–3, and 5–7 represent 10, 20 and 40 s reaction times for Q157A and Aa-RNase III, respectively. Lanes 4 and 8 show reactions that lacked Mg^{2+}, but were otherwise complete, and were incubated for 40 s. The figures on the left indicate the positions of the substrate and three cleavage products. The short arrow indicates the product of cleavage of a single phosphodiester at the target site. The slight disruption of two bands in lanes 6 and 7 reflect a physical discontinuity in the gel.

B. Gel shift assay of Aa-RNase III and the Q157A mutant binding to 5'-^{32}P-labeled Aa-16S[hp] RNA. Lanes 1–4, and lanes 5–8 show reactions containing 0, 100, 200 and 400 nM (dimer concentration) of Aa-RNase III or the Q157A mutant, respectively. The positions of free (F) and bound (B) RNA are indicated. The asterisk indicates the origin of electrophoresis.

C. Diagram, based on Figure 4B in Gan *et al*. (2006) (PDB code: 2EZ6) showing the interaction of the Q157 side chain of Aa-RNase III with the uridine at pb position 2. The Q157 side chain and uridine residue are shown, but the complementary adenine is not shown. The two hydrogen bonds are indicated by dotted lines, and involve the uracil O2 atom and the ribose 2'-OH group interacting with the Q157 carboxamide group.

activity, under conditions where Aa-RNase III efficiently processes Aa-16S[hp] RNA. A gel mobility shift assay (Figure 23B) reveals that the low catalytic activity of the Q157A mutant reflects a defect in substrate binding. In fact, the K'_D of the RNA-mutant enzyme complex was too large to be determined by this approach. We conclude that the Q157 interaction with the bp at pb position 2 is important for substrate binding.

A series of six variants of a shortened version of Aa-16S[hp] RNA were chemically synthesized, to further examine the pb-RBM1 interaction (Figure 24). The variants lacked 2'-OH groups at the positions that engage in hydrogen bonds with Aa-RNase III, based on the crystallographic analyses (Figure 3C; Figure 7D). These 2'-deoxyribose variants therefore provide a complementary assessment of the contribution of individual hydrogen bonds to processing reactivity. The dU_{30} variant (containing 2'-deoxyribose residue in the right strand at pb positions 2; Figure 24) showed the most severe effect on cleavage (retaining only a ~10% relative reactivity). This order of reactivity of the 2'-deoxy variants correlates with that of the corresponding alanine mutants (U at pb 2 with Q157; Table 3) and therefore further supports the important functional role of individual hydrogen bond in the RBM1-dsRNA interaction.

3.2.2.2 Interaction of Aa-RNase III RBM1 mutants with the pb of Aa-23S[hp] RNA

The Aa-RNase III RBM1 residues whose side chains contact specific functional groups in the pb include K153, T154, Q157, E158, and Q161 (Figure 7D). The K153 ε-amino group closely approaches a nonbridging oxygen atom of the phosphodiester between pb nt 4 and 3 on one strand. This interaction may therefore exhibit a largely ionic character (Figure 25). The T154 side chain hydrogen bonds with the 2'-OH

A

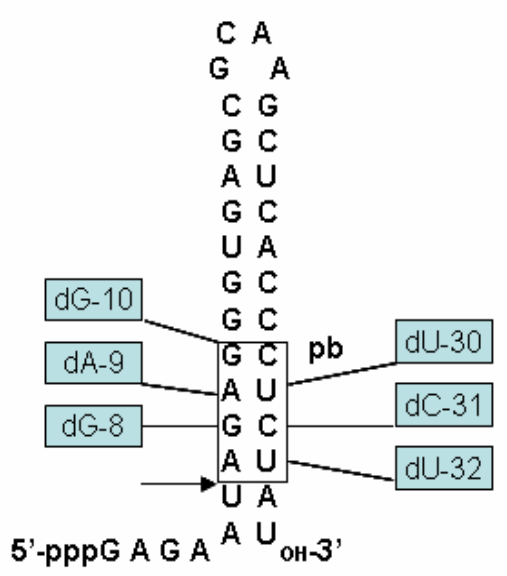
C A
G A
C G
G C
A U
G C
U A
G C
G C
G C
A U
G C
A U
U A
A U
dG-10
dA-9
dG-8
pb
dU-30
dC-31
dU-32
5'-pppG A G A
OH-3'

B

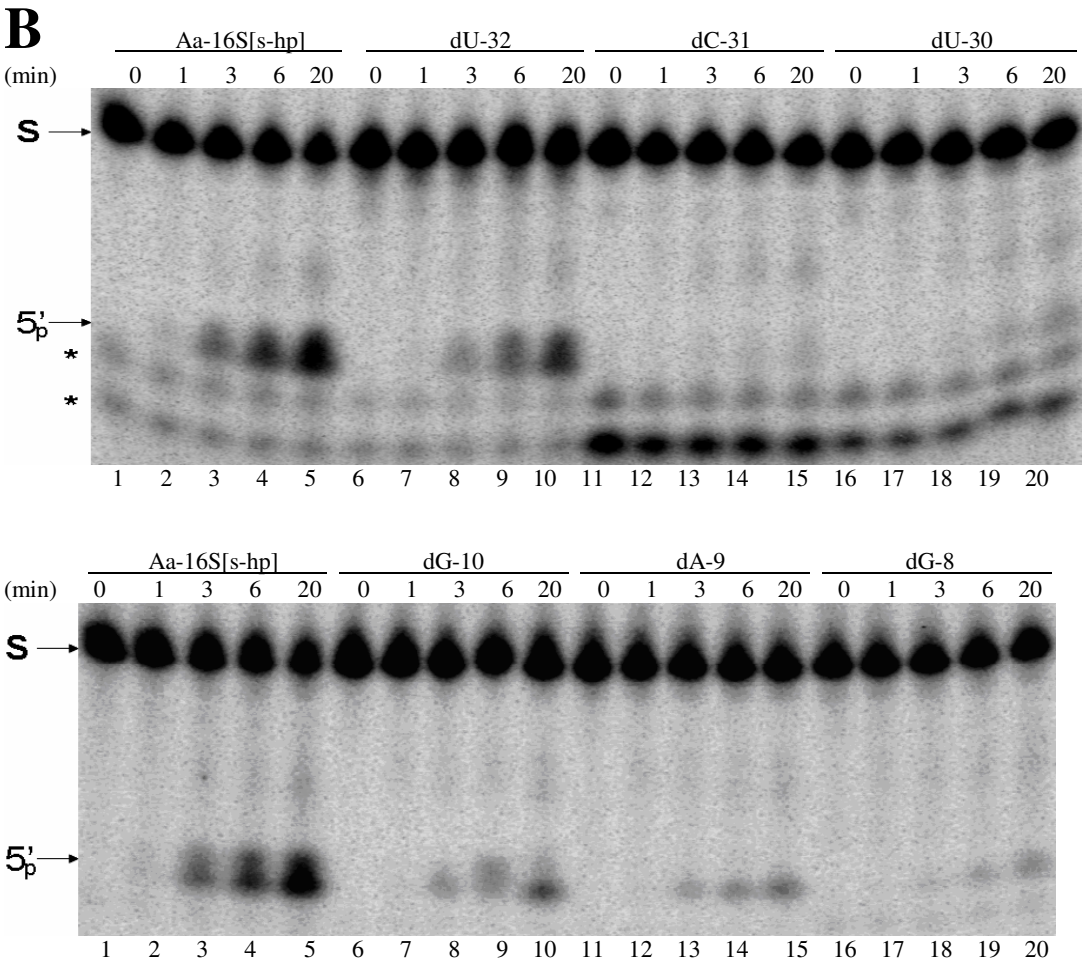
Aa-16S[s-hp]
dU-32
dC-31
dU-30
(min)
0 1 3 6 20 0 1 3 6 20 0 1 3 6 20 0 1 3 6 20
S
5'p
*
*
1 2 3 4 5 6 7 8 9 10 11 12 13 14 15 16 17 18 19 20
Aa-16S[s-hp]
dG-10
dA-9
dG-8
(min)
0 1 3 6 20 0 1 3 6 20 0 1 3 6 20 0 1 3 6 20
S
5'p
1 2 3 4 5 6 7 8 9 10 11 12 13 14 15 16 17 18 19 20

Figure 24. Aa-RNase III cleavage of 2'-deoxyribose variants of Aa-16S[s-hp] RNA.

A. Diagram of Aa-16S[s-hp] RNA, and specific 2'-deoxyribose variants. The arrow indicates the Aa-RNase III cleavage site.

B. Aa-RNase III cleavage of Aa-16S[s-hp] RNA and specific 2'-deoxyribose variants. Reactions were performed at 45°C in buffer containing 50 mM NaCl, 30 mM Tris-HCl (pH 8.0), and 10 mM Mg^{2+}. The Aa-RNase III concentration was 20 nM, and the RNA concentration was 150 nM. RNA was 5'-^{32}P-labeled (see Materials and Methods). The asterisks indicate non-enzymatic, nonspecific cleavage products.

A

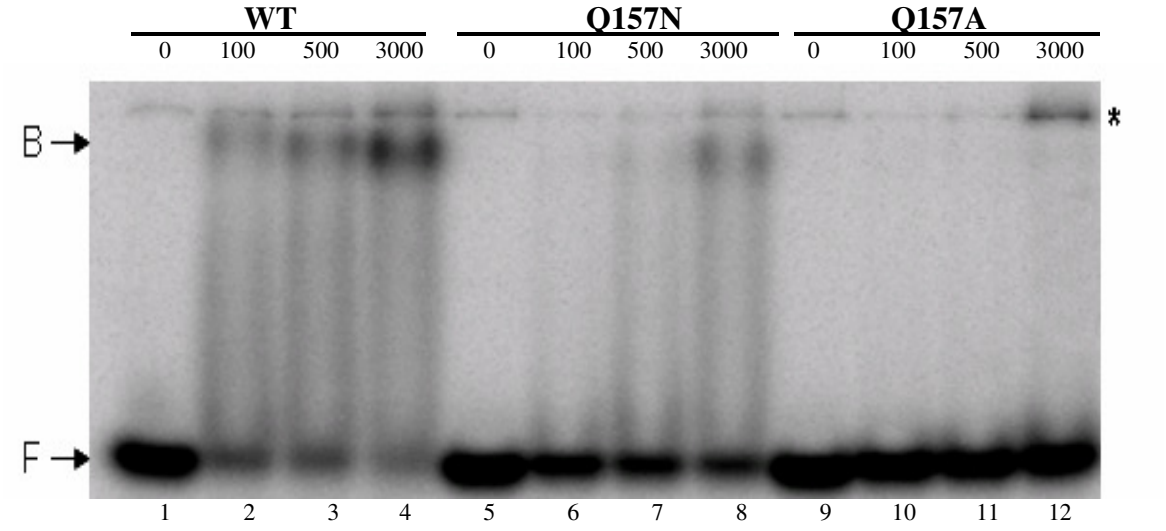
WT
Q157N
Q157A
0 100 500 3000 0 100 500 3000 0 100 500 3000
B
F
*
1 2 3 4 5 6 7 8 9 10 11 12

B

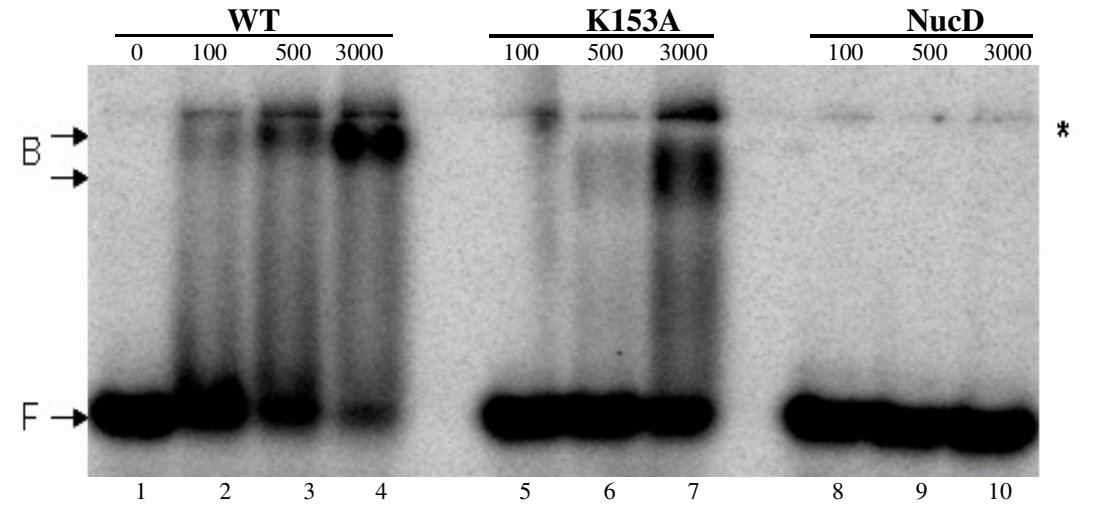
WT
K153A
NucD
0 100 500 3000 100 500 3000 100 500 3000
B
F
*
1 2 3 4 5 6 7 8 9 10

C

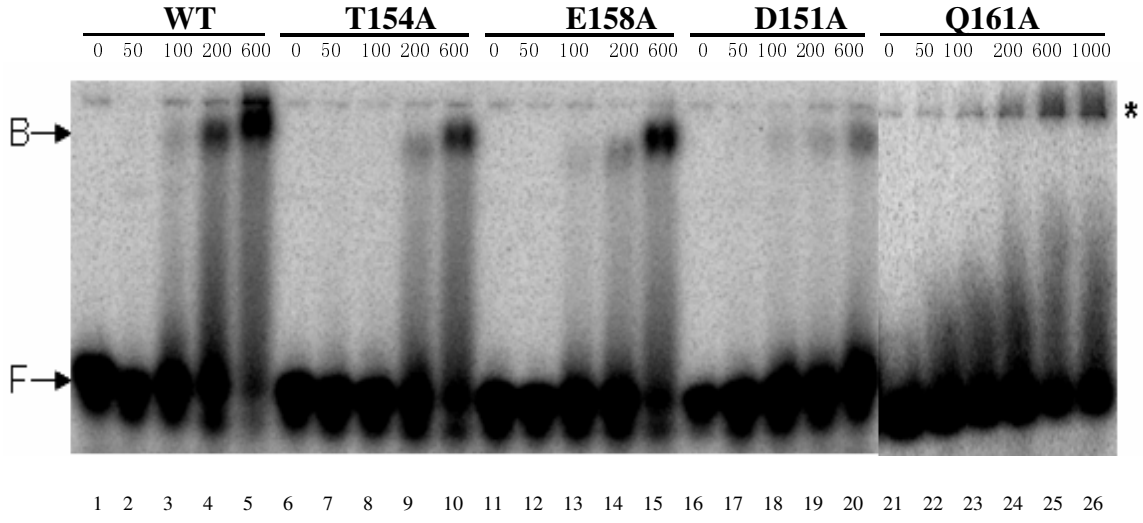
WT
T154A
E158A
D151A
Q161A
0 50 100 200 600 0 50 100 200 600 0 50 100 200 600 0 50 100 200 600 0 50 100 200 600 1000
B
F
*
1 2 3 4 5 6 7 8 9 10 11 12 13 14 15 16 17 18 19 20 21 22 23 24 25 26

Figure 25. Gel mobility shift assays of Aa-RNase III mutant binding to Aa-23S[hp] RNA.

Enzyme concentrations are reported in units of nM (dimer concentration). Reaction buffer consisted of 30 mM Tris-HCl (pH 8.0 at 20°C), 5 mM $CaCl_2$, 250 mM Potassium Glutamate, 5 mM Spermidine, 0.1 mM DTT, and 5% Glycerol (v/v). 15,000 cpm of 3'-labeled Aa-23S[hp] RNA was added per reaction. After 10 min incubation, reactions were electrophoresed at 20°C, 150 V for 6 h.

'F' and 'B' indicate the positions of free and protein-bound forms of the RNA, respectively. In Panel B, the upper arrow (B) indicates the complex formed by Aa-RNase III. The lower arrow (B) indicates the complex formed by K153A mutant, which migrates faster than the former complex. This faster mobility of the K153A mutant complex may reflect the greater negative charge of the complex, due to the loss of a positively-charged lysine side chain. The asterisk on the right side of the images indicates the origin of electrophoresis.

Table 3. Relative rates of Aa-RNase III cleavage of Aa-16S[s-hp] RNA and 2'-deoxyribose variants.

Substrate	16S- s	dU32	**dC31**	**dU30**	dG10	dA9	dG8
Relative rate	(1.0)	0.63 +/-0.07	0.08 +/-0.01	0.12 +/-0.01	0.41 +/-0.01	0.83 +/-0.05	0.35 +/-0.02
pb position	(N/A)	4	3	2	1'	2'	3'
Contact	(N/A)	-	**T154**	**Q157**	Q161	E158	-

': pb position on the complementary dsRNA strand.
Reaction conditions were described in Figure 24B.
Bases in bold-face indicate the greatest reduction in cleavage rate.

Table 4. Relative rates of cleavage of Aa-23S[hp] RNA by Aa-RNase III mutants.

RNase III	WT	D151A	**K153A**	T154A	**Q157A**	Q157N	E158A	**Q161A**	NucD
Relative rate	1.0	1.1 +/-0.06	0.01 +/-0.00	0.28 +/-0.08	0.05 +/-0.01	0.40 +/-0.00	0.18 +/-0.01	0.08 +/-0.01	0.01 +/-0.00

Reactions were performed at 45°C, and contained 5 nM enzyme and 200 nM substrate, in buffer containing 30 mM Tris-HCl (pH 8.0), 50 mM NaCl, and 10 mM $MgCl_2$.

Table 5. K'_D values of Aa-23S[hp] RNA•Aa-RNase III mutant complexes.

Enzyme	WT	D151A	**K153A**	T154A	Q157N	E158A	**Q161A**
K'_D (nM)	57 +/- 4	74 +/- 8	2386 +/- 50	486 +/-16	993 +/-6	1312 +/-226	4118 +/-913

The Q157A complex was too weak to determine a K'_D by gel shift assay.

Table 6. Relative rates of Aa-RNase III cleavage of Aa-23S[hp] RNA pb mutants.

Substrate	23S	U-CG	L-GC	UL-CG+GC	AA1	AA2	AA3	AA4
Rate	1.0	0.29 +/-0.01	0.39 +/-0.02	0.09 +/- 0.00	0.23 +/-0.00	0.21 +/-0.03	0.60 +/-0.00	0.32 +/-0.00

Enzyme concentration: 5 nM; substrate concentration: 200 nM; Reaction buffer: 30 mM Tris-HCl (pH 8.0), 50 mM NaCl, 10 mM $MgCl_2$; Reaction temperature: 45°C.

Table 7. K'_D values of complexes of Aa-RNase III and Aa-23S[hp] RNA pb mutants.

Substrate	23S	U-CG	L-GC	UL-CG+GC
K'_D	57 +/-4	140+/-22	588+/-54	694+/-61
Substrate	AA1	AA2	AA3	AA4
K'_D	348+/-60	308+/-33	200+/-2	1422+/-50

Substrate concentration: ~15 nM. Reaction buffer: 30 mM Tris-HCl (pH 8.0), 50 mM NaCl, 5 mM $CaCl_2$. Reaction were performed at 20°C, and gel electrophoresis was performed at 20°C (see Materials and Methods). K'_D reported in nM.

Table 8. Relative rates of Aa-NucD cleavage of Aa-23S[hp] RNA sequence variants.

Substrate	23S	U-CG	L-GC	UL-CG+GC	AA1	AA2	AA3	AA4
Rate	1	0.50+/-0.04	0.46+/-0.09	0.21+/- 0.00	0.42+/-0.18	0.57+/-0.18	1.17+/-0.32	0.38+/-0.02

Reaction conditions were described in Figure 30.

group at pb nt 3 (the effect is shown by dC_{31} variant at pb positions 3, Figure 24; retaining only a ~10% relative reactivity, Table 3), while the D151 side chain helps stabilize the hydrogen bond by forming another hydrogen bond with T154. As mentioned above, the Q157 side chain engages in two hydrogen bonds with the pb nt 2: one with the ribose 2'-OH group, and the other with the pyrimidine base O_2 atom. On the opposite strand of the pb the E158 side chain hydrogen bonds to the ribose 2'-OH at pb nt 2, while the Q161 side chain engages in two hydrogen bonds with pb nt 1: the ribose 2'-OH and the guanine 2-amino group (Figure 3C). The side chain of the highly conserved L156 engages in hydrophobic interactions with residues in the β_1, β_2 and α_2 segments of the dsRBD, and most likely stabilizes the tertiary structure of the dsRBD. Due to its function in stabilizing structure, rather than interacting with the pb, L156 was not subjected to a mutational analysis. Time course assays for cleavage of Aa-23S[hp] RNA by the Aa-RNase III mutants are shown in Figure 26. Each mutant exhibits decreased activity, with the K153A and Q157A mutants exhibiting the lowest activity. The Q157 side chain was further analyzed by creating the Q157N mutation, which assesses the positional stringency of the interaction by shifting the position of the carboxamide group by deletion of a methylene group. The Q157N mutation causes only a modest decrease (2.5-fold) in the rate of cleavage (Figure 26D; Table 4). Thus, there is no strict positional requirement for the Q157 side chain, which in turn suggests a local flexibility in the RNA-protein interactions that can largely adjust to accommodate the methylene deletion without abolishing the two hydrogen bonds.

The inhibitory effect of alanine substitution was more severe with Aa-16S[hp] RNA than with Aa-23S[hp] RNA (Figure 26B). This is consistent with the fewer number of protein contacts that the former substrate can engage it, since it has only

A

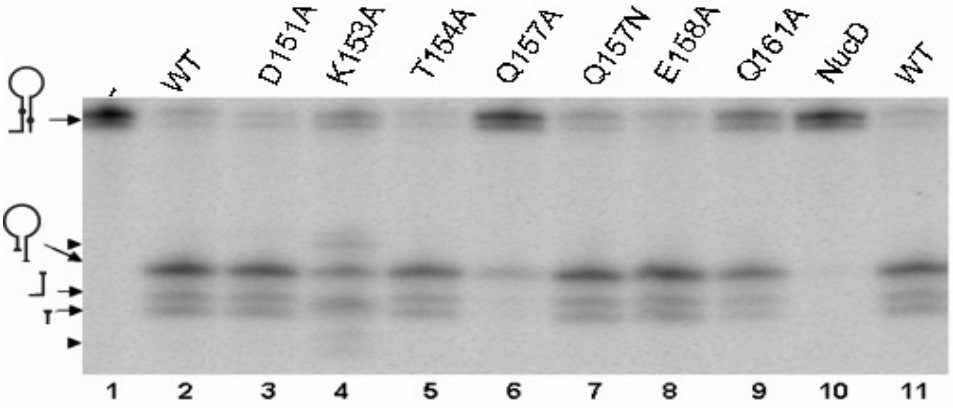

B

Aa-16S[hp] RNA

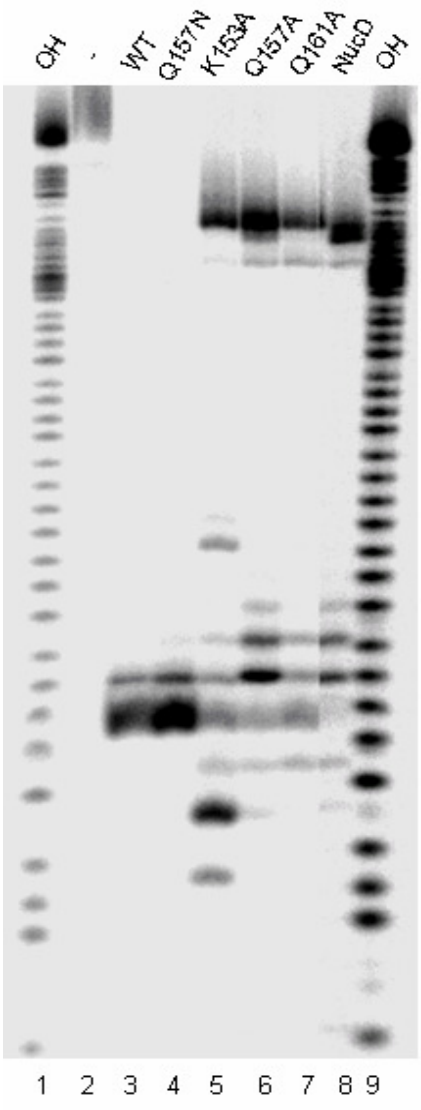

C

Aa-23S[hp] RNA

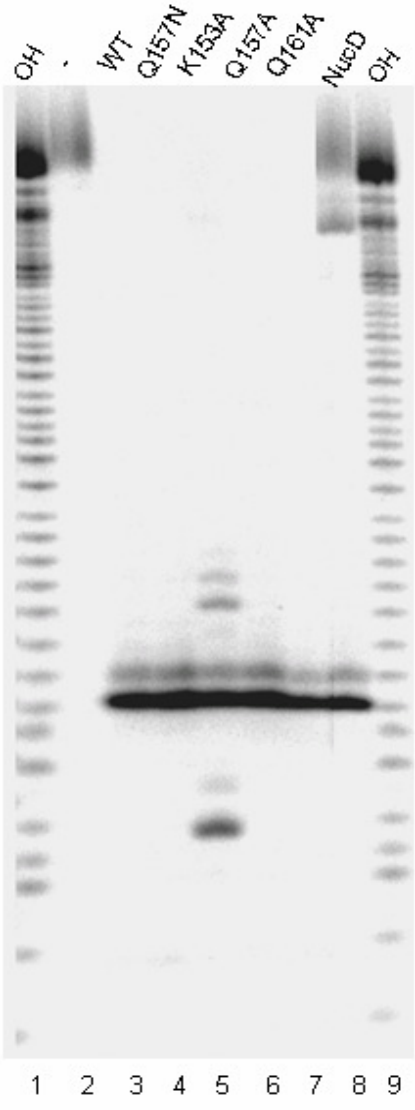

D

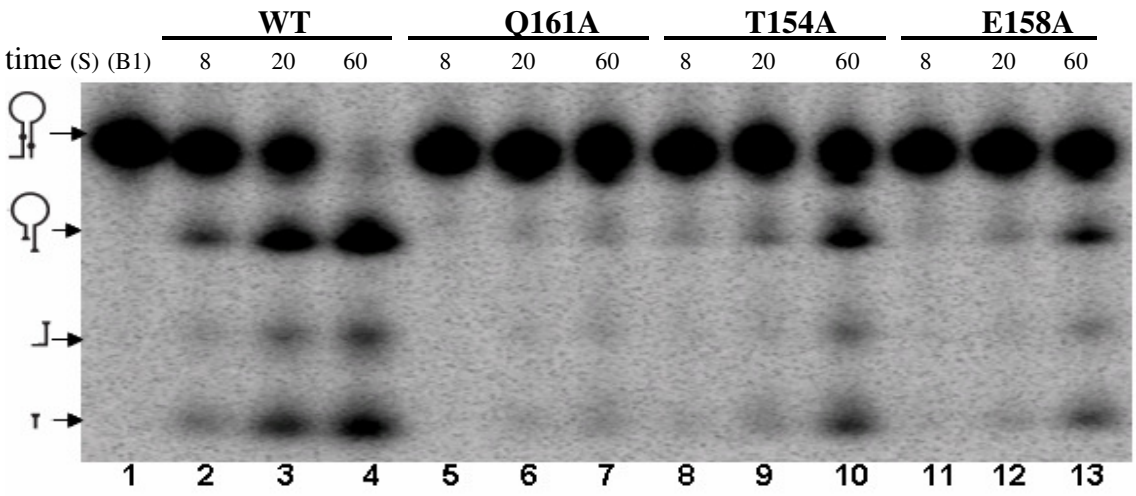
WT
Q161A
T154A
E158A
time (S) (B1) 8 20 60 8 20 60 8 20 60 8 20 60
1 2 3 4 5 6 7 8 9 10 11 12 13

E

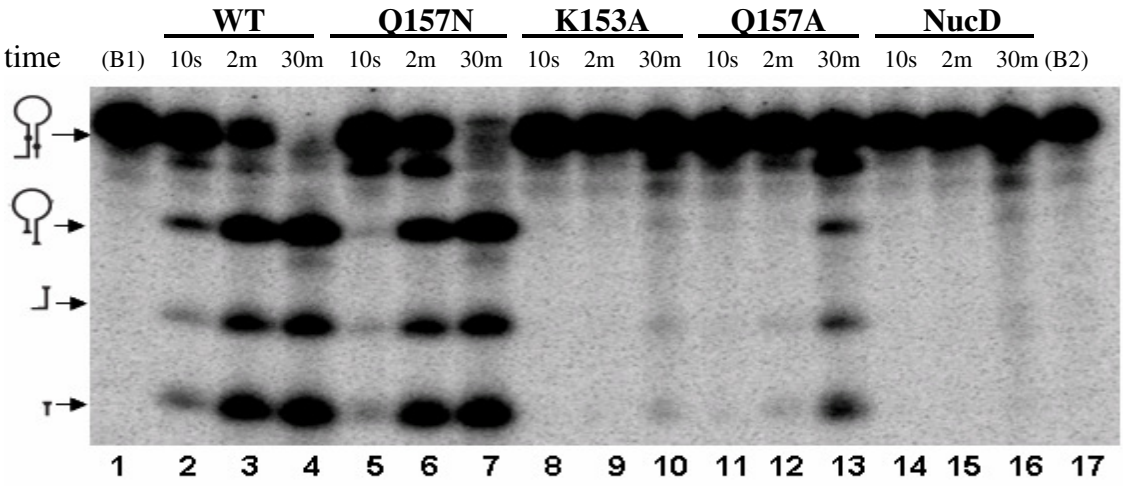
WT
Q157N
K153A
Q157A
NucD
time (B1) 10s 2m 30m 10s 2m 30m 10s 2m 30m 10s 2m 30m 10s 2m 30m (B2)
1 2 3 4 5 6 7 8 9 10 11 12 13 14 15 16 17

F

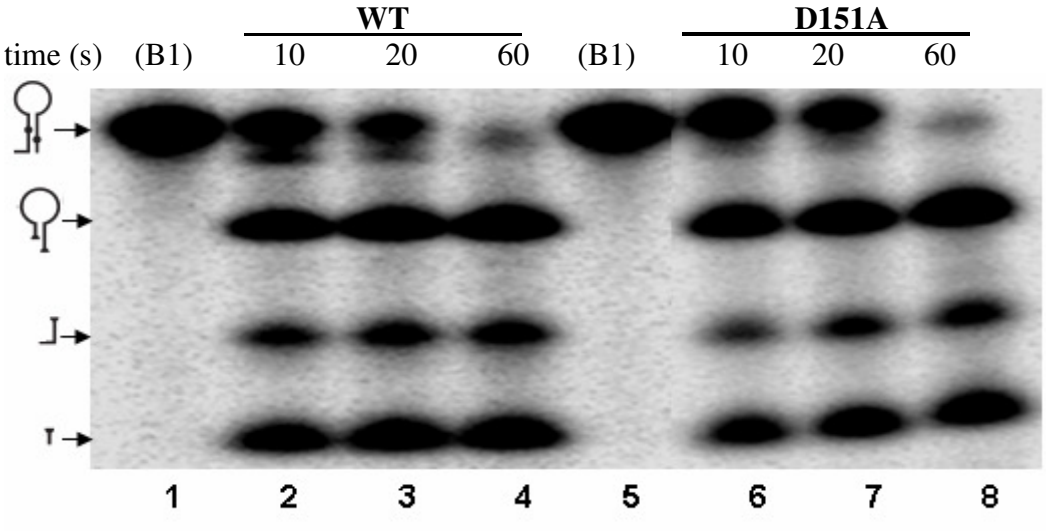
WT
D151A
time (s) (B1) 10 20 60 (B1) 10 20 60
1 2 3 4 5 6 7 8

Figure 26. Determination of cleavage rates and specificities of Aa-RNase III mutants, using Aa-16S[hp] RNA and Aa-23S[hp] RNA as substrates.

A. Comparison of cleavage specificities of Aa-RNase III mutants using internally ^{32}P-labeled Aa-23S[hp] RNA. Reactions were carried out in buffer containing 30 mM Tris-HCl (pH 7.25), 10 mM $MgCl_2$, 50 mM NaCl, 100 nM Aa-23S[hp] RNA. Reactions were assembled and pre-incubated at 40°C for 1 min, and RNase III mutant was added (concentrations provide below) to initiate the reactions (incubation temperature, 40°C). Lane 1, substrate incubated in reaction buffer without Aa-RNase III; lane 2, Aa-RNase III; lane 3, D151A mutant; lane 4, K153A mutant (note additional cleavage sites); lane 5, T154A mutant; lane 6, Q157A mutant; lane 7, Q157N mutant ; lane 8, E158A mutant; lane 9, Q161A mutant; lane 10, Aa-NucD; lane 11, Aa-RNase III. Lanes 2, 3, 5, 7, 8, and 9 show 3 min reactions involving 10 nM Aa-RNase III (or mutant). Lanes 4, 6, 9, and 10 show 30 min reactions containing 40 nM Aa-RNase III mutant. Arrowheads indicate additional cleavage products seen in lane 4.

B. Comparison of cleavage specificities of Aa-RNase III mutants, using 3'-^{32}P-labeled Aa-16S[hp] RNA as substrate. Lane 1, alkaline ladder; lane 2, substrate in reaction buffer without Aa-RNase III; lane 3, Aa-RNase III; lane 4, Q157N mutant; lane 5, K153A mutant; lane 6, Q157A mutant; lane 7, Q161A mutant; lane 8, Aa-NucD; lane 9, alkaline ladder. The reaction conditions were the same as in panel A, except the temperature was increased to 65°C.

C. Comparison of cleavage specificities of Aa-RNase III mutants, using 3'-^{32}P-labeled Aa-23S[hp] RNA as substrate. The order of the reactions are the same as in panel B.

D-F. Cleavage of internally ^{32}P-labeled Aa-23S[hp] RNA by Aa-RNase III mutants. The reaction conditions were the same as in panel A, and the reaction times are listed above each lane. B1, substrate in reaction buffer without Aa-RNase III; B2, substrate incubated for 30 min at 40°C in reaction buffer without Aa-RNase III.

one distal box (see Figure 27A). Thus, the presence of the additional distal box in Aa-23S[hp] RNA may partially compensate for any mutational perturbation of the RBM1-pb interaction. In addition to decreasing catalytic activity, the K153A mutation promoted cleavage of Aa-23S[hp] RNA at two additional sites that flank the canonical site (Figure 26, panel A, lane 4; panel C, lane 5). This result suggests a role of the lysine side chain in cleavage site selection as well as in binding energetics. For Aa-16S[hp] RNA, the mutations with the least effect on cleavage rate (D151A, T154A, Q157N, and E158A) do not alter specificity of cleavage (data not shown), while the three mutations with the greatest effect on cleavage rate (K153A, Q157A and Q161A) alter the pattern of cleavage (Figure 26B). Moreover, as shown below, the pattern of cleavage of the latter three mutants resembles the specificity of action of the isolated nuclease domain.

Gel mobility shift assays using 5'-^{32}P-labeled Aa-23S[hp] RNA (Figure 25) revealed that the RBM1 mutations influence the stability of the enzyme-substrate complex. The K'_D values of the enzyme-substrate complexes were determined by a protein titration assay, and are provided in Table 5.

3.2.2.3 Effect of pb mutations on RBM1 recognition and cleavage of Aa-23S[hp] RNA

The interaction of the highly conserved Q157 side chain with the O2 atom of the pyrimidine at pb position 2 (Gan *et al*., 2006, 2008) suggests a role for this residue in cleavage site selection. A UA→AU bp inversion at this position does not have a significant effect on reactivity (Figure 21A), suggesting that the repositioned minor groove O2 atom can still be recognized by adjustment of the Q157 side chain or that the adenine N3 atom can replace the O2 uracil atom. The apparent local structural flexibility of this interaction is also indicated by the near wild-type activity of the

A

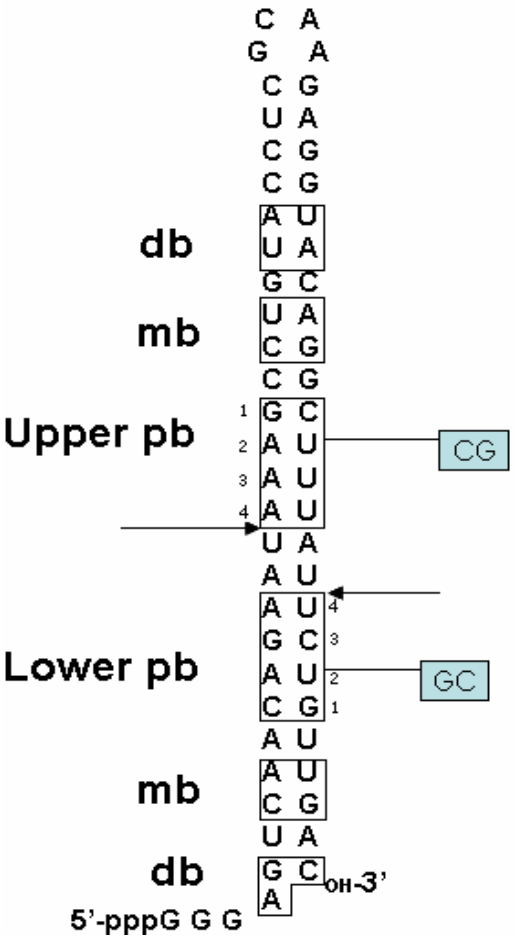

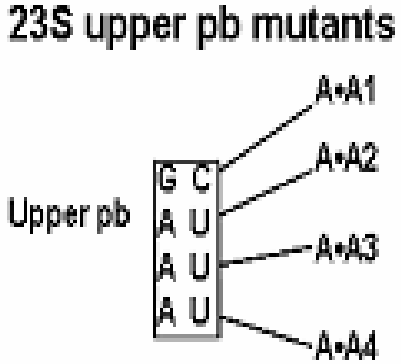

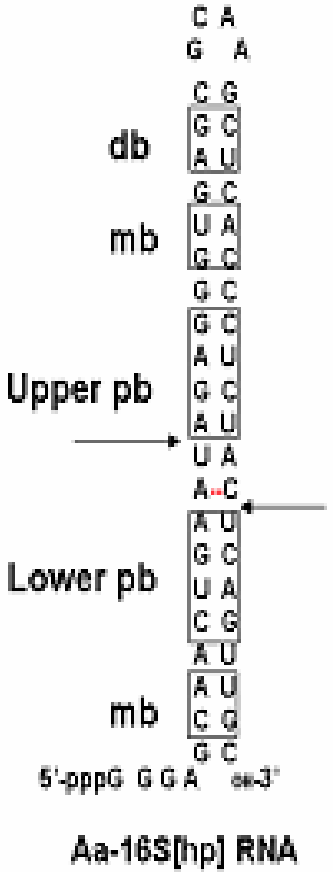

Aa-16S[hp] RNA

B

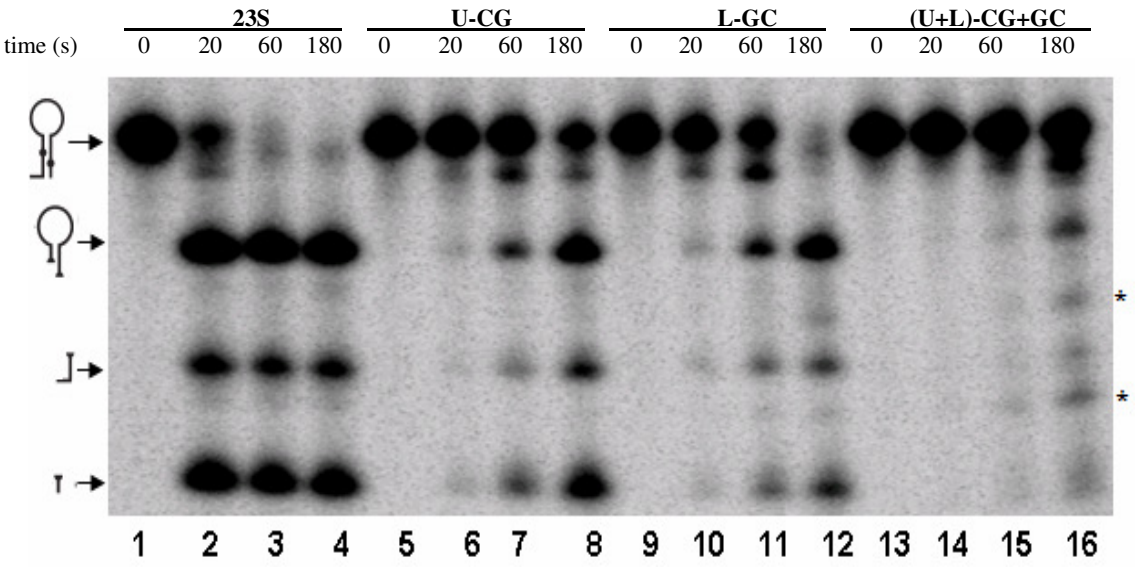
23S
U-CG
L-GC
(U+L)-CG+GC
time (s)
0 20 60 180 0 20 60 180 0 20 60 180 0 20 60 180
1 2 3 4 5 6 7 8 9 10 11 12 13 14 15 16

C

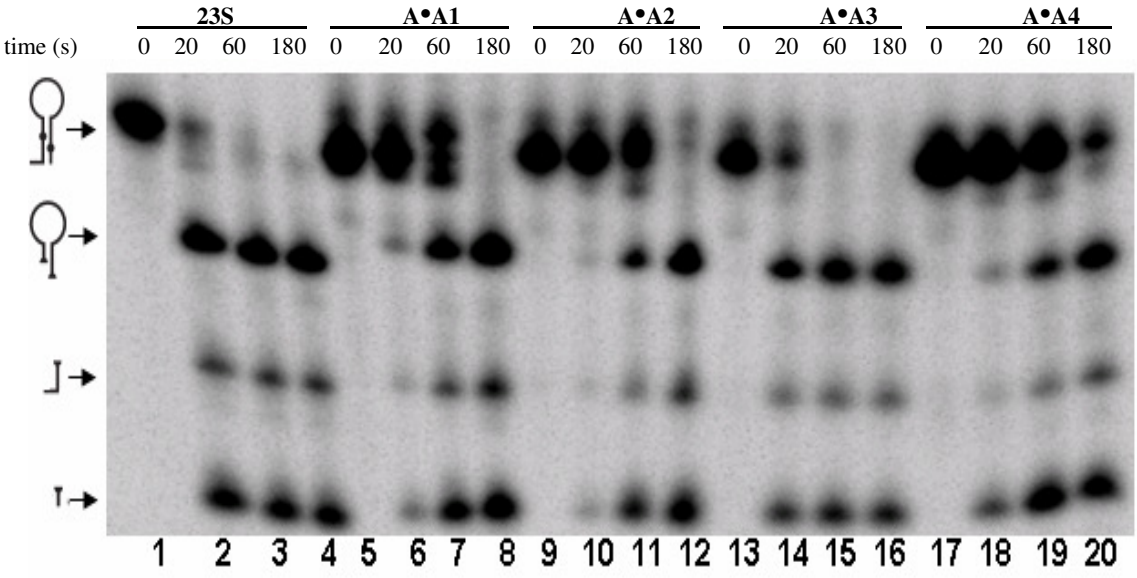
23S
A•A1
A•A2
A•A3
A•A4
time (s)
0 20 60 180 0 20 60 180 0 20 60 180 0 20 60 180 0 20 60 180
1 2 3 4 5 6 7 8 9 10 11 12 13 14 15 16 17 18 19 20

Figure 27. Aa-RNase III cleavage of pb sequence variants of Aa-23S[hp] RNA.

A. Diagrams of Aa-23S[hp] RNA and Aa-16S[hp] RNA, showing the distal box (db), middle box (mb) and proximal box (pb). Arrows indicate RNase III cleavage sites. The A-C mismatch in Aa-16S[hp] RNA is indicated by the dotted line.

B. Aa-RNase III cleavage of Aa-23S[hp] RNA pb mutants. The asterisks on the right indicate additional cleavage products caused by the GC or CG substitution in the L-pb position 2.

C. Aa-RNase III cleavage of Aa-23S[hp] RNA upper-pb A•A bp mutants

For Figures B and C, reactions were performed at 45°C, in buffer containing 30 mM Tris-HCl (pH 8.0), 50 mM NaCl, and 10 mM $MgCl_2$. The enzyme and substrate concentrations were 10 nM and 100 nM, respectively.

methylene-shifted Q157N mutant (Shi *et al*., 2011) (see also above). Specific bp substitutions at pb position 2 inhibit binding of Aa-RNase III (Shi *et al*., 2011). Thus, a CG or GC bp in place of the AU or UA bp causes a strong inhibition of enzyme binding. The inhibition is attributed to the presence of the guanine 2-amino group in the minor groove, since inhibition was not observed with an IC bp (I, inosine) substitution, which lacks the purine 2-amino group (Pertzev and Nicholson, 2006). Moreover, substitution of 2,6-diaminopurine for the A in the otherwise non-inhibitory AU bp also inhibited binding of RNase III (Pertzev and Nicholson, 2006). It was proposed that the Q157-O2 interaction is a positive determinant of recognition, and that the substitution of a 2-amino group for the O2 atom blocks this interaction through a direct steric effect (Pertzev and Nicholson, 2006; Shi *et al*. 2011). The CG/GC bp at this position can therefore act as a recognition antideterminant (Pertzev and Nicholson, 2006). To test this proposal, we considered a "missing contact' analysis, wherein the O2 atom would be deleted from the U of the UA bp, and substrate reactivity tested. Since a pyrimidine analog that lacks the O2 atom was not experimentally accessible, we replaced the pyrimidine with adenine, creating an AA base-pair. Although this represents a substitution of a pyrimidine with a bulkier purine, the adenine nonetheless lacks an oxygen atom at the position (C2) corresponding to the pyrimidine C2 atom, and as such could provide a measure of involvement of the pyrimidine O2 atom involvement in substrate binding. Figure 27 displays the substrate cleavage assays, and Table 6 provides the relative cleavage reactivities of Aa-23S[hp] RNA variants containing specific bp substitutions in the pb. Figure 28 shows the gel shift assays, and Table 7 summarizes the K'_D values. The results show that substitutions by AA bp at the upper pb positions lead to decreased cleavage reactivity and binding affinity.

A

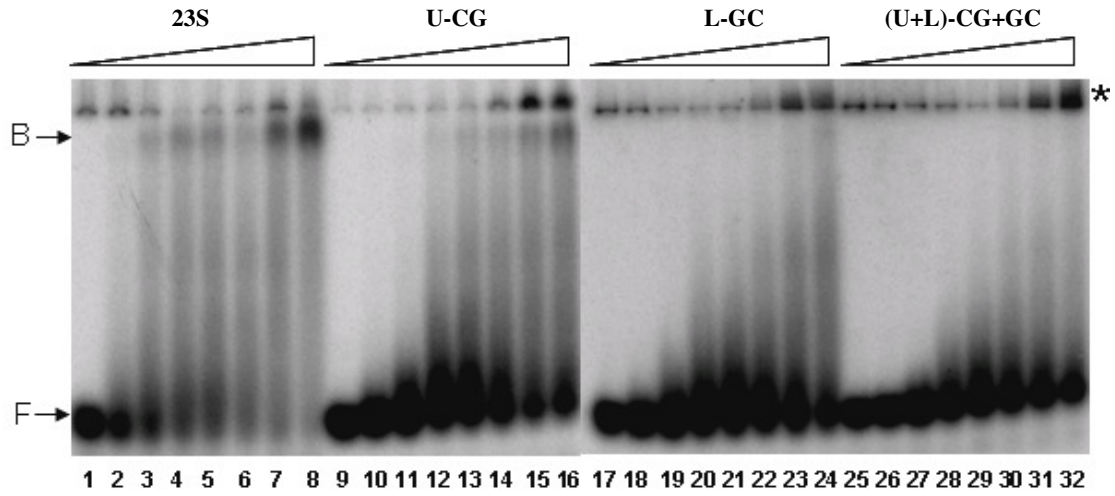
23S
U-CG
L-GC
(U+L)-CG+GC
B
F
*
1 2 3 4 5 6 7 8 9 10 11 12 13 14 15 16 17 18 19 20 21 22 23 24 25 26 27 28 29 30 31 32

B

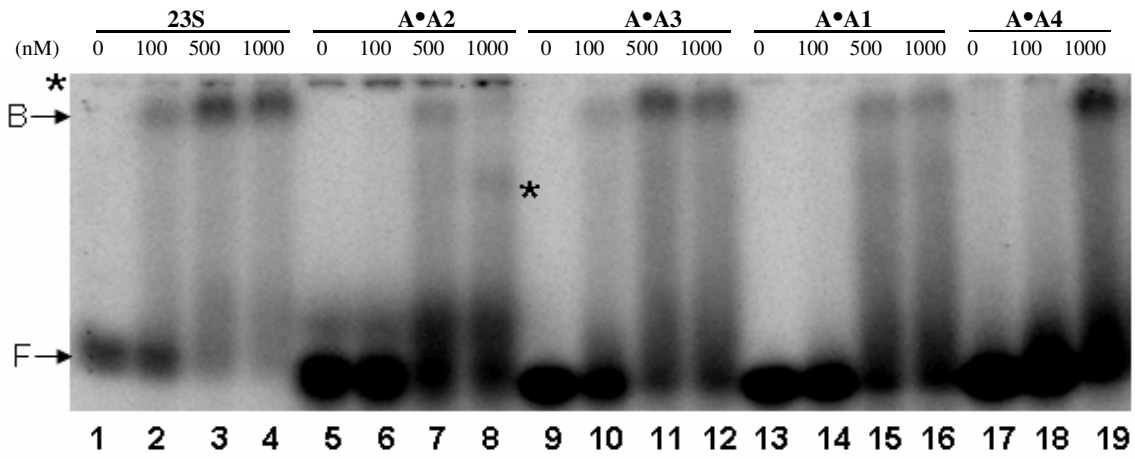
23S
A•A2
A•A3
A•A1
A•A4
(nM) 0 100 500 1000 0 100 500 1000 0 100 500 1000 0 100 500 1000 0 100 1000
*
B
*
F
1 2 3 4 5 6 7 8 9 10 11 12 13 14 15 16 17 18 19

Figure 28. Gel shift assay of Aa-RNase III binding to pb sequence variants of Aa-23S[hp] RNA.

A. Aa-RNase III binding to Aa-23S[hp] RNA pb sequence variants. For lanes 1-8, the substrate was Aa-23S[hp] RNA, and the Aa-RNase III concentrations were 0 nM, 50 nM, 100 nM, 200 nM, 400 nM, 600 nM, 1 μM, and 2 μM, respectively; For lanes 9-16, the substrate was "upper-pb2" CG (U-CG) bp mutant variants, and the Aa-RNase III concentrations were 0 nM, 50 nM, 100 nM, 200 nM, 400 nM, 600 nM, 1 μM, and 2 μM, respectively; For lanes 17-24, the substrate was "lower-pb2" GC (L-GC) bp variants, and Aa-RNase III concentrations were 0 nM, 50 nM, 100 nM, 200 nM, 400 nM, 600 nM, 1 μM, and 2 μM, respectively; For lanes 25-32, the substrate was "upper-pb2 + lower-pb2" GC (U+L-CG+GC) double bp mutant, and the Aa-RNase III concentrations were 0 nM, 50 nM, 100 nM, 200 nM, 400 nM, 600 nM, 1 μM, and 2 μM, respectively. 'F' and 'B' indicate the positions of free and protein-bound forms of the RNA, respectively. The asterisk on the right hand side of the image indicates the origin of electrophoresis.

B. Aa-RNase III binding to Aa-23S[hp] upper-pb A•A sequence variants. The asterisk to the right of lane 8 reflects the position of free RNA generated by dissociation of the complex during electrophoresis. The asterisk on the left hand side of the image indicates the origin of electrophoresis. The amount of radioactive RNA in lanes 1-4 was less than the amount used in lanes 5-19.

The same results are observed with substitutions of the AU bp by a CG/GC bp at the upper (U) /lower (L) respectively (or both) pb position 2. The GC bp substitution at the lower bp position 2 also causes two additional cleavage products (Figure 27B). Figure 29 shows a direct correlation between cleavage reactivity and binding affinity of the Aa-RNase III alanine mutants (panel A) and the Aa-23S[hp] RNA pb mutants (panel B).

3.2.3 Substrate cleavage specificity and catalytic activity of the Aa-RNase III nuclease domain

3.2.3.1 Substrate cleavage specificity of the Aa-RNase III NucD

Ec-RNase III lacking the dsRBD can cleave substrate *in vitro*, but the reaction is inefficient, and occurs only under non-physiological conditions that involve low salt concentrations, and Mn^{2+} in place of Mg^{2+} (Sun *et al*., 2001). Similarly, an excess amount of Aa-NucD, and prolonged reaction times provides only a limited level of cleavage of a cognate substrate (Figure 26), and no binding can be detected by a gel mobility shift assay (Figure 25B). Aa-NucD action on Aa-23S[hp] RNA also reveals that the truncated form can cleave with the same specificity as full-length enzyme (Figure 26B). Thus, the Aa-NucD contains the determinants sufficient for selection of the target site, at least for this substrate. By inference, there is no absolute requirement for the RBM1 (or other dsRBD feature) to establish specificity. Do the activities of the Aa-RNase III dsRBD point mutants, especially the more severe ones, exhibit similar behavior as Aa-NucD? The least active mutants, K153A and Q157A, exhibit a slightly higher activity than Aa-NucD (Figure 24A; Table 4). This suggests a residual ability of each mutant dsRBD to bind substrate. Aa-NucD cleaves Aa-16S[hp] RNA at several sites, including the canonical sites (Figure 26B, lane 8). The relaxed specificity of cleavage of this substrate by the NucD can be “corrected” to the

A

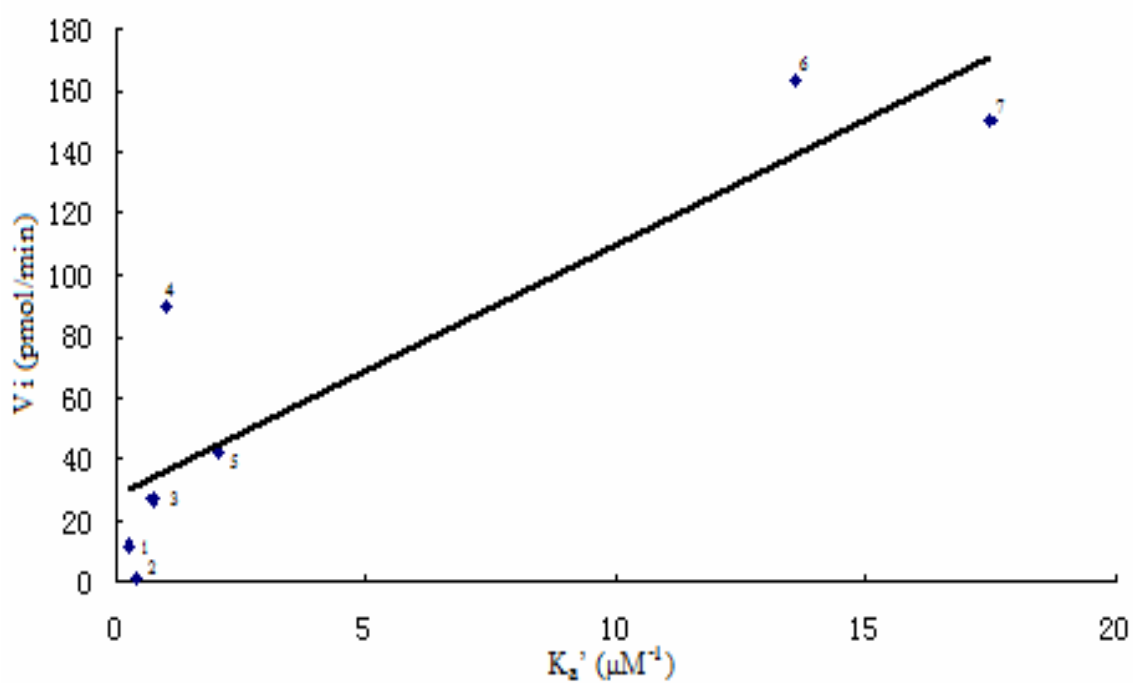
180
160
140
120
100
80
60
40
20
0
Vi (pmol/min)
0
5
10
15
20
Ka' (μM-1)
1
2
3
4
5
6
7

B

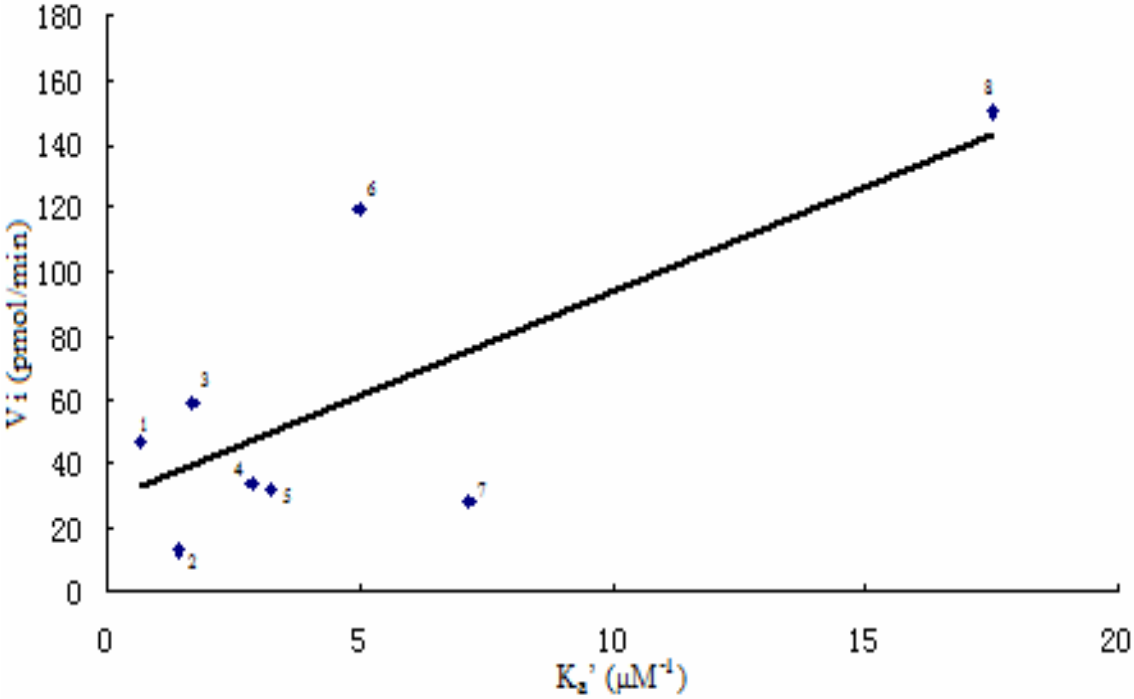
180
160
140
120
100
80
60
40
20
0
Vi (pmol/min)
0
5
10
15
20
Ka' (μM-1)
1
2
3
4
5
6
7
8

Figure 29. Correlation between initial cleavage rate (V_i) and substrate binding affinity (K'_A) (= $1/K'_D$).

The plotted V_i and K'_D values are the average of two experiments, based on the data in Table 4-9 (x-axis: K'_A, (μM^{-1}); y-axis: Vi, (pmol product/min).

A. Correlation of Aa-RNase III mutant affinity for, and cleavage of Aa-23S[hp] RNA. 1, Q161A; 2, K153A; 3, E158A; 4, Q157N; 5, T154A; 6, D151A; 7, WT.

B. Correlation of Aa-RNase III binding and cleavage of Aa-23S[hp] RNA pb mutant substrates. 1, A•A4; 2, upper-pb CG+ lower-pb GC; 3, L-GC; 4, A•A1; 5, A•A2; 6, A•A3; 7, U-CG; 8, 23S[hp].

canonical single site by the addition of the dsRBD (Figure 26B, lane 3), but the presence of either the K153A or Q157A mutation relaxes the specificity (Figure 26B, lanes 5 and 6). Thus, we conclude that for Aa-16S[hp] RNA, the dsRBD is required for specific recognition and cleavage of the canonical site. In turn, this evidence implies that the dsRBD is inherently capable of selecting the canonical cleavage site, independently of the NucD (see Discussion).

3.2.3.2 Aa-NucD cleavage of pb sequence variants of Aa-23S[hp] RNA

Since the Aa-NucD can select the correct cleavage site in Aa-23S[hp] RNA, it is possible that this domain is responsive to bp substitutions in the pb. To examine this, pb sequence variants of Aa-23S[hp] RNA were tested for their reactivity towards Aa-NucD. Figure 30 shows representative cleavage assays, and Table 8 provides the relative rates of cleavage of the Aa-23S[hp] RNA pb sequence variants. The Aa-NucD is able to cleave the mutant substrates at the canonical site, but less efficiently. The response to the bp substitutions is similar to that seen with Aa-RNase III. However, Aa-NucD exhibits an attenuated response, compared to Aa-RNase III, towards the Aa-23S[hp] RNA variants, including u-CG, u+l-CG+GC, AA1, AA2, and AA3 (Figure 30C). A potential mechanism by which the NucD can select the canonical cleavage site, and exhibit sensitivity towards bp substitution, is presented below (see Discussion).

3.2.3.3 A heterologous dsRBD can support Aa-RNase III catalytic activity

Given the strong conservation of the RBM1, and the similar sizes of bacterial Class 1 dsRBDs, a dsRBD from another RNase III may provide equivalent binding energy and support cleavage of the canonical site. To test this, two chimeric RNase III proteins were created by exchanging the dsRBDs of Aa-RNase III and Ec-RNase III. The $NucD^{Aa}$-$dsRBD^{Ec}$ and $NucD^{Ec}$-$dsRBD^{Aa}$ chimeric proteins were soluble, and the

A

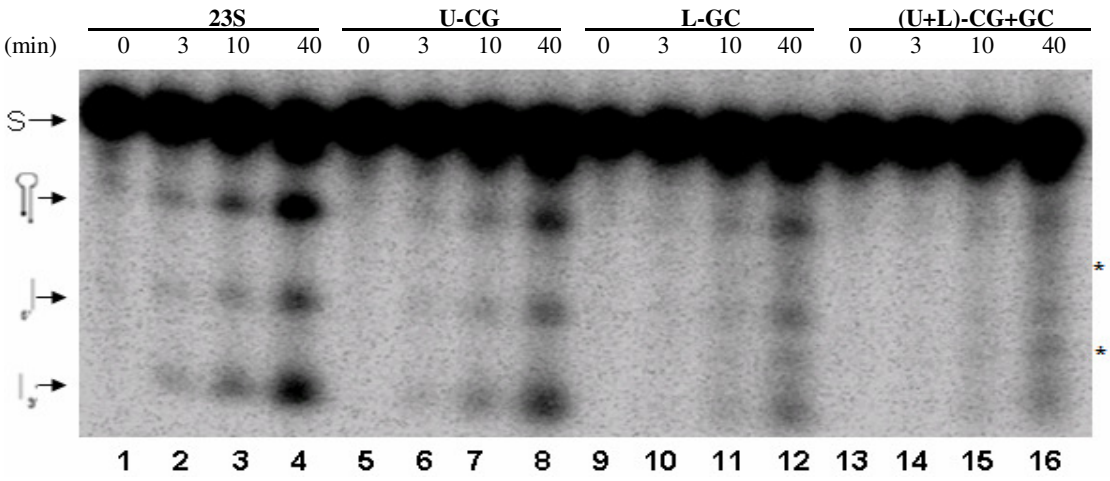
23S
U-CG
L-GC
(U+L)-CG+GC
(min)
0 3 10 40 0 3 10 40 0 3 10 40 0 3 10 40
1 2 3 4 5 6 7 8 9 10 11 12 13 14 15 16

B

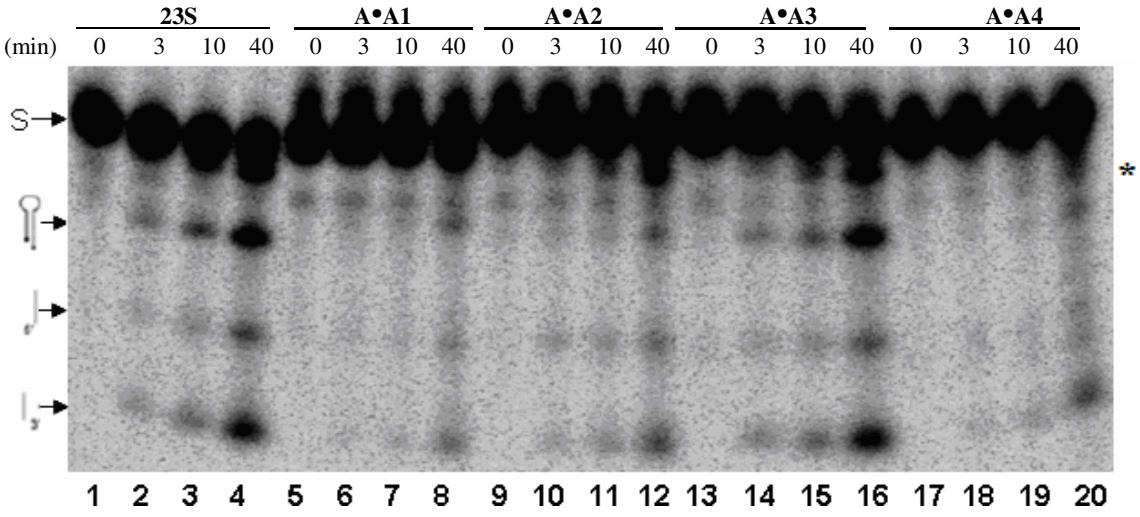
23S
A•A1
A•A2
A•A3
A•A4
(min)
0 3 10 40 0 3 10 40 0 3 10 40 0 3 10 40 0 3 10 40
1 2 3 4 5 6 7 8 9 10 11 12 13 14 15 16 17 18 19 20

C

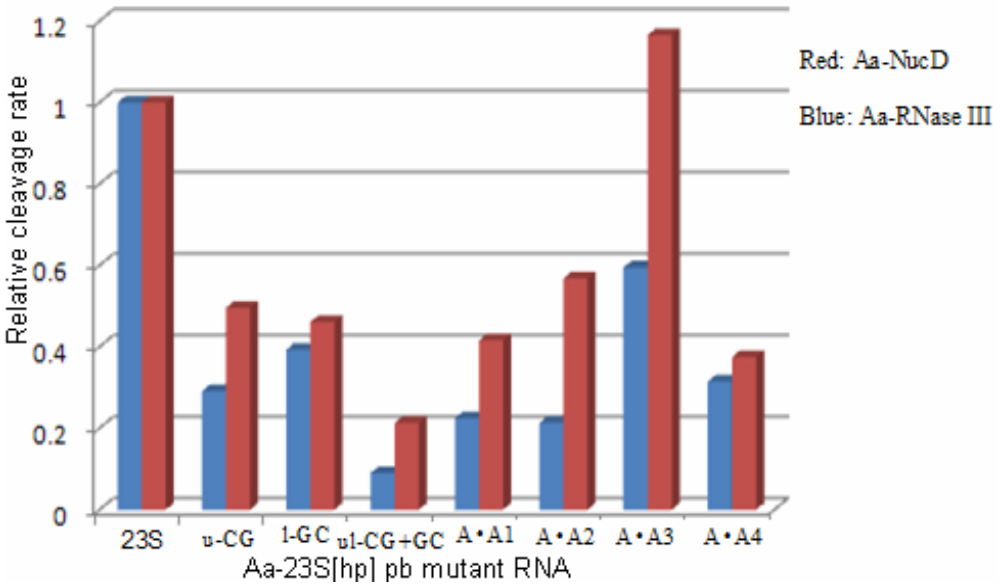
Relative cleavage rate
1.2
1
0.8
0.6
0.4
0.2
0
23S
u-CG
l-GC
ul-CG+GC
A•A1
A•A2
A•A3
A•A4
Aa-23S[hp] pb mutant RNA
Red: Aa-NucD
Blue: Aa-RNase III

Figure 30. Aa-NucD cleavage of pb sequence variants of Aa-23S[hp] RNA.

A. Aa-NucD cleavage of pb sequence variants of Aa-23S[hp] RNA.

B. Aa-NucD cleavage of (upper-pb) AA mismatch variants of Aa-23S[hp] RNA. The asterisks on the right indicate additional cleavage products caused by the CG substitution in the L-pb position 2.

For the experiments in A and B, cleavage reactions were performed at 65°C in reaction buffer containing 30 mM Tris-HCl (pH 8.0), 50 mM NaCl, 10 mM $MgCl_2$, 400 nM enzyme, and 100 nM internally ^{32}P-labeled substrate. Reaction times are labeled on top of the images. The asterisk on the right hand side indicates the product of cleavage of a single phosphodiester.

C. Comparison of cleavage reactivities. Graph derived from Tables 6 and 8. X-axis: Aa-23S[hp] pb mutant RNA. Y-axis, relative cleavage rate. 23S was set at 1 as a standard. Columns in blue represent WT Aa-RNase III relative cleavage rate, columns in red represent Aa-NucD relative cleavage rate.

CD spectra closely matched those of Aa-RNase III and Ec-RNase III (Figure 14E). Cleavage assays were performed using Aa-16S[hp] RNA as substrate, which showed that $NucD^{Aa}$-$dsRBD^{Ec}$ is catalytically active, and cleaves the RNA with essentially the same specificity as Aa-RNase III (Figure 31A, lanes 8-13). $NucD^{Ec}$-$dsRBD^{Aa}$ also is active, and is similar to Ec-RNase III in its specificity of action (Figure 31C, lanes 8-12). However, the overall activity of the two chimeras is reduced compared to Aa-RNase III or Ec-RNase III. This may reflect the differential temperature optima for the respective proteins, or subtle differences in the affinity of the chimeras for substrate. In conclusion, the behavior of the chimeras supports the proposal that the NucD establishes cleavage site specificity.

3.3 Exploring dsRBD-NucD functional interactions in substrate binding and catalytic action

3.3.1 Ec-RNase III heterodimer cleavage of R1.1[WC] RNA

Figure 32A shows the action of Ec-RNase III and specific heterodimeric forms on R1.1[WC] RNA. R1.1[WC] RNA is a variant of R1.1 RNA that has two scissile phosphodiesters at the target site. The E117A mutation suppresses catalytic activity without affecting substrate binding (Meng and Nicholson, 2008). Compared to WT/WT RNase III homodimer, the WT/NucD and WT/NucD[E117A] heterodimers exhibit significantly lower cleavage activities, and preferentially produce products that are the result of cleavage at only one phosphodiester. In contrast, the WT[E117A]/NucD heterodimer did not show detectable cleavage activity under the same conditions. These results indicate that the dsRBD exhibits a cis-acting functional behavior, wherein it preferentially interacts with the nuclease domain in the same subunit to enable cleavage of the phosphodiester in the catalytic site, but not the phosphodiester in the other catalytic site.

A

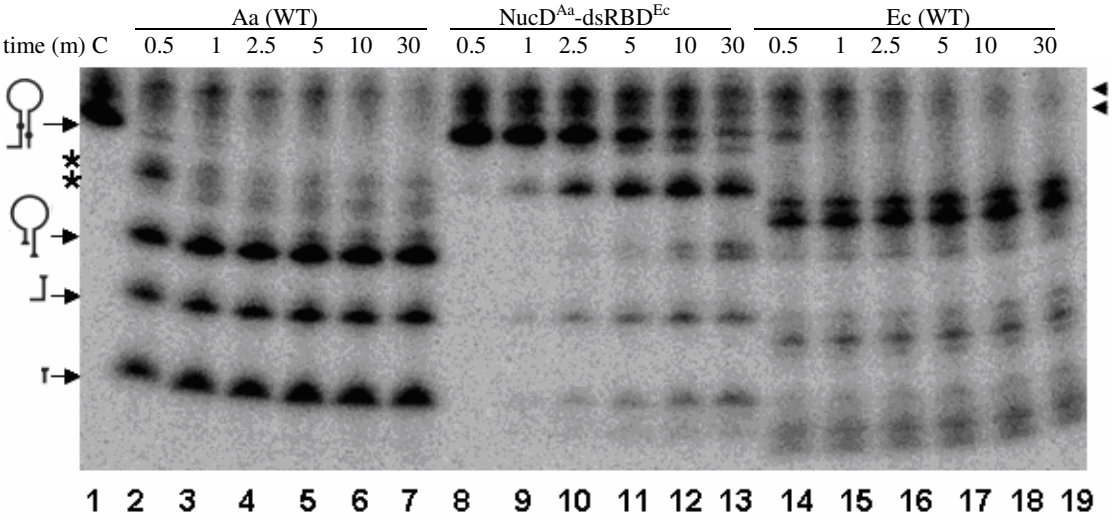
Aa (WT)
NucD^Aa-dsRBD^Ec
Ec (WT)
time (m) C 0.5 1 2.5 5 10 30 0.5 1 2.5 5 10 30 0.5 1 2.5 5 10 30
1 2 3 4 5 6 7 8 9 10 11 12 13 14 15 16 17 18 19

B

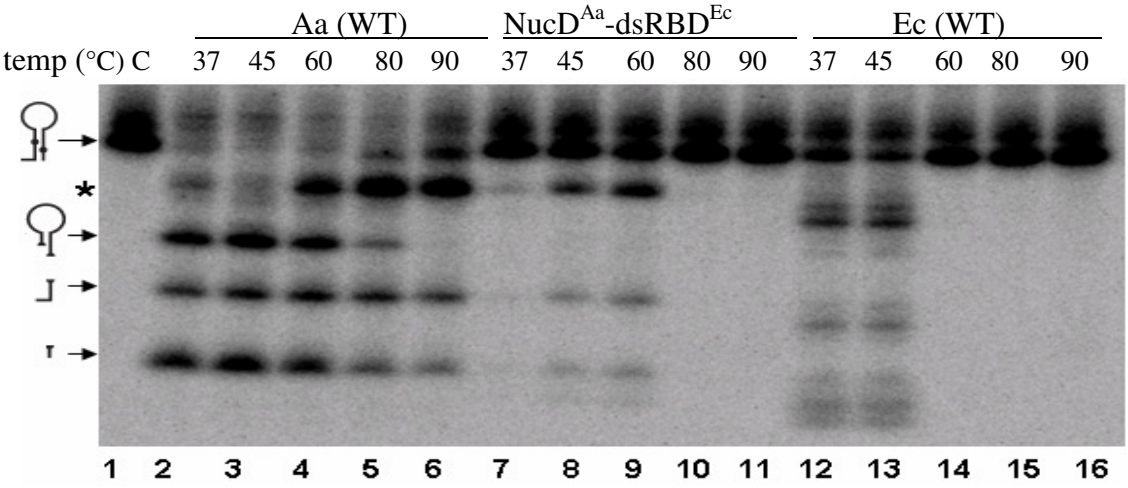
Aa (WT)
NucD^Aa-dsRBD^Ec
Ec (WT)
temp (°C) C 37 45 60 80 90 37 45 60 80 90 37 45 60 80 90
1 2 3 4 5 6 7 8 9 10 11 12 13 14 15 16

C

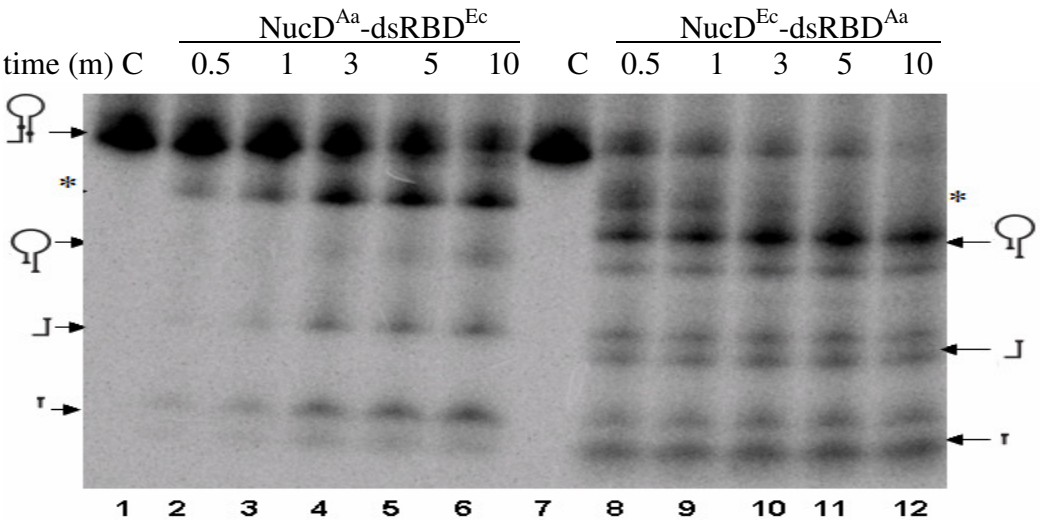
NucD^Aa-dsRBD^Ec
NucD^Ec-dsRBD^Aa
time (m) C 0.5 1 3 5 10 C 0.5 1 3 5 10
1 2 3 4 5 6 7 8 9 10 11 12

Figure 31. Aa-Ec RNase III chimera cleavage of Aa-16S[hp] RNA.

A. Time course assay of substrate cleavage by the $NucD^{Aa}$-$dsRBD^{Ec}$ RNase III chimera, compared with Aa-RNase III and Ec-RNase III. Protein concentration: 50 nM; substrate concentration: 100 nM. Reaction buffer: 10 mM $MgCl_2$, 30 mM Tris-HCl (pH 8.0), and 50 mM NaCl. Reactions were performed at 37°C. "C", Aa-16S[hp] RNA in reaction buffer without RNase III (no incubation). The asterisks indicate the product of cleavage of a single phosphodiester. The arrowheads on the right hand side indicate the positions of two slower-migrating RNA species present in the substrate, which may represent alternate, less reactive conformers.

B. Temperature dependence of Aa-16S[hp] RNA cleavage by the $NucD^{Aa}$-$dsRBD^{Ec}$ RNase III chimera, Aa-RNase III, and Ec-RNase III. Protein concentration, 50 nM; substrate concentration, 100 nM; reaction buffer: 10 mM $MgCl_2$, 30 mM Tris-HCl (pH 8.0), 50 mM NaCl; reaction time: 2 min.

C. Cleavage of Aa-16S[hp] RNA by $NucD^{Aa}$-$dsRBD^{Ec}$ and $NucD^{Ec}$-$dsRBD^{Aa}$ RNase III chimera. Substrate concentration: 100 nM. Enzyme concentration, 30 nM. Reaction conditions: 10 mM $MgCl_2$, 30 mM Tris-HCl (pH 8.0), 50 mM NaCl. Reaction temperature 37°C. "C", control, substrate and enzyme incubated in the absence of $MgCl_2$.

A

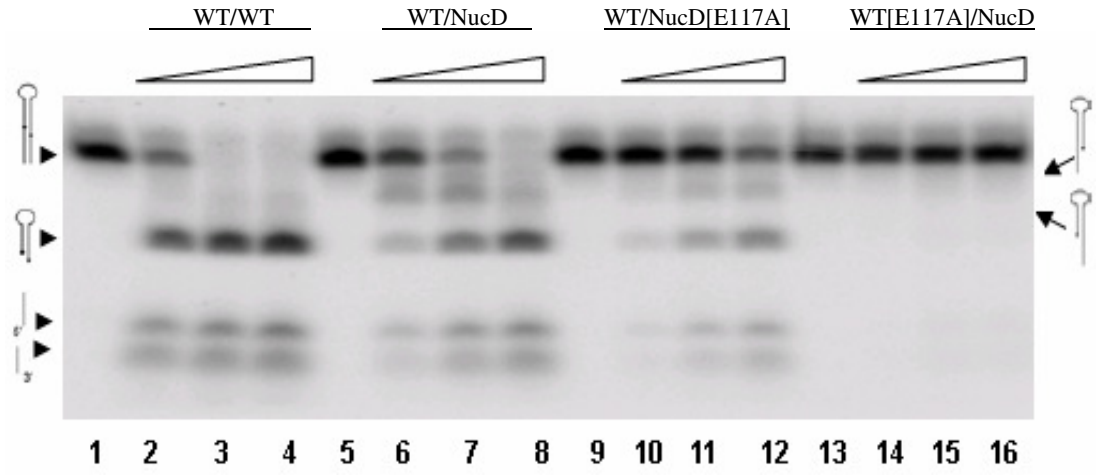
WT/WT
WT/NucD
WT/NucD[E117A]
WT[E117A]/NucD
1 2 3 4 5 6 7 8 9 10 11 12 13 14 15 16

B

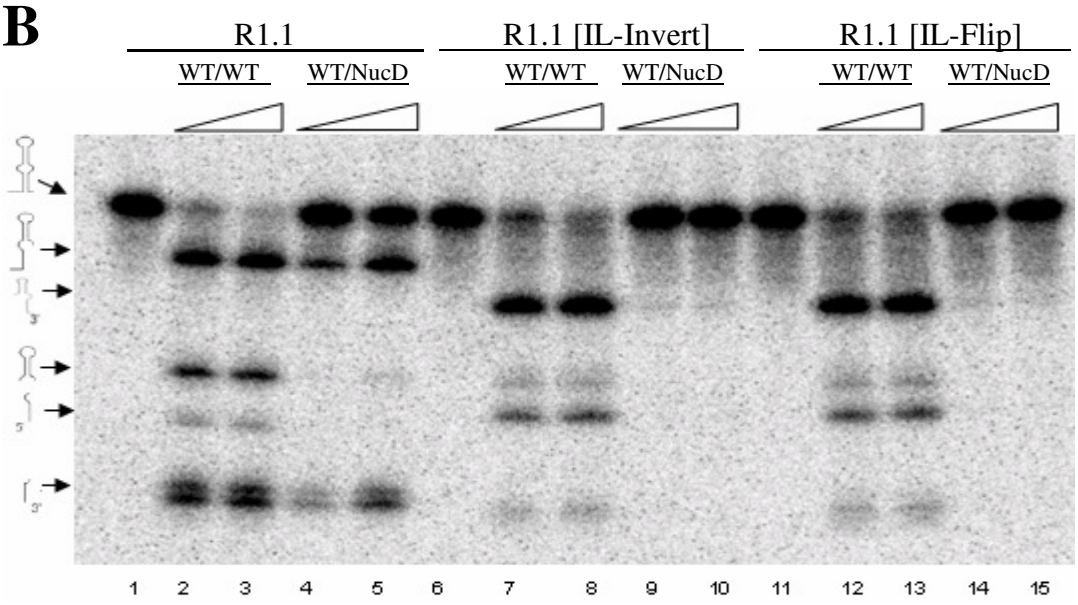
R1.1
R1.1 [IL-Invert]
R1.1 [IL-Flip]
WT/WT
WT/NucD
WT/WT
WT/NucD
WT/WT
WT/NucD
1 2 3 4 5 6 7 8 9 10 11 12 13 14 15

C

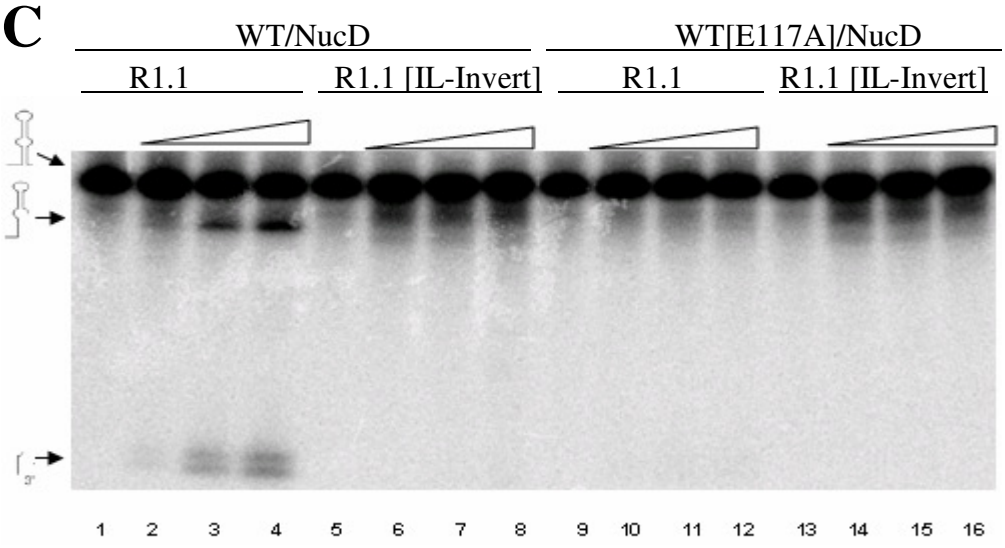
WT/NucD
WT[E117A]/NucD
R1.1
R1.1 [IL-Invert]
R1.1
R1.1 [IL-Invert]
1 2 3 4 5 6 7 8 9 10 11 12 13 14 15 16

Figure 32. Evidence for preferential cis-acting functional behavior of the dsRBD.

A. Ec-RNase III heterodimer cleavage of R1.1[WC] RNA. Lanes 1, 5, 9 and 13 show substrate incubated in reaction buffer without RNase III. Lanes 2-4, WT/WT enzyme; lanes 6-8, WT/NucD heterodimer; lanes 10-12, WT/NucD[E117A] heterodimer; lanes 14-16, WT[E117A]/NucD heterodimer. Reactions were performed in Ec-RNase III cleavage buffer at 37°C. Reaction times were 1, 3, and 10 min, respectively. Triangles on top of the image indicate increased reaction time.

B. WT/NucD heterodimer cleavage of R1.1, R1.1[IL-Invert] RNA and R1.1[IL-Flip] RNA. Lanes 1, 6 and 11 show substrate incubated in reaction buffer without RNase III. Lanes 1-5 show R1.1 RNA reaction; lanes 6-10 show R1.1 [IL-Invert] RNA reaction; lanes 11-15 show R1.1 [IL-Flip] RNA reaction. Lanes 2-3, 7-8 and 12-13 show Ec-WT/WT RNase III reaction; lanes 4-5, 9-10 and 14-15 show Ec-WT/NucD RNase III reaction. Reaction time was 1 and 3 min, respectively.

C. [E117A]/NucD cleavage of R1.1 [IL-Invert] RNA. Lanes 1, 5, 9 and 13 show substrate incubated in reaction buffer without RNase III. Lanes 1-4 and 9-12, R1.1 RNA reaction; lanes 5-8 and 13-16, R1.1 [IL-Invert] RNA reaction. Lanes 1-8 show Ec-WT/NucD RNase III reaction, and lanes 9-16 show Ec-WT[E117A]/NucD RNase III reaction. Reaction time was 1, 3, and 10 min, respectively.

In panels B and C, the doublet for the smallest product reflects the presence of transcripts with an extra, non-templated nucleotide added to the 3' end.

3.3.2 The action of RNase III heterodimers containing a single functional catalytic site towards R1.1 RNA and specific structural variants

R1.1 RNA, and two variants, R1.1[IL-Invert] RNA and R1.1[IL-Flip] RNA (IL, internal loop) were used as substrates to further analyze the pattern of cleavage and catalytic efficiency of Ec-RNase III heterodimers. The WT/WT enzyme cleaved R1.1[IL-Invert] RNA and R1.1[IL-Flip] RNA in a different pattern compared to R1.1 RNA(a fainter, 1 nt-shorter 3' fragment; a darker, 1 nt-longer 5' product; a lighter, similar-sized completely-cut upper hairpin fragment; and a 1 nt-shorter, 3' long fragment instead of a 5' long fragment; Figure 32B). Compared to WT/WT RNase III, the WT/NucD heterodimer exhibited reduced catalytic action towards all of the RNAs. These data suggest that the primary cleavage site "tracks" with the 5-nt component of the internal loop, but that the cleavage sites remain the same distance from the upper db (Calin-Jageman and Nicholson, 2003; Figure 8). The WT[E117A]/NucD heterodimer did not detectably cleave R1.1 RNA, and with WT/NucD[E117A], only single-site cleaved fragments were detected. Neither WT/NucD[E117A] nor WT[E117A]/NucD heterodimers cleaved R1.1[IL-Flip] RNA. These results suggest the existence of a functional requirement of directionality of bound substrate, and reflect the asymmetry of the substrate as well as the asymmetry of the heterodimers (see also Discussion).

CHAPTER 4. DISCUSSION

4.1 On the optimal conditions for Aa-RNase III catalytic activity *in vitro*

This project has characterized basic biochemical properties of Aa-RNase III, and analyzed the reactivities of small hairpin substrates based on the Aquifex pre-16S and pre-23S rRNA processing stem structures. Determining the optimal reaction conditions is necessary to establish *in vitro* assays of substrate binding and cleavage that accurately reflect the *in vivo* behavior of the enzyme. Aa-RNase III catalytic activity is supported by either Mn^{2+} or Mg^{2+} ion, with comparable efficiency. In contrast to Ec-RNase III (Sun *et al*., 2005), Aa-RNase III is not inhibited by higher Mn^{2+} concentrations. Regarding this difference in behavior, for Ec-RNase III it has been proposed that at higher concentrations, Mn^{2+} can bind to a third site near the two catalytic metal sites, thereby inhibiting product release (Sun and Nicholson, 2001). If this site also exists in Aa-RNase III (for which there is some evidence: see Gan *et al*., 2008), then its occupancy by Mn^{2+} does not cause inhibition. A salt concentration optimum at ~50 mM was observed, with increasing concentrations causing a progressive inhibition, perhaps reflecting ion competition with RNA for enzyme binding sites. Nonetheless, salt concentrations up to ~200 mM allow reasonably efficient cleavage of cognate substrates at 45°C. The pH dependence indicates that maximal catalytic activity requires the conjugate base forms of one or more enzyme groups. If the rate-limiting step under steady-state conditions is associated with product release, as is apparently the case with Ec-RNase III (Campbell *et al*., 2002), then deprotonation may optimize the rate of this step. It is possible that an increased negative charge on the enzyme at higher pH may accelerate release of the polyanionic RNA products from the post-catalytic complex.

4.2 The sources of thermostability of Aa-RNase III

Aa-RNase III exhibits a robust thermostability, with maximal activity achieved by ~70°C, and which is retained at temperatures approaching 90°C. It has been noted that the Charged-*versus*-Polar (C*v*P)-bias values in the amino acid compositions of thermophile proteins is larger than those of mesophile proteins (Cambillau and Claverie, 2000; Suhre and Claverie, 2003). The greater C*v*P-bias values probably reflect a functional preference for charged residues that can form stabilizing salt bridges, as well as reflecting a preference for Glu and Asp residues, instead of Gln and Asn residues that contain thermolabile carboxamide groups. The C*v*P-bias of Aa-RNase III is 22.2, which is about 2.6 times larger than the C*v*P-bias of Ec-RNase III. The C*v*P-bias values of Aa-RNase III and Ec-RNase III can be compared to the average C*v*P-bias values of 15.4 and 2.6 for *A. aeolicus* and *E. coli* proteins, respectively (Cambillau and Claverie, 2000; Suhre and Claverie, 2003). Thus, the larger C*v*P-bias of Aa-RNase III correlates with its thermostability. A similar correlation between C*v*P-bias and thermostable catalytic activity was noted for *Thermotoga maritima* RNase III (Nathania and Nicholson, 2010). Another contributor to protein thermostability is contact order (CO), which is a measure of the density of noncovalent, non-nearest neighbor interactions, which in turn influences protein structural compactness (Plaxco *et al*., 1998; Robinson-Rechavi *et al*., 2006; Robinson-Rechavi and Godzik, 2005). The relative CO value for the NucD of Aa-RNase III (PDB: 1I4S) is 0.1000, while the relative value of CO for the NucD of RNase III of the mesophile *Mycobacterium tuberculosis* (Mt), (PDB: 2A11) is 0.0927. Although the relative CO value for Aa-RNase III appears to be only slightly greater than that of Mt-RNase III, the difference (0.0073) is greater than that between the mean CO value for *Thermotoga maritima* proteins and the mean CO value for the

homologous mesophilic proteins [the difference is 0.0032 (*P*=0.013); Robinson-Rechavei and Godzik, 2006]. Based on this analysis it may be concluded that a greater CO also contributes to Aa-RNase III thermostability.

4.3 Functional relevance of the site-specific cleavage of small hairpin RNAs based on the Aquifex 16S and 23S pre-rRNAs

4.3.1 Aa-RNase III cognate substrate reactivity

The *A. aeolicus* pre-16S and pre-23S processing stems exhibit the greatest lengths and predicted thermodynamic stabilities among an examined set of phylogenetically broad pre-rRNA secondary structures (Saito *et al*., 2000). The extensive base pairing may reflect the ~80°C optimal growth temperature of the Aquificales that undoubtedly imposes demanding conditions on rRNA maturation and ribosome assembly *in vivo* (Deckert *et al*., 1998; Swanson, 2011). The positions of the cleavage sites in the pre-16S and pre-23S hairpins are consistent with a role for the enzyme in providing the immediate precursors to the mature rRNAs. Although the *in vivo* RNase III cleavage sites for the Aquifex pre-rRNA substrates are not known, a coincidence of the *in vitro* sites with the *in vivo* sites is expected, since the *in vitro* processing sites for RNase III substrates in general coincide with the *in vivo* sites (Court, 1993; Nicholson, 2003; Dunn and Studier, 1983; Dunn, 1976). The other enzymes that presumably act downstream to create the mature rRNA 5'- and 3'-ends have not been identified, but probably include RNase E/G, which has been implicated in Aquifex 5S rRNA maturation (Lombo and Kaberdin, 2008; Kaberdin and Bizebard, 2005), and one or more of the 3'→5' exonucleases identified thus far, including RNase R, RNase PH, and polynucleotide phosphorylase (Condon and Putzer, 2002). Besides creating the immediate precursors to the 16S and 23S rRNAs, the action of RNase III on the primary transcript also would release the precursors to $tRNA^{Ile}$,

$tRNA^{Ala}$ and $tRNA^{Arg}$ (Figure 6A). The tRNA precursors may be then acted upon by an RNase P-like activity that has been identified in *A. aeolicus* cell-free extracts that directly creates the mature tRNA 5'-ends (Wilkomm *et al*., 2002; Marszalkowski *et al*., 2008). Since the tRNAs already contain the 3'-terminal CCA sequence, the mature 3'-ends can be directly fashioned through exonucleolytic trimming, up to the 3'-terminal A, by one or more of the 3' →5' exoribonucleases mentioned above.

The minimal substrate, Aa-16S[μ-hp] RNA, which possesses a single cleavage site, allowed determination of the K_m and k_{cat} for an Aa-RNase III-catalyzed reaction, as well as demonstration of the base pair sequence control of reactivity. The reactivity of Aa-16S[μ-hp] RNA is independent of the distal box sequence (Shi *et al*., 2011), which differs from the strong db sequence dependence seen with Ec-RNase III substrates (Zhang and Nicholson, 1997; Pertzev and Nicholson, 2006). The db is a site of contact by one or more residues within a region in the NucD, termed RBM4, which exhibits variability in both length and sequence among RNase III orthologs (Figure 2C; Figure 3B) (Gan *et al*., 2006; Gan *et al*., 2008). For Aa-RNase III, the db-RBM4 interaction includes a ribose 2'-OH group that is hydrogen bonded to the R97 side chain (Figure 3C) (Gan *et al*., 2006). Thus, the db sugar-phosphate backbone, rather than base functional groups, appears to play a predominant role in db recognition by Aa-RNase III. Moreover, while the db-RBM4 interaction per se is conserved, the variability in dependence on the db sequence, and the variability in RBM4 sequence and length together suggest an idiosyncratic, species-specific interaction between RBM4 and the db. Base pair substitutions in the middle box (mb), which is also a site of RNase III interaction with the sugar-phosphate backbone, have moderate effects on reactivity (Figure 21A). This has been suggested to reflect local subtle changes in helical structure caused by the base pair substitutions (Gan *et al*., 2006; Gan *et al*.,

2008).

4.3.2 Aa-23S[hp] RNA is a more reactive substrate than Aa-16S[hp] RNA

The differential reactivities of Aa-23S[hp] RNA and Aa-16S[hp] RNA probably reflect the difference in helix length. Aa-23S[hp] RNA (58 nt) has a 25 bp stem that provides two db (more precisely, a full db and a "half" db), two mb, and two pb. In contrast, Aa-16S[hp] RNA (50 nt) has a 21 bp stem, providing only one db, two mb, and two pb (Figure 27A). As shown by gel shift assays (Figure 20), the shorter RNA is less stably bound to Aa-RNase III, and therefore less efficiently cleaved. This was further supported by the reactivity of Aa-16S[μ-hp] RNA, which is only 34 nt in total, and has one db, one mb, and one pb. For this substrate, the cleavage rate was further reduced, and the enzyme-substrate complex could not be detected by gel shift assay (data not shown).

Further evidence of reactivity differences due to altered substrate•RNase III contacts is provided by the observation that Aa-RNase III cleavage of Aa-16S[hp] RNA is more sensitive to mutations in RBM1. The Q157A and Q161A mutations cause multiple-site cleavage of Aa-16S[hp] RNA, while Aa-23S[hp] RNA is cleaved only at the canonical site, indicating that two db are needed for optimal specificity as well as reactivity. One possibility is that the two db function in concert to act as "anchors" to fix the site of cleavage. As shown in the RNase III•dsRNA diagram (Figure 3B), when both db are present (as with Aa-23S[hp] RNA), the Q157A or Q161A mutant enzymes remain properly anchored by both db, even though the pb interaction is weakened by mutation. As a result, the canonical site remains the exclusive site. In contrast, when there is only one db in the substrate (as with Aa-16S[hp] RNA), the Q157A and Q161A mutant enzymes are anchored less tightly, and coupled with the RBM1 mutation, cleave (albeit much less efficiently) substrate

at additional sites, due to increased positional flexibility of the enzyme on the substrate.

The NucD can specifically cleave Aa-23S[hp] RNA at the canonical target site (Figure 26C, lane 8), but exhibits relaxed specificity (i.e., cleaves at several sites) towards Aa-16S[hp] RNA (Figure 26B, lane 8). The NucD engages in several interactions with substrate, including the RBM4-db interaction. A normal precatalytic complex therefore exhibits two RBM4-db contacts (Figure 3B) that provide "anchors" of binding energy for the NucD as well as full-length enzyme. Although other interactions, yet to be characterized, are probably also involved in NucD selection of the cleavage site, the two db ensure proper positioning (also alluded to in Gan *et al*., 2008). The loss of one of the db-RBM4 anchors is sufficient to destabilize the proper binding mode, leading to loss of cleavage site-specificity as well as binding affinity. Considering that Aa-RNase III can cleave both Aa-23S[hp] RNA (Figure 26C, lane 3) and Aa-16S[hp] RNA (Figure 26B, lane 3) at the canonical target site, it follows that the NucD determines the cleavage site by RBM4-db anchoring. The presence of the dsRBD can restore the proper specificity of cleavage that is lost with Aa-16S[hp] RNA. This reflects the capability of the dsRBD to site-specifically bind substrate (probably by the RBM1-pb interaction), which in turn promotes correct positioning of the NucD in the absence of both db.

4.4 Dependence of substrate reactivity on the proximal box sequence

This project has shown that the proximal box (pb) plays a major role in determining the reactivity of Aa-RNase III substrates. For Aa-16S[μ-hp] RNA, specific base-pair substitutions at pb positions 2, 3 and 4 reduce cleavage reactivity by ≥5-fold *in vitro* (Figure 21A). The preference for an AU or UA bp at pb positions 2 and 4 is similar to what is observed with Ec-RNase III substrates (Pertzev and

Nicholson, 2006). The sequence preference at pb position 2 may be explained as follows. The uridine nucleoside at pb position 2 directly interacts with the side chain of Q157 in RBM1 *via* two hydrogen bonds: one involving the uracil O2 atom, and the other involving the ribose 2'-OH group (Figure 23C) (Gan *et al*., 2006; Gan *et al*., 2008). The functional equivalence of the UA and AU bp indicate that a uridine in either position can engage in energetically equivalent bonding, reflecting a local flexibility of the Q157 side chain. The inhibition of substrate binding by the Q157A mutation would reflect the loss of the two hydrogen bonds, together providing ~2–4 kcal/mol of binding energy (Lesser *et al*., 1990). The functional importance of the pb2-Q157 interaction is further underscored by the observation that a GC or CG bp substitution at this position inhibits cleavage. Since Aa-16S[μ-hp] RNA binding to Aa-RNase III could not be detected in a gel shift assay (data not shown), the effect of the CG/GC mutation on enzyme binding to this substrate could not be assessed by this assay. However, for a similar minimal substrate of Ec-RNase III, inhibition by a CG or GC bp at pb position 2 was attributed to the presence of the purine 2-amino group in the minor groove, which is predicted to interfere with positioning of the glutamine side chain (Pertzev and Nicholson, 2006). However, caution is needed in referring to the crystallographic data, since they are derived from complexes containing either a cleaved RNA, or a mutant RNase III that is catalytically inactive (Gan *et al*., 2006; Gan *et al*., 2008). A structural analysis of a true pre-catalytic complex would be needed to provide a more precise characterization of the pb–RBM1 interaction.

4.5 Role of substrate-Aa-RNase III domain interactions

4.5.1 Role of RBM1 in the catalytic activity of Aa-RNase III

An alanine mutation-based analysis has shown that highly conserved residues in the N-terminal α-helix of the dsRBD, termed RBM1 (Gan *et al*. 2006) provide key

contributions to RNase III binding and cleavage of substrate. Alanine substitution removes noncovalent bonding interactions, while minimizing any alteration in protein secondary structure (Wells, 1991). Using this approach it has been shown that the individual energetic contributions to substrate binding of the conserved side chains are unequal. Thus, mutation of either of the two invariant residues, Q157 and K153, has the most severe effects on substrate binding and cleavage, while mutation of D151, T154, E158, or Q161 has less of an effect.

Besides Q157, K153 also is invariant in bacterial class 1 RNases III, but is not present in fungal Class 1 enzymes. This suggests a role for this side chain that is specific for the Class 1 bacterial enzymes. However, despite the strong inhibitory effect of the K153A mutation on substrate binding and cleavage, the crystal structures do not show any hydrogen bond formed between K153 and dsRNA, which suggests a specialized function of the side chain in bacterial substrate recognition. In the absence of a crystal structure of a pre-catalytic complex, the precise interactions this side chain makes with substrate, and how it perturbs cleavage site selection remain obscure. However, some speculation on the K153 side chain function can be provided. K153 is the only residue in the RBM1 of Class 1 bacterial RNases III that provides a positively-charged side chain. The loss of a positive charge in the K153A mutant is manifested not only by a decreased substrate binding affinity and cleavage rate (Table 4 and 5), but it also confers a greater electrophoretic mobility of the K153A•substrate complex in gel mobility shift assay compared to the wild-type enzyme complex (Figure 25B). The greater mobility can be explained by an increased overall negative charge of the enzyme-substrate complex; however, a subtle conformational difference from the wild-type enzyme complex cannot be excluded. Intriguingly, K153A is the only mutation obtained thus far that promotes cleavage of Aa-23S[hp] RNA at

additional sites (Figure 26A,C). The source of this effect is unknown, but suggests a unique role of K153 in positioning RNase III on the substrate. The unique function of the K153 side chain may also involve the adjacent dipole moment of the RBM1 α-helix. Protein α-helices exhibit intrinsic dipole moments, created by the aggregate effect of all the individual dipoles from the carbonyl groups of the peptide bond, pointing in the same direction along the helix axis. The net dipole moment can be approximated by a ~0.5-0.7 positive charge near the N-terminus (and a corresponding ~0.5-0.7 negative unit charge near the C-terminus) of the helix (Hol, 1985). K153 is the N-terminal residue of the RBM1, and interacts with dsRNA through formation of a salt bridge with a nonbridging oxygen atom of the phosphodiester between pb nt 4 and 3, positioned at the edge of the minor groove. The positive charge of the α-helix dipole moment, and the positively-charged K153 side chain together create a localized environment of high positive charge that would provide a significant attractive force for the negatively charged substrate. The K153 side chain and the α-helix dipole in effect function as a "zipper head" at the edge of RBM1. The strong, localized electrostatic attraction may cause a structural distortion in the dsRNA in the precatalytic complex and reduce the transition state free energy barrier. In the absence of the K153 side chain, the strong electrostatic interaction at the zipper head is effectively lost, and the dsRBD-substrate interaction relies of the remaining residues in the RBM1 only inefficiently form weaker and/or alternative (mismatched) hydrogen bonds with other sites in the proximal box (not yet characterized), which can reposition the dsRBD in at least two new registers on the RNA. In turn, this causes the appearance of cleavage sites in addition to the preferred site. In contrast, mutation of Q157 does not have the same effect, as this does not disrupt the electrostatic interactions. The Q157 side chain may be dedicated to discriminating

AU/UA bp from CG/GC (antideterminant) bp at pb position 2 through hydrogen bonding, while K153 plays a role in positive identification of the pb sequence.

4.5.2 Function of proximal box antideterminants

Specific bp substitutions (CG or GC) at position 2 of either the upper or lower pb hinder binding of Aa-23S[hp] RNA to Aa-RNase III, presumably through a perturbation of dsRBD recognition. Substitution at the upper or lower pb has unequal effects: the Aa-23S[hp] RNA variant containing a GC bp at position 2 in the lower pb exhibits a four-fold greater K'_D value (Table 7), compared to the variant with the same bp substitution within the upper pb. The greater inhibitory effect of the GC bp in the lower pb position 2 as well as additional cleavage products may be due to a greater reliance of this recognition element, in the absence of a fully functional lower db, due to its proximity to the stem terminus. Furthermore, the K'_D value of the variant containing a GC bp at both positions reflects the independent (non-cooperative) contribution of each single mutation (Table 7). Interestingly, the relative initial rates of cleavage of the U-CG and L-GC pb variants of Aa-23[hp] RNA are similar (0.29 *vs* 0.39, Table 6), indicating that there is less of a differential effect of the mutations under catalytic conditions.

Aa-RNase III is moderately more sensitive to bp substitution at pb position 2 (~3-5 fold reduction in initial rate of cleavage of Aa-23S[hp] RNA; Table 7), compared to NucD (~2-3 fold reduction; Table 9). Thus, while target site specificity is preserved, bp discrimination is slightly reduced. An emerging model is one wherein the NucD selects the cleavage site, while the dsRBD provides binding energy, and confers additional responsiveness to antideterminant (AD) bp (CG or GC) at pb position 2. In this model, the dsRBD can regulate RNase III action by its control of binding energy through its responsiveness to bp sequence, including antideterminant

GC/CG bp. dsRBD regulation of ribonucleolytic activity would be critical for cell viability, as indiscriminate intracellular cleavage of RNA could be lethal.

4.6 A model for preferential *cis* presentation of substrate in the recognition step of the RNase III catalytic pathway

Based on a previous proposal by Ji and co-workers for RNase III recognition of dsRNA (Gan *et al*., 2005; Figure 33), a general pathway for substrate recognition by RNase III has been proposed (Meng and Nicholson, 2008; Figure 34C,D). The pathway involves initial recognition of the substrate by either of the two dsRBDs, followed by NucD engagement of the substrate, with an accompanying protein conformational change mainly involving the flexible linker. The other dsRBD then engages the substrate to form the precatalytic complex (Figure 34C). As discussed previously (Gan *et al.*, 2005), formation of the precatalytic complex is dependent on the flexibility of the linker connecting the dsRBD and NucD. The presence of only a single dsRBD, as occurs in a WT/NucD heterodimer, would provide a single pathway in step 1 (see Figure 34D), thus reducing substrate binding affinity from a statistical thermodynamic standpoint. The presence of only one dsRBD also may affect the catalytic step, if the dsRBD participates in catalysis (Meng and Nicholson, 2008). In Figure 34D (upper panel), when there is only one dsRBD (WT/NucD), the substrate is preferentially singly cleaved at either of the two scissile bonds at the target site, with one site slightly more reactive than the other site. The single-cleaved RNA may be slowly cleaved at the other site by the bound enzyme or be released from the enzyme, then inefficiently rebind for cleavage of the remaining scissile bond, and product release. This modified pathway would exhibit a decreased cleavage rate, compared to the pathway involving wild-type enzyme (Figure 32A, lanes 6-8). In the case of WT/NucD[E117A] (Figure 34A), substrate must go through two rounds of

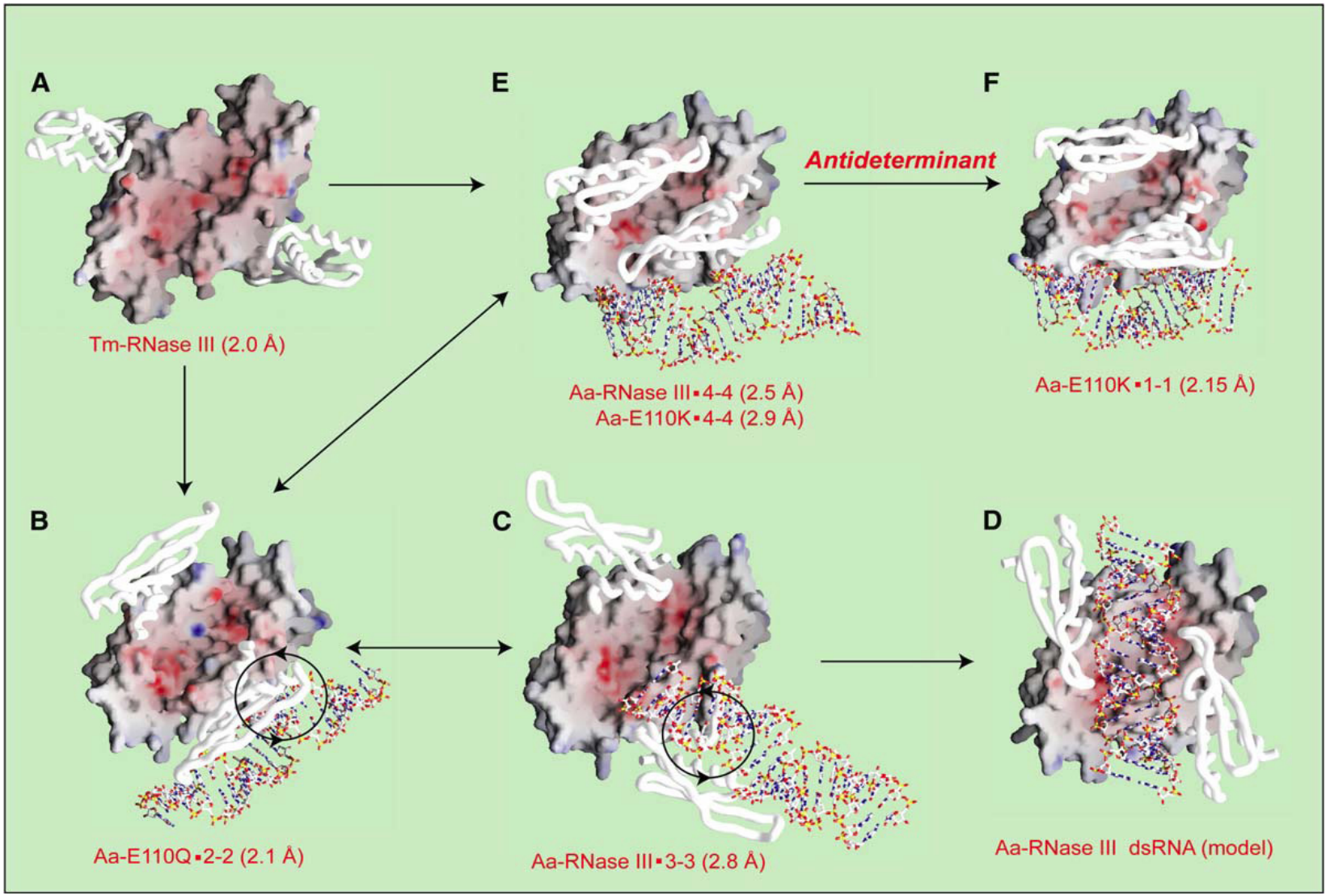
A
E
F
Antideterminant
Tm-RNase III (2.0 Å)
Aa-RNase III▪4-4 (2.5 Å)
Aa-E110K▪4-4 (2.9 Å)
Aa-E110K▪1-1 (2.15 Å)
B
C
D
Aa-E110Q▪2-2 (2.1 Å)
Aa-RNase III▪3-3 (2.8 Å)
Aa-RNase III dsRNA (model)

Figure 33. Proposed catalytic pathway for RNase III, based on the structure of RNase III, and two RNase III•dsRNA complexes (Gan *et al*., 2005).

A. Structure of Tm-RNase III (PDB Code, 1O0w).

B. Aa-RNase III[E110Q]•dsRNA (Gan *et al*., 2005).

C. Aa-RNase III•dsRNA (Gan *et al*., 2005).

D. Hypothetic functional RNA-processing form of Aa-RNase III•dsRNA.

E. Aa-RNase III• dsRNA and Aa-RNase III[E110K]• dsRNA (Gan *et al*., 2005).

F. Noncatalytic form of Aa-RNase III[E110K]•1-1 (Blaszczyk *et al*., 2004).

The NucD is displayed as a molecular surface, with positive and negative potentials indicated by blue and red color, respectively. The dsRBD is shown in white, and the dsRNA is represented as stick models, using the atomic color scheme (carbon in white, nitrogen in blue, oxygen in red, and phosphorus in yellow). The circles indicate a possible rotation of the dsRBD•dsRNA moiety, enabled by the flexible linker connecting the NucD and dsRBD. The direction of the predicted rotation is indicated by the arrowheads on the circles.

A

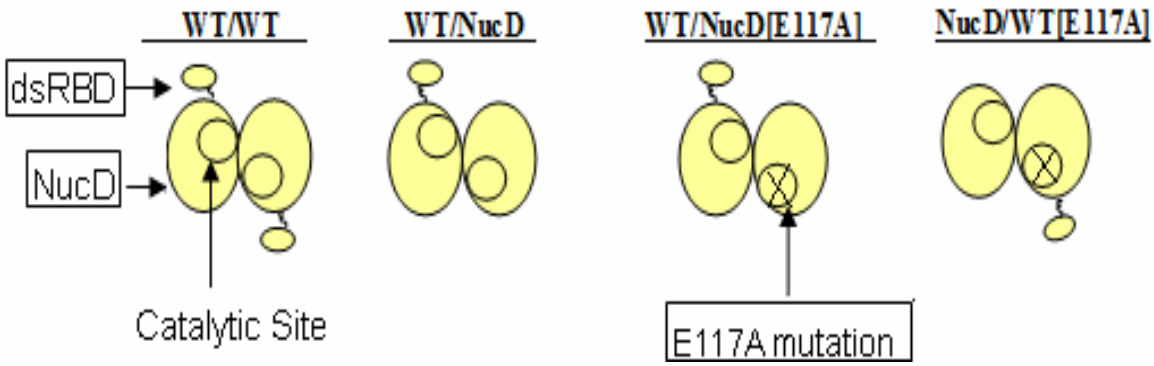
WT/WT
WT/NucD
WT/NucD[E117A]
NucD/WT[E117A]
dsRBD
NucD
Catalytic Site
E117A mutation

B

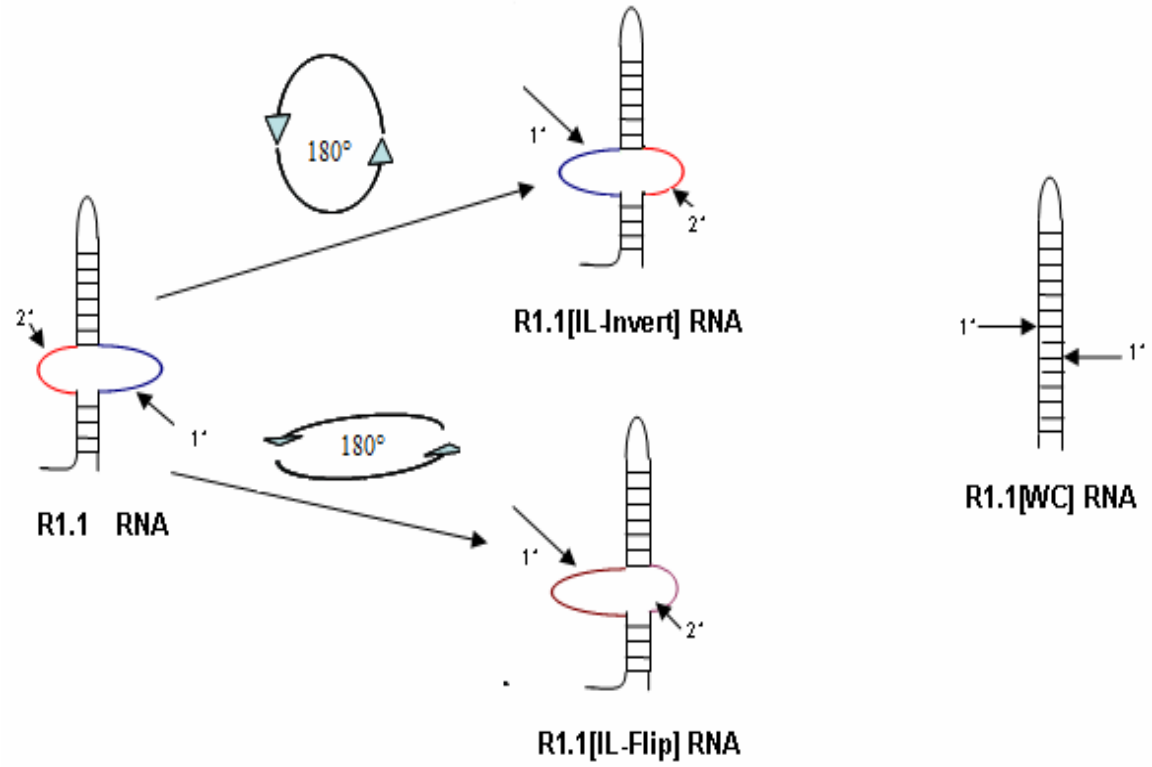
180°
1'
2'
R1.1[IL-Invert] RNA
2'
1'
180°
R1.1 RNA
1'
2'
R1.1[IL-Flip] RNA
1'
1'
R1.1[WC] RNA

C

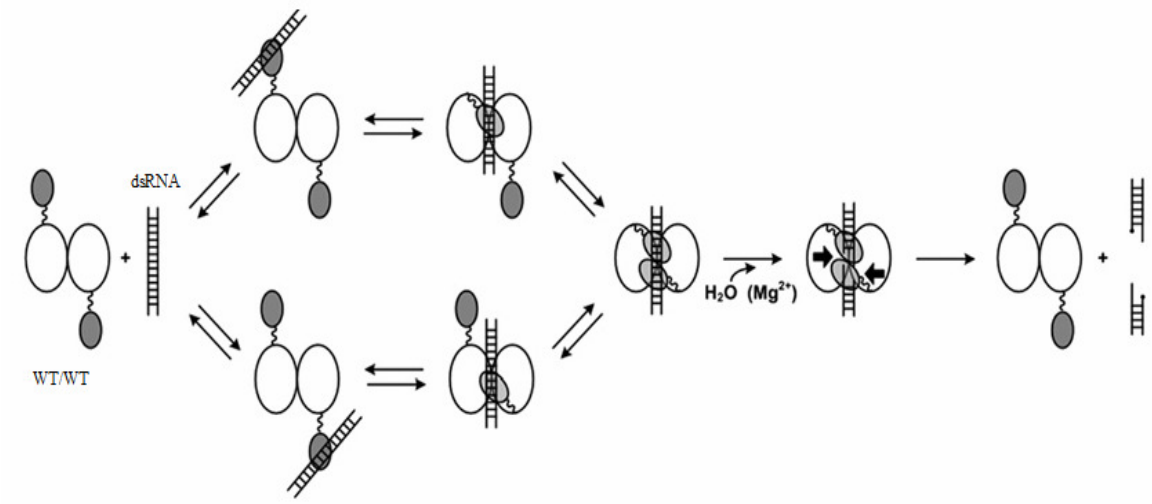

D

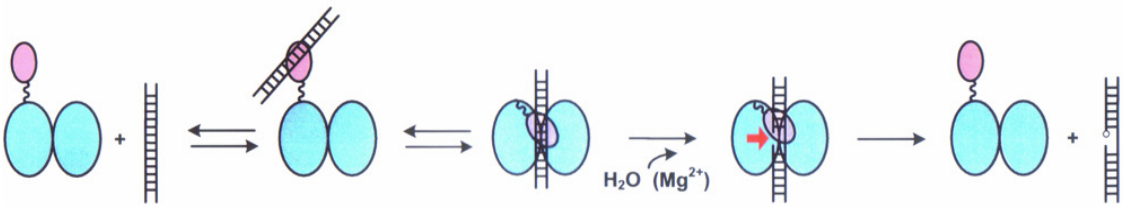

RNase III[NucD/wt]

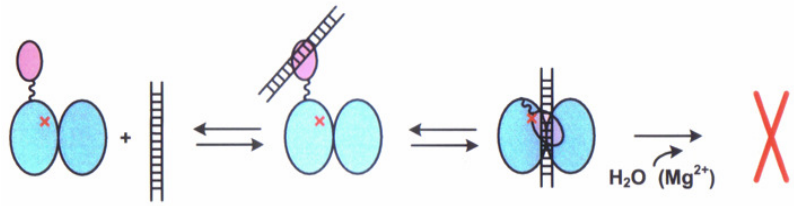

RNase III[NucD/E117A]

E

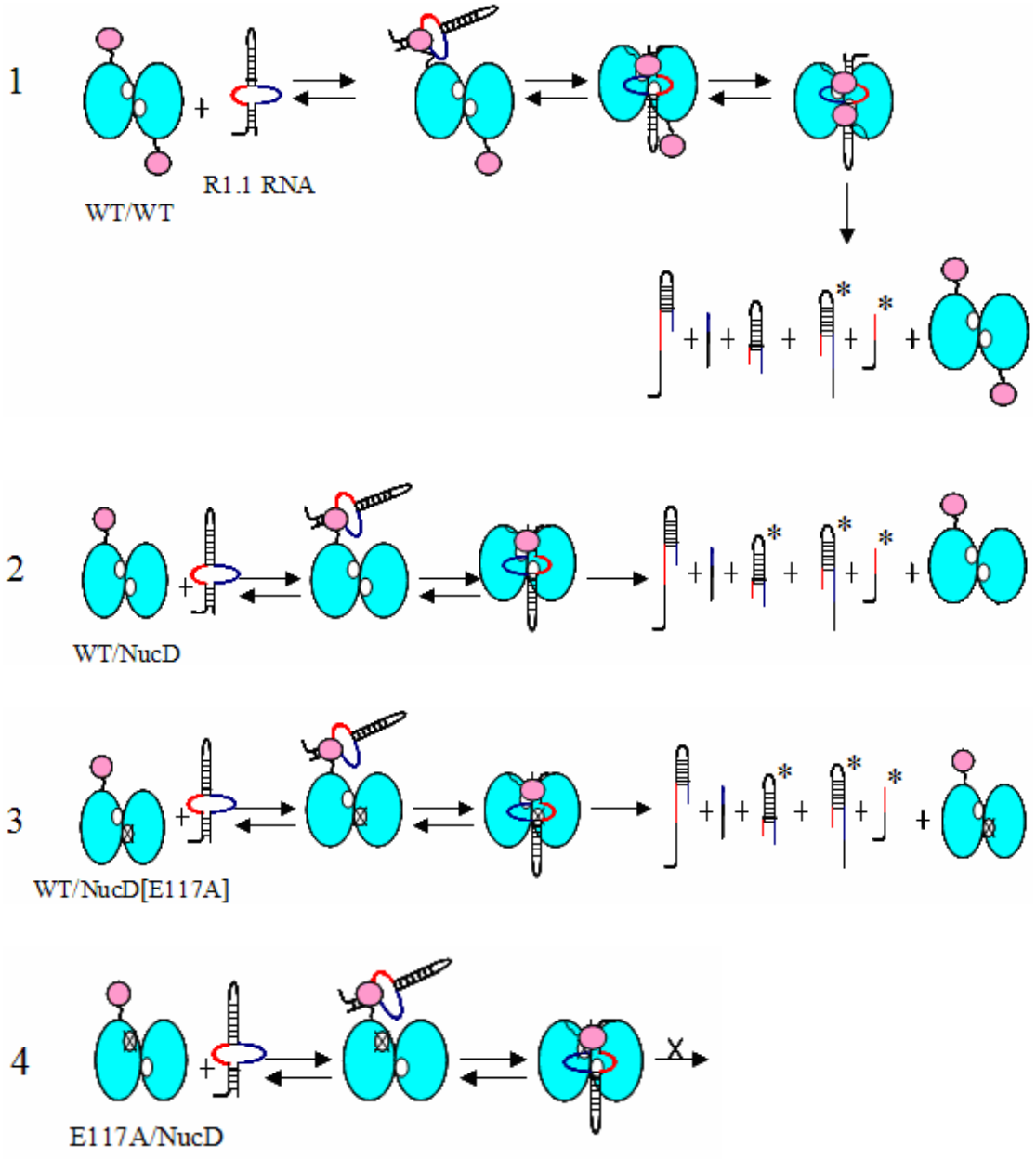

F

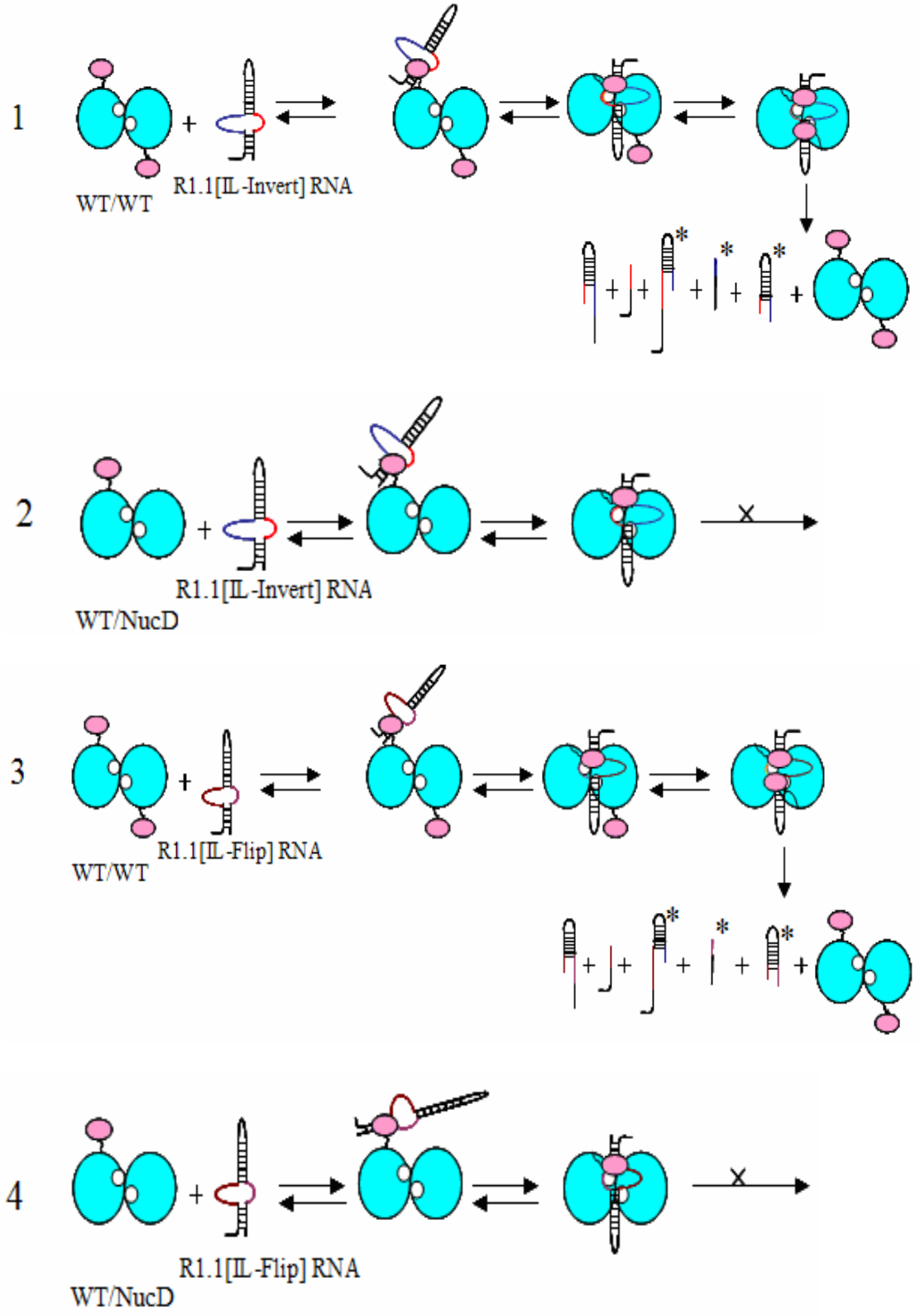
1
WT/WT
R1.1[IL-Invert] RNA
2
WT/NucD
R1.1[IL-Invert] RNA
3
WT/WT
R1.1[IL-Flip] RNA
4
WT/NucD
R1.1[IL-Flip] RNA

Figure 34. A proposed asymmetric pathway for substrate binding and cleavage by RNase III.

A. Diagrammatic structures of Ec-RNase III mutant heterodimers.

B. Structures of R1.1 RNA variants: R1.1 RNA, R1.1[WC] RNA, R1.1[IL-Flip] RNA, and R1.1[IL-Invert] RNA (based on Figure 8). R1.1 [IL-Invert] RNA is a variant of R1.1 RNA, in which the internal loop is rotated by 180°. R1.1 [IL-Flip] RNA is a variant of R1.1 RNA wherein the two strands of the internal loop are interchanged.
1°: Primary cleavage site, indicated by long arrow.
2°: Secondary cleavage site, indicated by short arrow.

C and D. *E. coli* RNase III WT/WT and mutant heterodimer cleavage of R1.1 [WC] RNA (Meng and Nicholson, 2008).

E. Pathway for Ec-RNase III and mutant heterodimer cleavage of R1.1 RNA (based on Figure 32, panel B and C). Cleavage fragments with asterisks represent minor products.

F. Ec-RNase III and mutant heterodimer cleavage of R1.1[IL-Invert] RNA and R1.1[IL-Flip] RNA (based on Figure 32B). Cleavage fragments with asterisks represent minor products.

binding-cleavage-release in order to achieve cleavage of both scissile bonds, thereby also imposing an additional overall decrease in cleavage rate (Figure 32A, lanes 10-12). The production of the singly-cleaved products is also more obvious in the latter two (WT/NucD and WT/NucD[E117A]) situations. In Figure 34D (lower panel), a functional NucD subunit that lacks the attached dsRBD cannot efficiently cleave a presented phophodiester, as neither a singly cleaved intermediate nor fully cleaved product can be detected (Figure 32A, lanes 14-16). Finally, the severely defective activity of the RNase III [NucD/E117A] heterodimer indicates that the dsRBD preferentially supports the action of the catalytic site of the same subunit. The limited length of linker may effectively prevent functional engagement of the dsRBD with the NucD of the other subunit. However, the specific interactions between the dsRBD and NucD remain to be characterized.

Based on the reactivities of asymmetric substrates towards asymmetric RNase III heterodimers, a pathway for formation of the precatalytic complex can be more precisely formulated (Figure 34E, F). Each of the target sites of the three asymmetric substrates examined (Figure 8; Figure 34B) has a primary (preferred) cleavage site on one strand and a secondary (i.e. minor) cleavage site on the other strand (Figure 32B). According to the model in Figure 34E and Figure 33B, C, and D, after initial recognition by the dsRBD, the dsRNA is rotated by ~180°, then placed in the intersubunit cleft of the NucD. As a consequence, the primary cleavage site is placed in the catalytic site of the functional NucD subunit which is connected in *cis* to the same dsRBD carrying the dsRNA. This pathway will lead to cleavage. In Figure 34E-4 (lower level), there will be no cleavage if the primary cleavage site is placed in the catalytically inactive NucD subunit containing the E117A mutation, even when the other subunit carries a functional catalytic site. This model was further tested by

examining the reactivity of internal loop-containing substrates in which the 5/4 nt internal loop was permuted by a vertical 180˚ rotation (R1.1[IL-Invert] RNA), or by a horizontal 180˚ "flip" (R1.1[IL-Flip] RNA). Since the primary cleavage site is associated with the 5 nt segment (Figure 32B; Calin-Jageman and Nicholson, 2003), the nondetectable cleavage of R1.1[IL-Invert] RNA and R1.1[IL-Flip] RNA by the WT/NucD heterodimer (Figure 32B, lanes 9, 10 and 14, 15) provides further support for the proposal that the dsRBD preferentially functions with the NucD of the same subunit.

4.7 Summary

A biochemical analysis of Aa-RNase III was carried out, and included the (i) demonstration of robust thermostability; (ii) dependence of catalytic activity on divalent metal cation type and concentration; and (iii) the effects of salt type, concentration, and pH. Small RNA hairpins based on the double-stranded stems associated with the Aquifex 16S and 23S rRNA precursors were developed and used to analyze the dependence of processing reactivity on base-pair sequence, and to characterize a conserved, functionally important RNase III–substrate interaction.

The contributions to substrate recognition were determined for conserved amino acid side chains in the RBM1 of Aa-RNase III. It was also shown that the dsRBD plays key dual roles in both substrate binding energetics and selectivity, primarily through RBM1 responsiveness to the substrate proximal box (pb) sequence. The dsRBD is responsive to an antideterminant GC/CG bp in pb position 2. The relative conformational inflexibility of both dsRNA and the dsRBD rationalizes the strong effect of an inhibitory bp at pb position 2, in that disruption of one RBM1 side chain interaction by an antideterminant bp can effectively disrupt neighboring interactions involving RBM1 side chains.

Structurally asymmetric mutant heterodimers of Ec-RNase III and asymmetric substrates were used to show how RNase III may bind and deliver hairpin substrates to the active site cleft, in a pathway that requires specific binding configurations between enzyme and substrate.

REFERENCES

Altuvia, S., Locker-Giladi, H., Koby, S., Ben-Nun, O. and Oppenheim, A.B. (1987). RNase III stimulates the translation of the cIII gene of bacteriophage lambda. Proc Natl Acad Sci USA 84, 6511-6515.

Blaszczyk, J., Tropea, J.E., Bubunenko, M., Routzahn, K.M., Waugh, D.S., Court, D.L. and Ji, X. (2001). Crystallographic and modeling studies of RNase III suggest a mechanism for double-stranded RNA cleavage. Structure 9, 1225-1236.

Blaszczyk, J., Gan, J., Tropea, J.E., Court, D.L., Waugh, D.S. and Ji, X. (2004). Noncatalytic assembly of ribonuclease III with double-stranded RNA. Structure 12, 457–466.

Calin-Jageman, I. and Nicholson, A.W. (2003). Mutational analysis of an RNA internal loop as a reactivity epitope for *Escherichia coli* ribonuclease III substrates. Biochemistry 42, 5025-5034.

Cambillau, C. and Claverie, J.M. (2000). Structural and genomic correlates of hyperthermostability. J Biol Chem 275, 32383–32386.

Campbell, F.E., Cassano, A.G., Anderson, V.E. and Harris,M.E. (2002). Pre-steady-state and stopped-flow fluorescence analysis of *Escherichia coli* ribonuclease III: insights into mechanism and conformational changes associated with binding and catalysis. J Mol Biol 317, 21–40.

Carey, J., Cameron, V., deHaseth, P.L. and Uhlenbeck, O.C. (1983). Sequence-specific interaction of R17 coat protein with its ribonucleic acid binding site. Biochemistry 22, 2601–2610.

Carey, J. (1991). Gel retardation. Methods Enzymol 208, 103–117.

Carmell, M.A. and Hannon, G.J. (2004). RNase III enzymes and the initiation of gene silencing. Nat Struct Mol Biol 11, 214–218.

Condon, C. and Putzer, H. (2002) The phylogenetic distribution of bacterial ribonucleases. Nucleic Acids Res 30, 5339–5346.

Court, D.L. (1993) RNA processing and degradation by RNase III. In: “Control of Messenger RNA Stability” (J.G. Belasco and G. Brawerman, eds). Academic Press, NY pp. 71-116.

Crick, F. (1970). Central dogma of molecular biology. Nature 27, 561-563.

Cruz-Reyes, J., Piller, K.J., Rusché, L.N., Mukherjee, M. and Sollner-Webb, B. (1998). Unexpected electrophoretic migration of RNA with different 3' termini causes a RNA sizing ambiguity that can be resolved using nuclease P1-generated sequencing ladders. Biochemistry 37, 6059-6064.

Deckert, G., Warren, P.V., Gaasterland, T., Young, W.G., Lenox, A.L., Graham, D.E., Overbeek, R., Snead, M.A., Keller, M., Aukjay, M., Huber, R., Feldman, R.A., Short, J.M., Olsen, G.J. and Swanson, R.V. (1998). The complete genome of the hyperthermophilic bacterium *Aquifex aeolicus*. Nature 392, 353–358.

Deutscher, M.P. (2009). Maturation and degradation of ribosomal RNA in bacteria. Prog Mol Biol Transl Sci 85, 369–391.

Dunn, J.J. (1976). RNase III cleavage of single-stranded RNA. Effect of ionic strength on the fidelity of cleavage. J Biol Chem 251, 3807–3814.

Dunn, J.J. (1982). Ribonuclease III. In P. Boyer (Ed.), The Enzymes, Vol. 15. (pp. 485–499). New York, Academic Press.

Dunn, J.J. and Studier, F.W. (1983). Complete nucleotide sequence of bacteriophage T7 DNA and the locations of T7 genetic elements. J Mol Biol 166, 477-535.

Ebright, R.H. (1985). Use of "loss-of-contact" substitutions to identify residues involved in an amino acid-base pair contact: effect of substitution of Gln18 of lac repressor by Gly, Ser, and Leu. J Biomol Struct Dyn 3,281-297.

Fire, A., Xu, S., Montgomery, M.K., Kostas, S.A., Driver, S.E. and Mello, C.C. (1998). Potent and specific genetic interference by double-stranded RNA in *Caenorhabditis elegans*. Nature 391, 806-11.

Gan, J., Tropea, J.E., Austin, B.P., Court, D.L., Waugh, D.S. and Ji, X. (2005). Intermediate states of ribonuclease III in complex with double-stranded RNA. Structure 13, 1435–1442.

Gan, J., Tropea, J.E., Austin, B.P., Court, D.L., Waugh, D.S. and Ji, X. (2006). Structural insight into the mechanism of double-stranded RNA processing by ribonuclease III. Cell 124, 355–366.

Gan, J., Shaw, G., Tropea, J.E., Waugh, D.S., Court, D.L. and Ji, X. (2008). A stepwise model for double-stranded RNA processing by ribonuclease III. Mol Microbiol 67, 143–154.

Grant, S.G., Jessee, J., Bloom, F.R. and Hanahan, D. (1990). Differential plasmid rescue from transgenic mouse DNAs into *Escherichia coli* methylation-restriction mutants. Proc Natl Acad Sci U S A 87, 4645-4649.

Hannon, G.J. (2002). RNA interference. Nature 418, 244-251.

Hol, W.G. (1985). Effects of the alpha-helix dipole upon the functioning and structure of proteins and peptides. Adv Biophys 19,133-165.

Huntzinger, E., Boisset, S., Saveanu, C., Benito, Y., Geissmann, T., Namane, A., Lina, G., Etienne, J., Ehresmann, B. Ehresmann, C., Jacquier, A., Vandenesch, F. and

Romby, P. (2005). *Staphylococcus aureus* RNAIII and the endoribonuclease III coordinately regulate spa gene expression. EMBO J 24, 824–835.

Jaskiewicz, L. and Filipowicz, W. (2008). Role of Dicer in posttranscriptional gene silencing. Curr Top Microbiol Immunol 320, 77–97.

Ji, X. (2006). Structural basis for non-catalytic and catalytic activities of ribonuclease III. Acta Crystallogr D Biol Crystallogr 62, 933-940.

Ji, X. (2008). The mechanism of RNase III action: how dicer dices. Curr Topics Microbiol Immunol 320, 99–116.

Kaberdin, V.R. and Bizebard, T. (2005) Characterization of *Aquifex aeolicus* RNase E/G. Biochem Biophys Res Comm 327, 382–392.

Kharrat, A., Macias, M.J., Gibson, T.J., Nilges, M. and Pastore, A. (1995). Structure of the dsRNA binding domain of *E. coli* RNase III. EMBO J 14, 3572-3584.

LaMontagne, B., Larose, S., Boulanger, J. and AbouElela, S. (2001). The RNase III family: a conserved structure and expanding functions in eukaryotic dsRNA metabolism. Curr Issues Mol Biol 3, 71–78.

Leulliot, N., Quevillon-Cheruel, S., Graille, M., van Tilbeurgh, H., Leeper, T.C., Godin, K.S., Edwards, T.E., Sigurdsson, S.T., Rozenkrants, N., Nagel, R.J., Ares, M. and Varani, G. (2004). A new alpha-helical extension promotes RNA binding by the dsRBD of Rnt1p RNAse III. EMBO J 23, 2468-2477.

Lesser, D.R., Kurpiewski, M.R. and Jen-Jacobson, L. (1990). The energetic basis of specificity in the Eco RI endonuclease-DNA interaction. Science 250, 776–786.

Lewin, B. (2003). Genes VIII (Oxford, U.K.: Oxford University Press).

Li, H. and Nicholson, A.W. (1996). Defining the enzyme binding domain of a ribonuclease III processing signal. Ethylation interference and hydroxyl radical footprinting using catalytically inactive RNase III mutants. EMBO J 15, 1421–1433.

Lamontagne B, Larose S, Boulanger J, Elela SA. (2001). The RNase III family: a conserved structure and expanding functions in eukaryotic dsRNA metabolism. Curr Issues Mol Biol 3, 71-8.

Lombo, T.B. and Kaberdin, V.R. (2008). RNA processing in *Aquifex aeolicus* involves RNase E/G and an RNase P-like activity. Biochem Biophys Res Comm 366, 457–463.

Macrae, I.J., Zhou, K., Li, F., Repic, A., Brooks, A.N., Cande, W.Z., Adams, P.D. and Doudna, J.A. (2006). Structural basis for double-stranded RNA processing by Dicer. Science 311, 195-198.

Marszalkowski, M., Willkomm, D.K. and Hartmann, R.K. (2008). 5'-end maturation of tRNA in *Aquifex aeolicus*. Biol Chem 389, 395–403.

Meng, W. and Nicholson, A.W. (2008). Heterodimer-based analysis of subunit and domain contributions to double-stranded RNA processing by *Escherichia coli* RNase III *in vitro*. Biochem J 410, 39-48.

Meng, W., Nicholson, R.H., Nathania, L., Pertzev, A.V. and Nicholson, A.W. (2008). New approaches to understanding double-stranded RNA processing by ribonuclease III. Purification and assays of homodimeric and heterodimeric forms of RNase III from bacterial extremophiles and mesophiles. Methods Enzymol 447, 119–129.

Nashimoto, H. and Uchida, H. (1985). DNA sequencing of the *Escherichia coli* ribonuclease III gene and its mutations. Mol Gen Genet 201, 25-29.

Nathania, L. and Nicholson, A.W. (2010). Thermotoga maritima ribonuclease III. Characterization of thermostable biochemical behavior and analysis of conserved base pairs that function as reactivity epitopes for the Thermotoga 23S rRNA precursor. Biochemistry 49, 7164–7178.

Nicholson, A.W. (2003). The ribonuclease III superfamily: forms and functions in RNA maturation, decay, and gene silencing. In RNAi: A Guide to Gene Silencing (Hannon, G.J. ed) Cold Spring Harbor Laboratory Press, Cold Spring Harbor, NY, 149-174.

Nicholson, A.W. (2011). Ribonuclease III and the role of double-stranded RNA processing in bacterial systems. Ribonucleases, Nucleic Acids and Molecular Biology 26, 269-297.

Pertzev,A. and Nicholson,A.W. (2006). Characterization of RNA sequence determinants and antideterminants of processing reactivity for a minimal substrate of *Escherichia coli* ribonuclease III. Nucleic Acids Res 34, 3708–3721.

Plaxco, K.W., Simons, K.T. and Baker, D. (1998). Contact order, transition state placement and the refolding rates of single domain proteins. J Mol Biol 277, 985–994.

Price, B., Adamidis, T., Kong, R. and Champness, W. (1999). A *Streptomyces coelicolor* antibiotic regulatory gene, absB, encodes an RNase III homolog. J Bacteriol 181, 6142–6151.

Redko, Y. and Condon, C. (2009). Ribosomal protein L3 bound to 23S precursor rRNA stimulates its maturation by mini-III ribonuclease. Mol Microbiol 71, 1145–1154.

Robinson-Rechavi, M., Alibe´s, A. and Godzik, A. (2006). Contribution of electrostatic interactions, compactness and quaternary structure to protein thermostability: lessons learned from structural genomics of *Thermotoga maritima*. J Mol Biol 356, 547–557.

Robinson-Rechavei, M. and Godzik, A. (2005). Structural genomics of *Thermotoga maritima* proteins shows that contact order is a major determinant of protein thermostability. Structure 13, 857–860.

Ryter, J.M. and Schultz, S.C. (1998). Molecular basis of double-stranded RNA-protein interactions: structure of a dsRNA-binding domain complexed with dsRNA. EMBO J 17,7505-7513.

Saito, H. and Richardson, C.C. (1981). Processing of mRNA by ribonuclease III regulates expression of gene 1.2 of bacteriophage T7. Cell 27, 533–542.

Saito, R., Ozawa, Y., Kuzuno, N. and Tomita, M. (2000). Computer analysis of potential stem structures of rRNA operons in various procaryotic genomes. Gene 259, 217–222.

Schmeissner, U., McKenney, K., Rosenberg, M. and Court, D. (1984). Removal of a terminator structure by RNA processing regulates int gene expression. J Mol Biol 176, 39–53.

Shi, Z., Nicholson, R.H., Jaggi, R. and Nicholson, A.W. (2011). Characterization of *Aquifex aeolicus* ribonuclease III and the reactivity epitopes of its pre-ribosomal RNA substrates. Nucleic Acids Res 39, 2756-2768.

Srivastava, A. and Schlessinger, D. (1990). Mechanism and regulation of bacterial ribosomal RNA processing. Annu Rev Microbiol 44, 105–129.

Suhre, K. and Claverie, J.M. (2003). Genomic correlates of hyperthermostability, an update. J Biol Chem 278, 17198–17202.

Sun, W., Jun, E. and Nicholson, A.W. (2001). Intrinsic double-stranded-RNA processing activity of *Escherichia coli* ribonuclease III lacking the dsRNA-binding domain. Biochemistry 40, 14976-14984.

Sun,W. and Nicholson,A.W. (2001). Mechanism of action of *Escherichia coli* ribonuclease III. Stringent chemical requirement for the glutamic acid 117 side chain, and Mn^{2+} rescue of the Glu117Asp mutant. Biochemistry 40, 5102–5110.

Sun, W., Pertzev, A. and Nicholson, A.W. (2005). Catalytic mechanism of *Escherichia coli* ribonuclease III. Kinetic and inhibitor evidence for the involvement of two Mg^{2+} ions in phosphodiester hydrolysis. Nucleic Acids Res 33, 807–815.

Swanson, R.V. (2001) Genome of *Aquifex aeolicus*. Methods Enzymol 330, 158–169.

Tian, B., Bevilacqua, P.C., Diegelman-Parente, A. and Mathews, M.B. (2004). The double-stranded-RNA-binding motif: interference and much more. Nat Rev Mol Cell Biol 5,1013-1023.

Wells, J.A. (1991). Systematic mutational analyses of protein-protein interfaces. Methods Enzymol 202, 390-411.

Wilkomm, D.K., Feltens, R. and Hartmann, R.K. (2002). tRNA maturation in *Aquifex aeolicus*. Biochimie 84, 713–722.

Woese, C.R., Kandler, O. and Wheelis, M.L. (1990). Towards a natural system of organisms: proposal for the domains Archaea, Bacteria, and Eucarya. Proc Natl Acad Sci U S A 87,4576-4579.

Wu, H., Henras, A., Chanfreau, G. and Feigon, J. (2004). Structural basis for recognition of the AGNN tetraloop RNA fold by the double-stranded RNA-binding domain of Rnt1p RNase III. Proc Natl Acad Sci U S A 101, 8307-8312.

Zhang, H., Kolb, F.A., Jaskiewicz, L., Westhof, E. and Filipowicz, W. (2004). Single processing center models for human Dicer and bacterial RNase III. Cell 118, 57–68.

Zhang, K. and Nicholson, A.W. (1997). Regulation of ribonuclease III processing by double-helical sequence antideterminants. Proc Natl Acad Sci USA 94, 13437–13441.